Crystal Growth of Some Rare Earth Molybdates by Gel Diffusion Technique

Dissertation

submitted for the award of the degree of

Master of Philosophy

in

Physics

by

Zahoor Ahmad Bhat

Under the Supervision of

Dr. Basharat Want

Department of Physics, University of Kashmir,

Hazratbal, Srinagar, 190006

November, 2012

Post Graduate Department of Physics,

University of Kashmir, Srinagar.

Certificate

This is to certify that the dissertation entitled "***Crystal Growth of Some Rare Earth Molybdates by Gel Diffusion Technique***" submitted by ***Zahoor Ahmad Bhat***, in partial fulfillment for the award of the degree of ***Master of Philosophy*** in ***Physics***, is the original research work carried out by him under my supervision and guidance. It is further certified that the dissertation has not been submitted for the award of M. Phil or any other degree to this University or any other University. The scholar has attended the department for statutory period as required under rules.

Dr. Basharat Want
(*Supervisor*)

Prof. Sheikh Javid Ahmad
(*Head of the Department*)

Acknowledgments

It gives me great pleasure and satisfaction to acknowledge the endowment of the creator and sustainer of this universe, Allah Almighty, the most gracious, compassionate and beneficent to His creature, Who blessed me with knowledge and potential to plan my research work. I offer my humblest words of thanks to His most noble messenger Muhammad (P.B.U.H), who is forever, a torch of guidance and Knowledge for all humanity.

I owe my indescribable special indebtedness to my Research Supervisor, **Dr. Basharat Want** who was very affectionate and cooperative during this research work and guided me at every step very politely, without his kind and sincere efforts it might not be possible for me to end this task in time. May he live long and prosper.

I am thankful to **Prof. Sheikh Javid Ahmad**, Head of Physics Department, University of Kashmir for the provision of all possible facilities and full co-operation. I also extend my thanks to the whole teaching faculty of the department for their generous help whenever needed.

My sincere thanks to my labmates Mr. Mehraj-U-din Shah, Mr. Ferooz Ahmad and Mr. Bilal Hamid Bhat for their timely suggestions. My special thanks to other research scholars of the department for their help during the completion of my course work. I am also thankful to my room-mates Mr.

Touseef Raja, Mr. Mudasir Rather, Mr. Reyaz Mir and Mr. Parveez Wani for their encouragement and continuous moral support.

I sincerely thank all the members of technical and non-technical/non-teaching staff of the department for their affection and kind co-operation.

I extend cordial thanks from the core of my heart to my mother, sisters, brother and other faimly members who encouraged me for higher studies and always wished to see me glittering high at the skies of success. I shall always remain indebted to them for their unstinted support, be it financially, morally or inspirationally.

May the Almighty Allah give them a happy life and bless them with good health (Amin!).

Zahoor Ahmad Bhat

Dedicated

To

The Unfathomable Depths Of Love

Ever Strengthening Prayers Of

My Sweet Mother

(To Whom's Feet My Heaven Lies)

Preface

The work presented in this thesis was carried out at the Solid-State Research Laboratory, Department of Physics, University of Kashmir, Srinagar. Due to the large applicability of rare earth molybdate crystal, it was thought with an aim of this thesis to investigate how to grow and also to characterize some of the rare earth molybdate crystals for scientific investigations by a very simple and inexpensive technique, known as gel technique.

The thesis is divided into seven chapters. First chapter gives an introduction to crystals and a brief overview of crystallization processes. These include classical theory of nucleation and many growth theories. Chapter two describes the different techniques of growing crystals, the main emphasis has been put on gel diffusion method.

Chapter three consists of experimental techniques used for the characterization of samples, such as scanning electron microscopy (SEM), powder X-ray diffraction (XRD), Energy-Dispersive Analysis of X-rays (EDAX), Thermal methods (TGA, DTA) etc.

Chapter four describes the literature survey. The chapter is divided into three parts, the first part gives a brief review of general rare earth compounds, the second part gives an overview of applications and growth process of rare earth molybdate and the third part gives an overview of spherulites, their morphology, characters etc.

Chapters five and six discuss the growth and characterization of the holmium molybdate crystals and gadolnium molybdate crystals respectively. Chapter seven gives summary and future scope of the present work. References to the literature are mentioned at the end of each chapter.

Abstract

Holmium molybdate and gadolnium molybdate crystal were grown via a very simple and inexpensive gel diffusion technique. The effect of various factors such as gel age, growth period, temperature, gel pH, concentration of lower reactant and concentration of upper reactant on the crystallization process were investigated.

As-grown samples were characterized by polarizing optical microscope, scanning electron microscopy (SEM), powder X-ray diffraction (XRD), Energy-Dispersive Analysis of X-rays (EDAX), Thermal methods (TGA, DTA).

The powder X-ray diffraction (pxrd) results revealed these samples are of crystalline nature and the EDAX results provided their elemental composition. The pxrd studies revealed that the structure of both the laboratory-grown holmium molybdate and gadolnium molybdate crystals is triclinic belonging to the space group of P1 with a = 7.80 $\mathring{A}$, b = 9.01 $\mathring{A}$, c = 13.54 $\mathring{A}$, $\alpha = 76.39^0$, $\beta = 131.38^0$ and $\gamma = 76.73^0$; a = 7.1560 $\mathring{A}$, b = 10.1980 $\mathring{A}$, c = 10.1740 $\mathring{A}$, $\alpha = 48.140^0$, $\beta = 58.220^0$ and $\gamma = 44.840^0$ as cell parameters respectively.

The optical images showed them to be of spherulitic form and the SEM results revealed them to be composed of nano-crystallites. Holmium molybdate spherulites grown at room temperature are composed of nano-plates and those grown at a temperature of 45 $^\circ C$ are composed of nano-rods. Gadolnium molybdate spherulites were grown only at 45 $^\circ C$ and were also composed of nano-rods. The thermal analysis curves provided their thermal decomposition behaviour and revealed that the holmium molybdate and gadolnium molybdate crystals shows an isomorphic phase transion at 520 $^\circ C$.

Contents

List of Tables

List of Figures

Chapter 1

Crystallization-Nucleation and Growth Kinetics: An Overview

1.1 Introduction to Crystals

People have been always surprised by the external shape or morphology of crystals. Crystals have fascinated human civilization for thousands of years and have attracted their intention owing to their beauty and rarity. Man practiced crystal growth and or crystallization processes as early as 1500 BC in the form of salt and sugar crystallization. Thus, crystal growth can be treated as an ancient scientific activity. However, the scientific approach to the field of crystal growth started in 1611 when Kepler correlated crystal morphology and structure, followed by Nicolous Steno, who explained the origin of a variety of external forms. Since then crystal growth has evolved steadily to attain its present status. Crystals are now the unacknowledged pillars of modern technology. The growth of crystals is both scientifically and technologically important, and the applications of such crystals today range

from electronics to thermal management to synthetic gemstones. Without crystals, there would be no electronic industry, no photonic industry, no fiber optic communications, which depend on materials/crystals such as semiconductors, superconductors, polarizers, transducers, radiation detectors, ultrasonic amplifiers, ferrites, magnetic garnets, solid state lasers, non-linear optics, piezo-electric, electro-optic, acousto-optic, photosensitive, refractory of different grades, crystalline films for microelectronics and computer industries. The current impetus in crystal growth started in the past few decades. It has greatly attracted the attention of researchers, particularly in view of the increasing demand of materials for technological applications (Brice 1986, Nalwa and Miyata 1997). The operating abilities of a large part of modern technological hardware (electronic and optic devices, control and operating systems, watches, etc.) is based on active and/or passive crystalline core pieces. For various applications the crystalline state is required to be polycrystalline (ceramics), multigrained (solar cells), crystalline designed (thin film sequences) or single crystalline (semiconductor and NLO devices, CaF_2 lenses, prisms, etc.). The dimension of the crystallites and crystals covers a wide range from nanometer (nanocrystallites) and micrometer (ceramics, thin-film arrangements) up to millimeter and centimeter scales (electronics, optics), in special cases up to meter scale (silicon single crystals, natural ice and quartz crystals).

Crystal growth is a highly interdisciplinary subject covering number of subjects such as physics, chemistry, material science, chemical engineering, metallurgy, crystallography, mineralogy, etc. The significance of the beauty and rarity of crystals is now well knitted with their symmetry, molecular

structure, and purity, and the physiochemical environment of their formation. These characteristics endow crystals with unique physical and chemical properties, which have transformed electronic industries for the benefit of human society. Prior to commercial growth or production of crystals, man depended only on the availability of natural crystals for both jewelery and devices. Today the list of uses of artificially grown crystals is growing exponentially for a variety of applications, such as electronics, electrooptics, crystal bubble memories, spintronics, magnetic devices, optics, nonlinear devices, oscillators, polarizers, transducers, radiation detectors, lasers, etc. Besides inorganic crystal growth, the world of organic, semiorganic, biological crystal growth is expanding greatly to make crystal growth activity more cost-effective. Today, the quality, purity, and defect-free nature of crystals is a prerequisite for their technological application.

Crystal growth is basically a process of arranging the units of a substance (atoms, ions, molecules or molecular assemblies) into a regular three dimensional periodic arrays. However, this perfect regularity has been never found in real crystals. This is because of the presence of different kinds of local disorder and long-range imperfections such as dislocations. So crystals are often polycrystalline in nature. Crystal growth techniques and characterization tools have advanced greatly in recent years. This has facilitated the growth and characterization of a large variety of technologically important crystals. Crystal growth can be treated as an important branch of materials science leading to the formation of technologically important materials of different sizes. Hence, it covers crystals from bulk to small and even to fine, ultrafine, and nanoscale sizes. In this respect, crystal growth has a close

relationship with crystal engineering, and also polyscale crystal growth is relevant. This concept becomes even more relevant with progress achieved in nanotechnology, where in the size effect explains changes in the physical properties of crystalline materials with size.

1.2 The Process of Crystallization

Crystallization is the (natural or artificial) process of formation of solid crystals by mass transfer of a solute from a liquid solution, melt or more rarely directly from a gas to a pure solid crystalline phase. Crystallization is an aspect of precipitation, obtained through a variation of the solubility conditions of the solute in the solvent, as compared to precipitation due to chemical reaction. The process of crystallization occurs in two steps, nucleation and crystal growth. For crystallization to occur from a solution it must be supersaturated which is the driving force for both the nucleation and growth [1-2]. This means that the solution has to contain more solute entities (molecules or ions) dissolved than it would contain under the equilibrium (saturated solution). This can be achieved by various methods, with (1) solution cooling, (2) addition of a second solvent to reduce the solubility of the solute (technique known as antisolvent or drown-out), (3) chemical reaction and (4) change in pH being the most common methods used in industrial practice. Other methods, such as solvent evaporation, can also be used. Figure 1.1 shows a typical (super)solubility diagram.

The diagram can be described in terms of three distinct zones:

1. The stable zone of an undersaturated solution where no nucleation or crystal growth is possible. Existing crystals will simply dissolve.

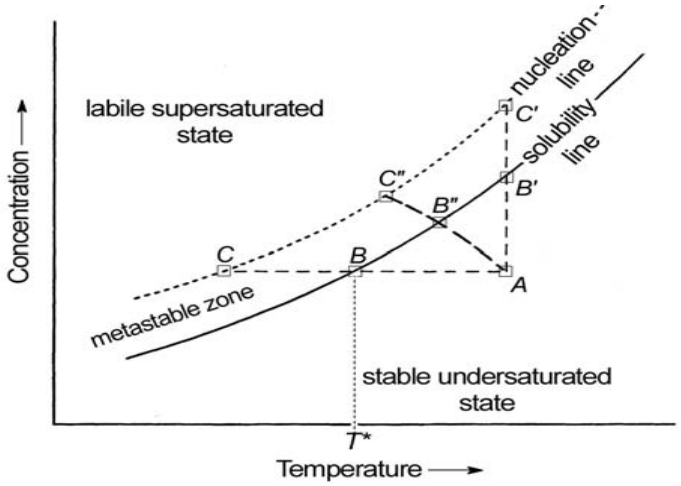

Figure 1.1: Typical solubility/super-solubility plot.

2. The supersaturated metastable zone where growth may occur but spontaneous nucleation does not.

3. The labile supersaturated zone of spontaneous and rapid nucleation.

1.3 Nucleation

Nucleation is the step where the solute molecules dispersed in the solvent start to gather into clusters, on the nanometer scale (elevating solute concentration in a small region), that become stable under the current operating conditions. These stable clusters constitute the nuclei. However, when the clusters are not stable, they redissolve. Therefore, the clusters need to reach a critical size (r_c) in order to become stable nuclei [3-4] as shown in figure 1.2. Such critical size is dictated by the operating conditions (temperature, supersaturation, etc.). It is at the stage of nucleation that the atoms arrange in a defined and periodic manner that defines the crystal structure. Nucle-

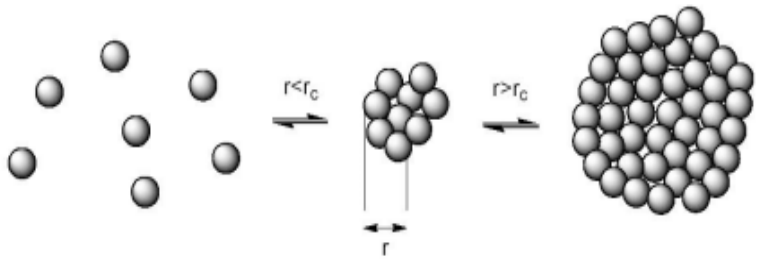

Figure 1.2: The process of nucleation.

ation is the extremely localized budding of a distinct thermodynamic phase. It is the initiation of a phase change in a small region. It is a consequence of rapid local fluctuations on a molecular scale in a homogeneous phase that is in a state of metastable equilibrium. Nucleation may occur at a seed crystal, but in the absence of seed crystals usually occurs at some particle of dust or at some imperfection in the surrounding vessel. Crystals grow by the ordered deposition of material from the fluid or solution state to a surface of the crystal. Total nucleation is the sum effect of two categories of nucleation primary and secondary as shown in figure 1.3.

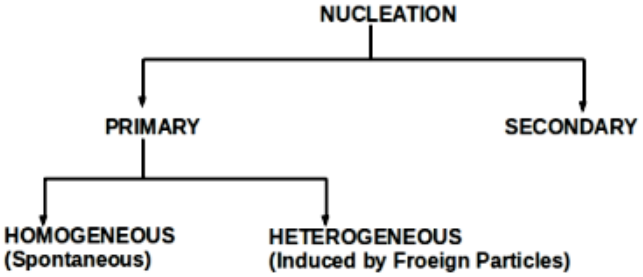

Figure 1.3: Structure of total nucleation process.

1.3.1 Primary Nucleation

Primary nucleation is the initial formation of a crystal where there are no other crystals present or where, if there are crystals present in the system, they do not have any influence on the process. This can occur in two conditions. The first is homogeneous nucleation, which is nucleation that is not influenced in any way by solids. These solids include the walls of the crystallizer vessel and particles of any foreign substance. The second category, then, is heterogeneous nucleation. This occurs when solid particles of foreign substances cause an increase in the rate of nucleation that would otherwise not be seen without the existence of these foreign particles. Homogeneous nucleation rarely occurs in practice due to the high energy necessary to begin nucleation without a solid surface to catalyse the nucleation.

Generally, heterogeneous nucleation takes place more quickly since the foreign particles act as a scaffold for the crystal to grow on, thus eliminating the necessity of creating a new surface and the incipient surface energy requirements. Heterogeneous nucleation can take place by several methods. Some of the most typical are small inclusions, or cuts, in the container the crystal is being grown on. This includes scratches on the sides and bottom of glassware. A common practice in crystal growing is to add a foreign substance, such as a string or a rock, to the solution, thereby providing nucleation sites for facilitating crystal growth and reducing the time to fully crystallize. The number of nucleating sites can also be controlled in this manner. If a brand-new piece of glassware or a plastic container is used, crystals may not form because the container surface is too smooth to allow heterogeneous nucleation. On the other hand, a badly scratched container

will result in many lines of small crystals. To achieve a moderate number of medium sized crystals, a container which has a few scratches works best.

1.3.2 Secondary Nucleation

A supersaturated solution nucleates much more readily, i.e. at a lower supersaturation, when crystals of the solute are already present or deliberately added (known as seeding). While in primary nucleation crystals can grow but cannot spontaneously nucleate in the metastable zone, so the term secondary nucleation is used for this particular pattern of behavior to distinguish it from so called primary nucleation (no crystals initially present). Secondary nucleation is the formation of nuclei attributable to the influence of the existing microscopic crystals in the magma. Secondary nucleation is widely used in industrial processes [6-9].

Strickland-Constable (1968) described several possible mechanisms of secondary nucleation, such as initial breeding (crystalline dust swept off a newly introduced seed crystal), needle breeding (the detachment of weak out-growths), polycrystalline breeding (the fragmentation of a weak polycrystalline mass) and collision breeding (a complex process resulting from the interaction of crystals with one another or with parts of the crystallization vessel). Conact nucleation has been found to be the most effective and common method for nucleation. The benefits include the following:

- Low kinetic order and rate-proportional to supersaturation, allowing easy control without unstable operation.
- Occurs at low supersaturation, where growth rate is optimum for good quality.

- Low necessary energy at which crystals strike avoids the breaking of existing crystals into new crystals.
- The quantitative fundamentals have already been isolated and are being incorporated into practice.

1.4 Classical Theory of Nucleation

The classical theory of nucleation, stemming from the work of Gibbs (1948), Volmer (1939), Becker and Doring (1935) and others, is based on the condensation of a vapour to a liquid, and this treatment may be extended to crystallization from melts and solutions. The free energy changes associated with the process of homogeneous nucleation may be considered as follows.

The overall excess free energy, ΔG, between a small solid particle of solute (assumed here, for simplicity, to be a sphere of radius r) and the solute in solution is equal to the sum of the surface excess free energy, ΔG_S, i.e. the excess free energy between the surface of the particle and the bulk of the particle, and the volume excess free energy, ΔG_V, i.e. the excess free energy between a very large particle ($r = \infty$) and the solute in solution. ΔG_S is a positive quantity, the magnitude of which is proportional to r^2. In a supersaturated solution ΔG_V is a negative quantity proportional to r^3 . Thus

$$\begin{aligned} \Delta G &= \Delta G_S + \Delta G_V \\ &= 4\pi r^2\sigma + \frac{4}{3}\pi r^3 \Delta G_v \end{aligned} \tag{1.1}$$

where ΔG_v is the free energy change of the transformation per unit volume and is the interfacial tension, i.e., between the developing crystalline surface

and the supersaturated solution in which it is located. The term surface energy is often used as an alternative to interfacial tension, but the latter term will be used throughout here for consistency.

For rapid crystallization ($\Delta G < 0$) the first term in equation (1.1) expresses the formation of the new surface, and the second term expresses the difference in chemical potential between the crystalline phase (μ) and the surrounding mother liquor (μ_0). The two terms are of opposite sign and depend differently on r, so the free energy of formation, ΔG, passes through a maximum (see Figure 1.4). This maximum value of the free energy, ΔG^*, corresponds to the critical nucleus of radius, r*, which is obtained by maximizing equation 1.1, setting $d\Delta G/dr = 0$, that is

$$\frac{d\Delta G}{dr} = 8\pi r\sigma + 4\pi r^2 \Delta G_v = 0 \tag{1.2}$$

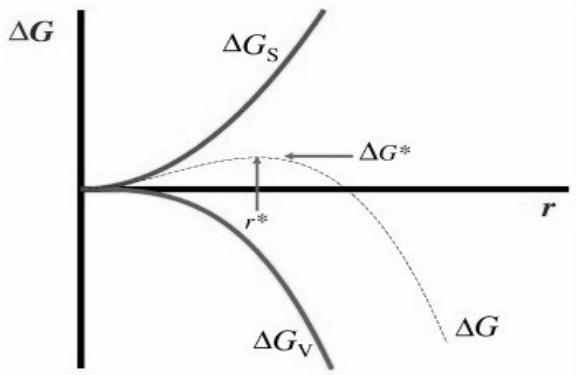

Figure 1.4: Free energy diagram for nucleation explaining the existence of a critical nucleus.

Hence, the radius of the critical nucleus is expressed as

$$r* = \frac{-2\sigma}{\Delta G_v} \tag{1.3}$$

where ΔG_v is a negative quantity. From equations (1.1) and (1.3), the critical free-energy barrier is given by

$$\Delta G^* = \frac{16\pi\sigma^3}{3(\Delta G_v)^2} = \frac{4\pi\sigma r*^2}{3} \tag{1.4}$$

The behaviour of a newly created crystalline lattice structure in a supersaturated solution depends on its size; it can either grow or redissolve, but the process which it undergoes should result in the decrease in the free energy of the particle. The critical size r* , therefore, represents the minimum size of a stable nucleus. Particles smaller than r* will dissolve, or evaporate if the particle is a liquid in a supersaturated vapour, because only in this way can the particle achieve a reduction in its free energy. Similarly, particles larger than r* will continue to grow. Although it can be seen from the free energy diagram why a particle of size greater than the critical size is stable, it does not explain the amount of energy, ΔG^*, necessary to form a stable nucleus is produced. This may be explained as follows. The energy of a fluid system at constant temperature and pressure is constant, but this does not mean that the energy level is the same in all parts of the fluid. There will be fluctuations in the energy about the constant mean value, i.e. there will be a statistical distribution of energy, or molecular velocity, in the molecules constituting the system, and in those supersaturated regions where the energy level rises temporarily to a high value nucleation will be favoured.

The number of molecules in the critical nucleus is given as follows:

$$I = \frac{4}{3}\pi\sigma r*^3 \tag{1.5}$$

The crucial parameter between a growing crystal and the surrounding mother liquor is the interfacial tension (σ). This complex parameter can be determined by conducting nucleation experiments.

1.5 Crystal Growth

Once an ordered structure is formed by nucleation, the growth units (atoms, ions or molecules) can diffuse from the surrounding supersaturated solution to the surface of the nuclei and incorporate into the lattice resulting in crystal growth [10]. So crystal growth is the development of the stable three-dimensional nuclei into crystals with well-developed faces. The formation of three-dimensional nuclei is usually discussed in terms of reduction in the Gibbs free energy of the system. At a given supersaturation and temperature, there is a critical value of the free energy at which three-dimensional nuclei of a critical radius are formed. Only those nuclei that are greater than the critically sized nucleus are capable of growing into crystals of visible size by the attachment of growth species (i.e. molecules, atoms, or ions) at energetically favorable growth sites. The surfaces of growing crystals may be flat (F), stepped (S), or kinked (K), as shown for a simple cubic crystal in figure 1.5 which is referred as Kossel crystal [11].

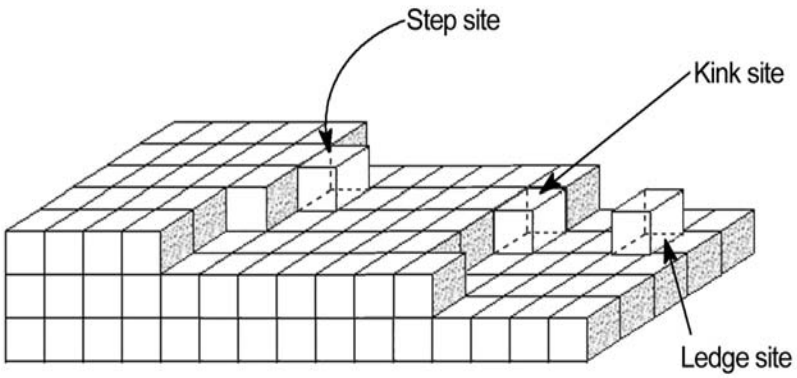

Figure 1.5: Incorporation of crystal forming elements on the surface of a growing crystal.

As indicated, adsorption of the growth units (depicted as a cube) on the surface structure of a growing crystal may occur at three possible sites:

1. Ledge sites (incorporation at a flat surface (terrace) having only one site of intermolecular interaction available),

2. Step sites (incorporation at a surface having two sites of intermolecular interactions available), or

3. Kink sites (three possible sites of intermolecular interactions).

Incorporation at a kink site will be the most energetically favorable because of higher coordination number. Furthermore, since incorporation at a kink site will provide a new kink site, the kink site is thus a repeatable step in the formation of the crystal.

1.6 Theories of Crystal Growth

Once stable nuclei, i.e. particles larger than the critical size (section 1.5), have been formed in a supersaturated or supercooled system, they begin to grow into crystals of visible size. Crystal growth has for long been in the centre of the interest of scientists, but are still not well understood up to now. Several theories to explain crystal growth have been proposed from time to time, involving the mechanism and the rate of growth of crystals. But none has succeeded to be generalized for the growth mechanism. This is due to the fact that many varieties of mechanisms needs to be considered before growth units, from the solution, reach and incorporated in to the crystal surface.

The important crystal growth theories are the surface energy theory, diffusion theory, adsorption layer theory, and screw dislocation theory. Gibbs

proposed the first theory of crystal growth, in which he assumed growth of crystals to be analogous to the growth of a water droplet from mist. Later Kossel and others explained the role of step and kink sites on the growth surface in promoting the growth process [12].

According to Garside there are three main ways to express the growth rate of a crystals or population of crystals:

1. Face growth rate, V_{hkl}. This is the rate of advance of the crystallographic face, measured perpendicular to the face. It means the individual crystal face needs to be observed and measured. The illustration of these theories can be taken from Burton, Cabrera, Frank (BCF model), or birth and spread (BS) model, purposed by OHara and Reid.

2. Overall mass growth rate, best expressed as the total mass flux to the crystal surface, R_G. This is the growth rate over the whole crystal.

$$R_G = \frac{1}{A_C}.\frac{dM_C}{dt} \tag{1.6}$$

If the face growth rates, Vhkl, and areas Ahkl of all the faces on a crystal are known, RG can be related to the different values of Vhkl by the expression:

$$R_G = \frac{\rho_C}{A_C} \sum V^*_{hkl} A_{hkl} \tag{1.7}$$

The overall mass growth rate is mainly used for calculations in batch systems.

3. Overall linear growth rate, which is defined as the time rate of change of a characteristic dimension, L, of the crystal.

$$G = \frac{dL}{dt} \tag{1.8}$$

The overall linear growth rate is widely used in population balance theory for calculating continuous and batch crystallizers.

1.6.1 Surface Energy Theory

The surface energy theory is based on the thermodynamic treatment of equilibrium states put forward by Gibbs [13]. He pointed out that the total free energy of a crystal in equilibrium with its surroundings at constant temperature and pressure would be a minimum for a given volume. If the volume free energy per unit volume is assumed to be constant throughout the crystal, then

$$\sum_{1}^{n} a_i g_i = minimum \tag{1.9}$$

where a_i is the area of the ith face of a crystal bounded by n faces, and g_i the surface free energy per unit area of the ith face. Therefore, if a crystal is allowed to grow in a supersaturated medium, it should develop into an 'equilibrium' shape, i.e. the development of the various faces should be in such a manner as to ensure that the whole crystal has a minimum total surface free energy for a given volume.

He compared the growth of crystals with the formation of water droplets in mist. Of course, a liquid droplet is very different from a crystalline particle; in the former the constituent atoms or molecules are randomly dispersed, whereas in the latter they are regularly located in a lattice structure. Gibbs was fully aware of the limitations of his simple analogy, but Many researchers later applied this idea and found it useful. Curie [14] worked out the shapes and morphologies of crystals in equilibrium with solution or vapor and found it a useful starting point for an attempt to evolve a general theory of crystal growth. Later, Wulff [15] deduced expressions for the growth rate at different faces and the surface free energies. According to him, the crystal faces would grow at rates proportional to their respective surface energies. Marc

and Ritzel [16] considered the effect of surface tension and solution pressure (solubility) on the growth rate. In their opinion, different faces have different values of solubility. When the difference in solubility is small, growth is mainly under the influence of surface energy, and the change in the surface of one form takes place at the expense of the other. Bravais [17] proposed that the velocities of growth of the different faces of a crystal depend inversely on the reticular or lattice density of the respective lattice plane, so that faces having low reticular densities would grow rapidly and eventually disappear. In other words, high index faces grow faster than low.

Figure 1.6(a) shows the ideal case of a crystal that maintains its geometric pattern as it grows. Such a crystal is called 'invariant'. The three equal A faces grow at an equal rate; the smaller B faces grow faster; while the smallest face C grows fastest of all. A similar, but reverse, behaviour may be observed when a crystal of this type dissolves in a solvent; the C face dissolves at a faster rate than the other faces, but the sharp outlines of the crystal are soon lost once dissolution commences.

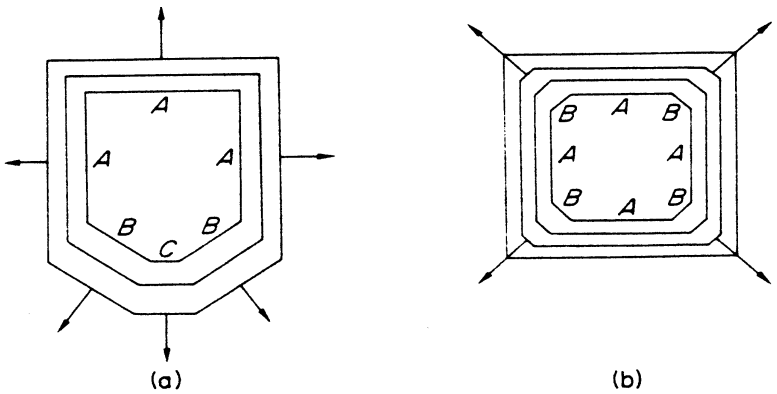

Figure 1.6: Velocities of crystal growth faces: (a) invariant crystal; (b) overlapping.

In practice, a crystal does not always maintain geometric similarity during growth; the smaller, faster-growing faces are often eliminated, and this mode of crystal growth is known as overlapping. Figure 1.6(b) shows the various stages of growth of such a crystal. The smaller B faces, which grow much faster than the A faces, gradually disappear from the pattern.

So far there is no general acceptance of the surface energy theories of crystal growth, since there is little quantitative evidence to support them. These theories, however, still continue to attract attention, but their main defect is their failure to explain the well-known effects of supersaturation and solution movement on the crystal growth rate.

1.6.2 Diffusion Theory

The diffusion theory proposed by Noyes and Whitney [18] in 1897. They developed the theory on the basis of following assumptions:

1. The deposition of solid on the face of a growing crystal was essentially a diffusional process;

2. Crystal growth is the reverse process of dissolution and that the rates of both processes were governed by the difference between concentration at the solid surface and in the bulk of the solution.

An equation for crystallization was proposed in the form

$$\frac{dm}{dt} = K_m A(C - C_0) \tag{1.10}$$

where m = mass of solid deposited in time t; A = surface area of the crystal; C = solute concentration in the solution (supersaturated); C_0 = equilibrium saturation concentration; and k_m = coefficient of mass transfer.

On the assumption that there would be a thin stagnant film of liquid adjacent to the growing crystal face, through which molecules of the solute would have to diffuse, Nernst in 1904 [19] modified equation 1.10 to the form

$$\frac{dm}{dt} = \frac{D}{\delta} A(C - C_0) \tag{1.11}$$

where D = coefficient of diffusion of the solute, and δ = length of the diffusion path.

The δ thickness of the stagnant film would obviously depend on the relative solid-liquid velocity, i.e. on the degree of agitation of the system. Film thicknesses up to 150 mm have been measured on stationary crystals in stagnant aqueous solution, but values rapidly drop to virtually zero in vigorously agitated systems. As this could imply an almost infinite rate of growth in agitated systems, it is obvious that the concept of film diffusion alone is not sufficient to explain the mechanism of crystal growth. Furthermore, crystallization is not necessarily the reverse of dissolution. A substance generally dissolves at a faster rate than it crystallizes at, under the same conditions of temperature and concentration.

1.6.3 Adsorption Layer Theory

The concept of a crystal growth mechanism based on the existence of an adsorbed layer of solute atoms or molecules on a crystal face was first suggested by Volmer in 1939. Many other workers have contributed to, and modified Volmer's original postulation. The brief account of this subsequent development given below will serve merely to indicate the important features of layer growth and the role of crystal imperfections in the growth process.

Kossel viewed crystal growth based on atomistic considerations. He assumed that crystal is in equilibrium with its solution when it is just saturated. Also, the attachment energy unit on growing surface is a simple function of distance only. The attachment energy is due to van der Waals forces if the crystal is homopolar, while it is due to electrostatic forces if the crystal is heteropolar (ionic). A growth unit arriving at a crystal surface finds attachment sites such as terraces, ledges, and kinks. The attachment energy of a growth unit can be considered to be the resultant of three mutually perpendicular components. The binding energy or attachment energy of an atom is maximum when it is incorporated into a kink site in a surface ledge, whilst at any point on the ledge it is greater than that for an atom attached to the flat surface (terrace). Hence, a growth unit reaching a crystal surface is not integrated into the lattice immediately. Instead it migrates to a step and moves along it to a kink site, where it is finally incorporated. Based on this consideration of attachment, Kossel was able to determine the most favorable face for growth. According to the Kossel model, growth of a crystal is a discrete process and not continuous. Also, a new layer on a preferably flat face of a homopolar crystal will start growing from the interior of the face. For heteropolar crystals, the corners are the most favorable for growth, while mid-face is least avored. According to Stranski, the critical quantity that determines the growth process is the work necessary to detach a growth unit from its position on the crystal surface. Growth units with the greatest detachment energy are most favored for growth, and vice versa. The greatest attraction of atoms to the corners of ionic and metallic crystals often leads to more rapid growth along these directions, with the result that the crystal

grows with many branches called dendrites radiating from a common core.

A crystal should grow fastest when its faces are entirely covered with kinks, and the theoretical maximum growth rate can be estimated. It is unlikely, however, that the number of kinks would remain at this high value for any length of time; it is well known, for example, that broken crystal surfaces rapidly 'heal' and then proceed to grow at a much slower rate. However, many crystal faces readily grow at quite fast rates at relatively low supersaturation, far below those needed to induce surface nucleation. Crystals of iodine, for example, can be grown from the vapour at 1 per cent supersaturation at rates some 101000 times greater than those predicted by classical theory (Volmer and Schultz, 1931). So it must be concluded that the Kossel model, and its dependence on surface nucleation, is unreasonable for growth at moderate to low supersaturation.

1.6.4 Screw Dislocation Theory

However, the Kossel, Stranski, and Volmer theory could not explain the moderately high growth rates observed in many cases at relatively low supersaturation, far below those needed to induce surface nucleation. A solution to the dilemma came when Frank in 1949 [20] proposed that few crystals ever grow in the ideal layer-by-layer fashion without some imperfection occurring in the pattern. Most crystals contain dislocations which cause steps to be formed on the faces and promote growth. Of these the screw dislocation is considered to be important for crystal growth, since it obviates the necessity for surface nucleation. Once a screw dislocation has been formed, the crystal face can grow perpetually up a spiral staircase. Growth takes place by rotation of the

steps around the dislocation point. Figure 1.7 indicates the successive stages in the development of a growth spiral starting from a screw dislocation. The curvature of the spiral cannot exceed a certain maximum value, determined by the critical radius for a two-dimensional nucleus under the conditions of supersaturation in the medium in which the crystal is growing. Dislocations

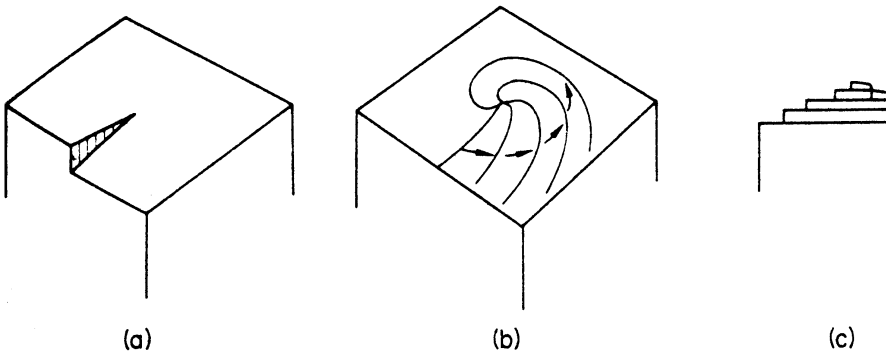

Figure 1.7: Development of a growth spiral starting from a screw dislocation.

are not necessary for crystal growth: large dislocation-free crystals of silicon are grown every day. However, growth on defects can be important when there is a barrier to the formation of new layers. When the rate at which new layers nucleate is very low, then growth can occur at the growth sites provided by defects. A growth rate that is proportional to ΔT^2, as Frank predicted is often observed at small undercoolings on surfaces where there is a nucleation barrier to growth. At larger undercoolings, the nucleation rate increases so that the nucleation of new layers takes over the growth process. At still larger undercooling, surface nucleation takes over, and the growth rate increases dramatically.

The defect density varies from crystal to crystal, and the nucleation rate depends on the crystal face as well as the crystal structure, as will be dis-

cussed below, so the magnitude of the rates, and the cross-over point from defect-dominated growth to surface nucleation growth varies widely. As a completely smooth face never appears under conditions of spiral growth, surface nucleation is not necessary and the crystal grows as if the surface were covered with kinks. Growth continues uninterrupted at near the maximum theoretical rate for the given level of supersaturation. The behaviour of a crystal face with many dislocations is practically the same as that of a crystal face containing just one. Burton, Cabrera and Frank (BCF) in 1951 [21] developed a kinetic theory of growth in which the curvature of the spiral near its origin was related to the spacing of successive turns and the level of supersaturation. By the application of Boltzmann statistics they predicted kink populations, and by assuming that surface diffusion is an essential step in the process they were able to calculate the growth rate at any supersaturation.The Burton-Cabrera-Frank (BCF) relationship may be written

$$R = A\sigma^2 tanh(B/\sigma) \tag{1.12}$$

where R = crystal growth rate. The supersaturation $\sigma = S - 1$, where S = C/C*. A and B are complex temperature-dependent constants which include parameters depending on step spacings.

At low supersaturations the BCF equation approximates to $R \propto \sigma^2$, but at high supersaturations $R \propto \sigma$. In other words, it changes from a parabolic to a linear growth law as the supersaturation increases. The volume diffusion model proposed by Chernov (1961) gives the same result. The general form of these expressions is shown in Figure 1.8. The Burton-Cabrera-Frank (BCF) supersaturation-growth relationship (I, $R \propto \sigma^2$; II, an approach to $R \propto \sigma$).

It should be pointed out that the BCF theory was derived for crystal

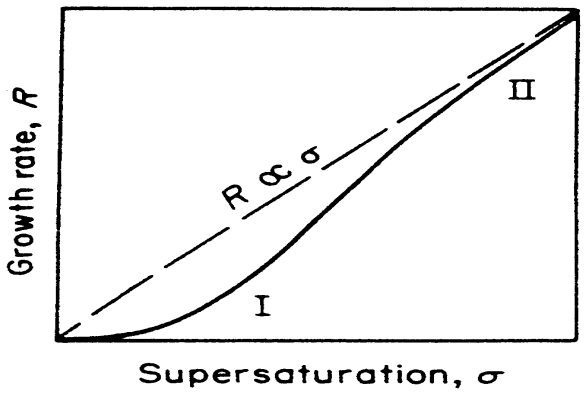

Figure 1.8: The Burton-Cabrera-Frank (BCF) supersaturation-growth relationship (I, $R \propto \sigma^2$; II, an approach to $R \propto \sigma$).

growth from the vapour; and while it should also apply to growth from solutions (and melts), it is difficult to quantify the relationships because of the more complex nature of these systems. Viscosities, for example, are higher and diffusivities lower in solutions ($\sim 10^{-3} Nsm^{-2} (1cP)$ and $10^{-9} m^2 s^{-1}$) than in vapours ($\sim 10^{-5} Nsm^{-2}$ and $10^{-4} m^2 s^1$). In addition, the dependence of diffusivity on solute concentration can be complex. Transport phenomena in ionic solutions can be complicated, especially if the different ions exhibit complex hydration characteristics. Furthermore, little is known about surface diffusion in adsorbed layers, and ion dehydration in or near these layers must present additional complicating factors.

1.7 Conclusion

The field of crystallization is very complicated as for as its theoretical background is considered. The theories used to explain the processes of nucleation and crystal growth have not yield satisfactory results. As some theories do

not stand on the experimental basis and some others are too complicated to calculate experimentally the different components included in them. Though the literature on crystallization is expanding very fast but lot is needed in order to have some good understanding of the field.

Bibliography

[1] A. N. Collins, G. N. Sheldrake and J. Crosby, **Chirality in Industry II**, Wiley, New York, 1997, Chapter 7, W. M. L. Wood.

[2] A. Mersmann, Trans. I Chem. E. 1996, **74**, 812.

[3] A. Collet, M. J. Brienne and J. Jacques, Chem. Rev. 1980, **80**, 215-230.

[4] R. Boistelle and J. P. Astier, J. Crystal Growth 1988, **90**, 14-30.

[5] Sunil Verma1 and K. Muralidhar., Res. Devel. Crystal Growth, **5**(2009), pp 146.

[6] J. Jacques, A. Collet and S. H. Wilen, **Enantiomers, Racemates, and Resolutions**, Wiley, New York, 1981.

[7] R. A. Sheldon, **Chirotechnology**, Marcel Dekker, New York, 1993, Chapter 6, W. M. L. Wood.

[8] P. Newman, **Optical Resolutions Procedures for Chemical Compounds**, Optical Resolution Information Center, New York, 1971.

[9] G. Amiard, **Bull. Soc. Chim. Fr.** 1956, 447-448.

[10] K. Sangwal, Prog. Cryst. Growth and Charact. 1998, **36**, 163-167.

[11] I. N. Stranski, Z. Phys. Chem. 1928, **136**, 259.

[12] W. Kossel, Nachr. Ges. Wiss. Gttingen **135**, 135-143 (1927)

[13] Gibbs, J. W. (1878), **"Collected Works"**, Longmans, Green and Co., New-York, 1928.

[14] P. Curie, Bull. Soc. Franc. Mineral. **8**, 145-150 (1885).

[15] G. Wulff, Z. Kristallogr. **34**, 449 (1901)

[16] R. Marc, A. Ritzel, Z. Phys. Chem. **76**, 584(1911).

[17] A. Bravais, A. Etudes: **Crystallographiques** (Gauthier Villers, Paris 1866).

[18] A.A. Noyes, W.R. Whitney, Z. Phys. Chem. **23**, 689-692 (1897)

[19] W. Nernst, Z. Phys. Chem. **47(1)**, 52-55 (1904)

[20] F.C. Frank, **5**, 48-54 (1949)

[21] W.K. Burton, N. Cabrera, F.C. Frank, **243**, 299-358(1951)

Chapter 2

Crystal Growth Techniques

2.1 Introduction

Crystal growth is a heterogeneous or homogeneous chemical process involving solid or liquid or gas, whether individually or together, to form a homogeneous solid substance having three dimensional atomic arrangement. A number of techniques/methods to grow crystal has been developed and employed. The methods of growing crystals, classified on the basis of their phase transformation, are as follows [1-4]:

- Solid growth solid-solid phase transformation.
- Vapor growth vapor-solid phase transformation.
- Liquid growth liquid-solid phase transformation.

There are number of growth methods in each category. Among the various methods of growing single crystals, solution growth at low temperature (a liquid growth technique) occupies a prominent place, owing to its versatil-

ity and simplicity [5-7]. Growth from solution occurs close to equilibrium conditions and hence crystals of high perfection can be grown.

2.2 Solid Growth Technique

In solid growth technique, single crystals are developed by the preferential growth of a polycrystalline mass. The commonly used solid-state growth techniques are annealing or sintering, strain annealing, heat treatment, deformation growth, polymorphic phase transitions, quenching, etc., and most of these are popularly used in metallurgical processes for tailoring material properties. Large crystals of several materials, especially metals have been grown by this method [8]. The main advantage of solid growth method is that this technique permits the growth at low temperatures without the presence of additional component. But as the growth takes place in the solid, density of sites for nucleation is high and it is difficult to control nucleation.

2.3 Vapour Growth Techniques

Vapor-phase growth is particularly employed in mass production of crystals for electronic devices because of its proven low cost and high throughput, in addition to its capability to produce advanced epitaxial structures. But, for growth from the vapor phase, the material should have high vapor pressure, and it should not decompose on vaporization if it is a compound. Alternatively, if the components have high vapor pressures, the desired compound can be assembled during deposition. One such scheme is illustrated in Fig. 2.1, where two components are vaporized separately, and combine at the

growing crystal. The technique is especially suitable for growth of semiconductors, despite the rather complex chemistry of the vapor-phase process. The fundamental reason for their success is the ease of dealing with low- and high-vapor-pressure elements. This is achieved by using specific chemical precursors in the form of vapor containing the desired elements. These precursors are introduced into the reactor by a suitable carrier gas and normally mix shortly before reaching the substrate, giving rise to the nutrient phase of the crystal growth process. The release of the elements necessary for construction of the crystalline layer may occur at the solidgas interface or directly in the gas phase, depending on the type of precursors and on the thermodynamic conditions.

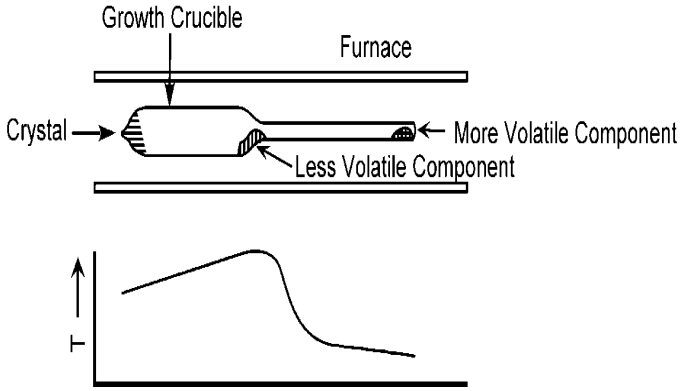

Figure 2.1: Vapor-phase growth of a compound from its components.

The advantage of vapor growth technique is that crystals tend to have a low concentration of point defects and low dislocation densities compared with crystals grown from the melt, as the temperatures employed are usually considerably lower than the melting temperature. Moreover, if the material undergoes a phase transformation or melts incongruently, vapor growth may be the only choice for the growth of single crystals. Although the method

was initially used to grow bulk crystals, with the enormous importance of thin films in electronic and metallurgical applications, vapor growth is now widely used to grow thin films, epitaxial layers, and substrates in the field of semiconductor technology [9-10].

Vapor-phase growth primarily involves three stages: vaporization, transport, and deposition. The vapor is formed by heating a solid or liquid to high temperatures. Transportation of vapor may occur through vacuum, driven by the kinetic energy of vaporization. Deposition of the vapor may occur by condensation or chemical reaction.

Various techniques exist in vapor-phase growth, differentiated by the nature of the source material and the means and mechanism by which it is transported to the growing crystal surface. Conceptually, the simplest technique is that of sublimation, where the source material is placed at one end of a sealed tube and heated so that it sublimates and is then transported to the cooler region of the tube, where it crystallizes.

Among vapor-phase growth techniques, vapor-phase epitaxy is the most popularly used, especially for the growth of p- and n-type semiconductor whose dimers and monomers are difficult to achieve by other methods (e.g., physical evaporation) or too stable to be reduced to the necessary atomic form. Furthermore, there are different variants such as metalorganic vapor-phase epitaxy (MOVPE), plasma-assisted molecular beam epitaxy (MBE), etc. to suit the growth of particular compounds.

2.4 Liquid Growth Technique

The liquid growth technique can be further classified as:

- Melt growth
- Solution growth
- Gel growth

2.4.1 Melt Growth Techniques

Melt growth of crystals is undoubtedly the most popular method of growing large single crystals at relatively high growth rates ($\sim cm/hr$). In fact, more than half of technological crystals are currently obtained by the technique. The method has been popularly used for growth of elemental semiconductors and metals, oxides, halides, chalcogenides, etc.

Growth from the melt requires some conditions:

1. The material must melt congruently (no change in composition during melting) e.g. Yttrium Iron garnet (YIG) is grown from solutions because it does not melt congruently.

2. The material must not decompose before melting. e.g. SiC is grown from vapor phase (sublimation-condensation) because it decomposes before melting.

3. The material must not undergo a solid state phase transformation between melting point and room temperature. e.g.SiO_2 is grown from solution (hydrothermal growth) because of a $\alpha - \beta$ quartz transition at $583\,^{\circ}C$.

4. The interaction between the melt and crucible, or the presence of a third component derived from the crystallization atmosphere, can affect melt

growth. Usually, an oxygen-containing atmosphere is used for oxides, a fluorine-containing atmosphere for fluorides, a sulfur-containing atmosphere for sulfides, and so on. In melt growth, crystallization can be carried out in a vacuum, in a neutral atmosphere (helium, argon, nitrogen), or in a reducing atmosphere (air, oxygen).

Variety of techniques have been developed for the growth of crystals of a material from its melt. These include Verneuil, Czochralski, Bridgman, Stockbarger, Kyropoulos method, etc. All have in common the characteristics that a material of approximately the correct composition is melted congruently, i.e., the same crystalline phase is maintained before and after melting. The melt is then solidified in a carefully controlled fashion to cause the formation of a single crystal. In most crystal growth experiments, this solidification is accomplished using a well oriented seed material of the same crystal composition. Unfortunately, since most interesting materials have high melting temperatures ($1500 - 2400\,^{\circ}C$), the melt techniques cannot always be useful because many materials decompose or vaporize at such high temperatures. Also, in some cases the melt may be viscous, so that a glass forms instead of a crystal.

Selection of a particular melt growth technique is done on the basis of the physical and chemical characteristics of the crystal to be grown. Metal single crystals with melting point $< 1800\,^{\circ}C$ are grown by Stockbarger method, and those with melting point $> 1800\,^{\circ}C$ by zone melting. Semiconducting crystals are grown chiefly by Czochralski method, and by zone melting. Single crystals of dielectrics with melting point $< 1800\,^{\circ}C$ are usually grown by the Stockbarger or Czochralski methods, while higher-melting materials are pro-

duced by flame fusion (Verneuil method). If the physicochemical processes involved in crystallization are taken into account, it is possible to establish optimum growth conditions.

One of the earliest melt techniques used to grow large quantity of high-melting materials was the Verneuil method (flame fusion technique), first described by Verneuil in 1902 [11]. This marks the beginning of commercial production of large quantities of high-melting crystals, which were essentially used as gems or for various mechanical applications. Today, the technique is popular for growth of a variety of high-quality crystals for laser devices and precision instruments, as well as substrates. The essential features are a seed crystal, the top of which is molten and is fed with molten drops of source material, usually as a powder through a flame or plasma. Following this, the Czochralski method, developed in 1917 and later modified by several researchers, became the most popular technique to grow large-size single crystals which were impossible to obtain by any other techniques in such large quantity. This technique has several advantages over the other related melt-growth technique, viz. the Kyropoulos method, which involves a gradual reduction in the melt temperature. In the Czochralski technique the melt temperature is kept constant and the crystal is slowly pulled out of the melt as it grows. This provides a virtually constant growth rate for the crystal. Several versions of Czochralski crystal pullers are commercially available. A large variety of semiconductor crystals such as Si, Ge, and several IIIV compounds are being commercially produced using this technique [12-14]. Besides, several other crystals of oxides, spinel, garnets, niobates, tantalates, and rare-earth gallates have been obtained by this method.

There are several other popularly used melt growth techniques that are feasible for commercial production of various crystals. Amongst them, the BridgmanStockbarger, zone melting, and floating zone methods are the most popular. The Bridgman technique [15] is characterized by the relative translation of the crucible containing the melt to the axial temperature gradient in a vertical furnace. The Bridgman technique is most frequently applied for the growth of metals, semiconductors and alkaline earth halides [16-18]. The Stockbarger method [19] is a more sophisticated modification of the Bridgman method. There is a high-temperature zone, an adiabatic loss zone, and a low-temperature zone. The upper and lower temperature zones are generally independently controlled, and the loss zone is either unheated or poorly insulated.

2.4.2 Solution Growth

This is one of the oldest and most widely used crystal growth techniques compared with vapor-phase or melt growth. In this process, a saturated solution of the material in an appropriate solvent is used from which crystallization takes place as the solution becomes critically supersaturated. The supersaturation can be achieved either by lowering the temperature of the solution or by slow evaporation. The advantage of the method is that crystals can be prepared from a solution at temperatures well below its melting point, perhaps even at room temperature and therefore it turns out to be more applicable in many cases [20].

Solution growth is used not only for growth of technologically important crystals but also for a variety of crystalline products for daily life such as the

growth of foods, medicines, fertilizers, pesticides, dye stuffs, etc. Most crystallization processes of ionic salts are conducted in aqueous solutions or in some cases in solvents which are a mixture of miscible and organic solvents. Solution growth is used for substances that melt incongruently, decompose below the melting point, or have several high-temperature polymorphic modifications, and is also often efficient in the absence of such restrictions. The important advantage of solution growth is the control that it provides over the growth temperature, control of viscosity, simplicity of equipment, and the high degree of crystal perfection since the crystals grow at temperatures well below their melting point.

For successful growth of a crystal from solution, it is essential to understand certain basic properties (physicochemical features) of the solution. The behavior of water with temperature and pressure; the critical, subcritical, and supercritical conditions; its structure, the variation in pH; viscosity; density; conductivity; dielectric constant; and coefficient of expansion are critical for successful crystal growth. The change in ionic strength of the solution during crystal growth results in formation of defects, and variation in the crystal habit and even the phases, and therefore has to be maintained constant, often with the help of swamping-electrolyte solutions. Similarly, chelating agents are frequently used to sequester ions and form respective complexes,which are later thermodynamically broken to release their cations very slowly into the solution, which helps in controlling the growth rate and crystal habit. In the last decade crystal growth from solution under microgravity conditions has been studied extensively to grow a wide variety of crystals such as zeolites, compound semiconductors (InP, GaAs, GaP, AlP,

etc.), triglycine sulfate, etc.

We can divide solution growth into three types depending upon the temperature, the nature of the solvent, solute, and the pressure:

- low-temperature aqueous solution growth,
- superheated aqueous solution growth, and
- high-temperature solution growth.

2.4.2.1 Low-temperature aqueous solution growth

It is the most effective and easy way for growing crystals. A variety of crystals can be grown by this technique at room temperature. In this method, a saturated solution of the material is prepared in a suitable solvent and crystallization is initiated by making the solution supersaturated. The supersaturation can be achieved by changing the solution temperature (slow cooling of the solution) or by changing the composition of the solution (solvent evaporation) or by some chemical method.

The greatest advantages of crystal growth from low-temperature aqueous solutions are the proximity to ambient temperature, which helps to retain a high degree of control over the growth conditions, especially with reference to thermal shocks, and reduction of both equilibrium and nonequilibrium defects to a minimum (even close to zero). Large and perfect crystals of industrially important materials are grown by this method [21-25].

2.4.2.2 Superheated aqueous solution growth

This method is commonly known as the hydrothermal method and is highly suitable for crystal growth of compounds with very low solubility and phase

transitions. The term hydrothermal refers to any heterogenous (usually for bulk crystal growth) or homogeneous (for fine to nanocrystals) chemical reaction in the presence of aqueous solvents or mineralizers under high-pressure and high temperature conditions to dissolve and recrystallize (recover) materials that are relatively insoluble under ordinary conditions. A number of metals and metal oxides show an appreciable increase in solubility when the temperature and pressure are increased.

It can be treated as aqueous solution growth at elevated temperature and pressure. Growth is usually carried out in steel autoclaves with gold or silver linings. A charge of crystals is dissolved in the lower part of the autoclave. The hot saturated solution is directed towards the upper (colder) part, where it cool and become supersaturated hence the growth of crystal. The spent solution returns to the other part and this process continues until the whole charge is recrystallized. The solution simply acts as a transporting agent for the solid phase. This method is extensively used for the growth of large high quality synthetic quartz crystals [26].

2.4.2.3 High-temperature solution growth

This is popularly known as flux growth and gained its importance for growing single crystals of a wide range of materials, especially complex multicomponent systems. Flux growth is the term used to describe the growth of crystals from molten salt solvents at high temperatures. A high temperature solvent which reduces the melting temperature of the solvent is referred as flux [27]. This reduction in temperature is probably, the main advantage of flux growth. The materials to he crystallized are dissolved in a proper solvent

at a temperature slightly above the saturation temperature and then slowly cool the crucible so that growth occurs in a spontaneously formed nucleus. The growth of crystals by the slow cooling of the flux is also effective.

Flux growth is carried out at much lower temperatures than corresponding growth from melt. A distinct advantage of the method is that this is the only method for obtaining certain oxide solid solutions. However flux growth is very slow and requires precise temperature control. The purity of the crystals grown by this method is often marginal. Flux growth is an expensive technique.

2.4.3 Gel Growth

2.4.3.1 Introduction

Crystal growth in gels has recently gained the interest because of its suitability to grow crystals of biological macromolecules and in studies involving biomineralization. It is an alternative technique to solution growth with controlled diffusion and the growth process is free from convection. The gel method of crystal growth is probably the most simple and versatile technique, compared with other methods of crystal growth from solutions under ambient conditions [28]. In 1896, Liesegang first observed the periodic precipitation of slightly soluble salts in gelatin [29]. Later, this technique was used extensively to crystallize many organic, inorganic, and even biological macromolecules in various colloidal media. The gel method of crystallization is well described by Henisch [28, 30], Arora [31], and Patel and Venkateswara Rao [32] as well as by Lefaucheux and Robert [33].

2.4.3.2 Types of Gels

Gel growth is a particular case of solution growth where the solution is trapped in a polymeric structure. The gel is a loosely linked polymer of a two-component system formed by the establishment of a three-dimensional system of cross-linkages between molecules of one of the components. The system as a whole is permeated by the other component as a continuous phase, giving a semisolid, generally rich in liquid. Gels can be prepared by a variety of techniques and materials. The most commonly used ones for crystallization are gels of silica, agar, gelatin, clay (bentonite), and polyacrylamide.

Silica gel is prepared [28] by mixing aqueous solution of sodium metasilicate and mineral or organic acid. Gelation takes place in times ranging from a few seconds to a few months, depending on the pH, temperature, and concentration of the gel solution. To form agar gel [34], agar-agar powder is dissolved in water (12% by weight) and boiled. When this solution cools down, gelation takes place. Gelatin gel is prepared [35] by dissolving gelatin in water, stirring at a constant temperature of $50\,^{\circ}C$ for 1h and cooling to room temperature. A small quantity of formaldehyde is added to strengthen the gel. To prepare clay gel, powdered clay is slowly sifted on rapidly stirred water making a blend until about 9% clay has been added; the gel sets immediately. Polyacrylamide gel [36] is prepared by dissolving 3.99 wt % acrylamide and 0.02 wt % of a cross-linking agent in water. The solution is bubbled with nitrogen and degassed by lowering the pressure. This results in a rigid transparent gel. Crystallization has also been attempted using other gels such as pectin, polyethylene oxide (PEO), polyvinyl alcohol (PVA), and

tetramethoxysilane (TMOS) [28, 30-34].

2.4.3.3 Mechanism of Gelling

Gels can be formed by cooling of a sol, by chemical reaction or by addition of a precipitating agent or incompatible solvents. The time taken for the gelling process varies from minutes to days, depending on the nature of the reagents and its temperature, pH, and history. The mechanical properties of fully developed gels can vary, depending on the gel density. In the case of silica gels, when sodium metasilicate (Na_2SiO_3) is dissolved in water, monosilicic acid and sodium hydroxide are produced initially as per the following reaction

$$Na_2SiO_3 + 3H_2O \rightarrow H_4SiO_4 + 2NaOH$$

Later on, monosilicic acid polymerizes with the liberation of water. The process of polymerization continues, until a three-dimensional network of Si-O links is established as shown in figure 2.2. The hydrogen ion concentration (pH) plays a vital role in the gelling process. During polymerization, it is known that two types of ions, viz. $H_3SiO_4^-$ and $H_2SiO_4^{2-}$, are produced, whose relative amounts depend on the pH. The formation of the more reactive $H_2SiO_4^{2-}$ is favored at high pH values. However, higher charge implies a

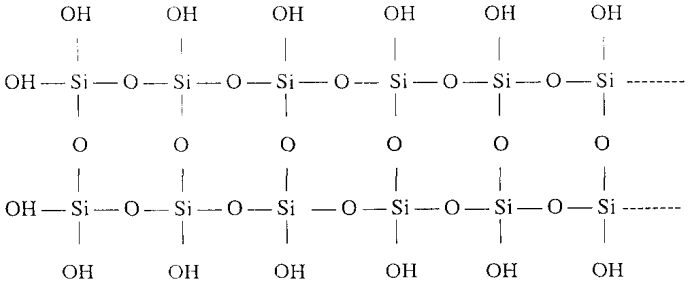

Figure 2.2: Network of Si-O links in silica gel.

greater degree of mutual repulsion. $H_3SiO_4^-$ is favored at low pH values and is responsible for the sharp increase in viscosity. Very high or very low pH values inhibit gelation. Gelling mechanism regarding agar and TMOS gels are reviewed by Lefaucheux and Robert [33].

2.4.3.4 Experimental Methods

Crystal growth methods in gels fall into the following classes [32]:

- Chemical reaction
- Complex dilution
- Reduction of solubility
- Chemical reduction, and
- Electrochemical techniques

Chemical Reaction

This method is suitable for crystals which are mostly insoluble or sparingly soluble in water and which decompose before melting. Here, two soluble reactants are allowed to react inside the gel medium by incorporation of one of the reactants (I) in the gel, whereas the other reactant (II), which is used as the supernatant, diffuses into the gel medium (Fig. 2.3).

The reaction, can be represented as shown below, inside the gel leads to the formation of an insoluble or sparingly soluble crystalline product.

$$AX + BY \rightarrow AY + BX$$

The basic requirements of this method are:

(a) The gel must remain stable in the presence of reacting solutions

(b) It must not react either with the solutions or with the product.

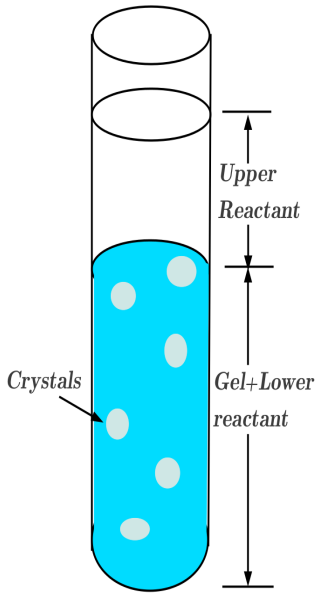

Figure 2.3: Schematic representation of single gel diffusion process.

U-tubes are used, where the two reactants are allowed to react by diffusion into an inactive gel. This technique can also be adopted to crystallize compounds which have poor aqueous and organic solubility (uric acid and cystine) using the displacement reaction method [37-38].

Complex Dilution

In this method, the material to be crystallized is first complexed in some reagents which enhance its solubility. It is then allowed to diffuse into a gel which is free from active reagents. As the complex solution diffuses through the gel it gets diluted. This results in a high supersaturation of the material

to be crystallized and hence nucleation and subsequent crystallization occurs. Crystals of mercuric sulfide, cuprous, and silver halides and selenium have been grown using this method [32].

Solubility Reduction

This method is generally used for crystallization of highly water-soluble substances. The substance to be grown is dissolved in water and incorporated in the gel before gelation. After the gel has been set, a solution that reduces the solubility of the substance (solute) is added as a supernatant solution to induce crystallization. Compounds which have low aqueous solubility can also be crystallized using this technique. Steroids which have low aqueous solubility have been crystallized using this technique by reducing the water content in the gel by incorporating an organic solvent [39]. During this process of crystallization, crystals can be observed in the supernatant solution above the gel due to the reverse diffusion of the precipitating solvent [40-41].

Chemical Reduction

This method is particularly suitable for growing metallic crystals (Cu, Au, and Ni). The metallic salt is incorporated with the gel and an aqueous solution of a reducing agent is slowly allowed to diffuse through the gel, where chemical reduction takes place to form metallic crystals[32].

Electrochemical/Electrolysis

Gels can be used to crystallize metals by electrolysis. George and Vaidyan [42] reported growth of single crystals and dendrites of silver. Recently, Muzikar et al. [43] reported crystallization of microcrystals of gold. Here, a small current was passed between two gold electrodes through a silica gel doped with $HAuCl_4$. Single crystals of gold of sizes ranging from hundreds of

nanometer to hundreds of micrometer were grown by this technique. Muzikar et al. [44] have also crystallized platinum particles and a platinum complex by an identical procedure.

Crystal Growth in the Presence of a Magnetic Field

The effect of a magnetic field (up to 3 T) on the crystallization of calcium tartrate [45] and strontium tartrate [46] has been reported. The magnetic field has the effect of reducing the number of crystals formed but helps in the growth of a few, larger crystals. Crystallization of cholesterol in gels in a magnetic field was studied by Sundaram et al. [47-48]; it was found that the presence of the magnetic field reduced the nucleation time and number of crystals but that there was an increase in the size of the crystals grown.

2.4.3.5 Nucleation Control in gels

During crystallization in gels, the growing crystals compete with one another for the solute atoms, leading to a reduction in crystal size and perfection. Hence, nucleation has to be suppressed until only a few crystals are formed. The commonly used methods to minimise the spurious nucleation in gels are

- Optimisation of gel density
- Ageing of the gel
- Neutral gel technique
- Concentration of the nutrients
- Stabilising the thermal condition
- Use of additives

- Field utillsation

The use of a particular combination of reactants, to grow the required crystals, has been found to reduce the nucleation density [49]. Acid-set gels, choosing a particular acid (based on experiments with various acids), is known to yield larger crystals [49]. It has been reported that changing the gel structure by varying one or more of the parameters, viz. pH and density, and by gel aging, can decrease the number of nucleation centers [28, 3-7]. The use of an intermediate neutral gel is also found to slow down the reaction and thereby reduce the number of nucleated crystals [50]. In another method, the concentration of the diffusing reactant is initially kept below the level at which nucleation is known to occur and then increased gradually in a series of small steps. Crystals grown by this method are more perfect and larger than those grown otherwise.

2.4.3.6 Pattern Formation in Gel Systems

Pattern formation is widespread in nature and can be found in structures ranging from agate rocks and gold veins to the growth of bacterial rings in agar and gallstones [51-53]. A specific example discussed below is the Liesegang ring structure, discovered in 1896 [29]. When coprecipitated ions interdiffuse in a gelatinous medium, the sparingly soluble salt may precipitate discontinuously in a spectacular pattern of parallel bands. The pleasing appearance of Liesegang bands, as well as their spatiotemporal distribution, has elicited a steady proliferation of publications on the subject [30, 54-56]. It is quite easy to produce the patterns in the laboratory. Liesegang rings can be produced in gels by diffusing one of the reactants into an inert gel

medium containing another reactant. The simplest and usual way to perform a Liesegang ring experiment is to fill a tube with an inert semisolid medium which contains one of the reactants (B), called the inner electrolyte. The other reactant (A), referred to as the outer electrolyte, is poured over the gel column as the supernatant solution. Usually the concentration level of the outer electrolyte is maintained high to minimize the possible loss of ions due to evaporation and other such transport mechanisms during the experimental processes. It involves the formation of concentric laminated rings or bands clearly separated in the direction perpendicular to the motion of the front [54].

The structures, which are often rings in circular geometries and bands in linear geometries, are formed by the nonuniform spatial distribution of crystals in a precipitation reaction in a gel [55-56]. Recently, George and Varghese reported the formation of triplet Liesegang ring patterns [57]. Terada et al. [58] described the formation of sheets and helices of strontium carbonate in silica gel. Helical rings of calcium phosphates (Fig. 2.4) were formed in silica gels by the diffusion of calcium ions into a phosphate-containing gel [59].

Though in vivo occurrence is rare, chemical concentration, geometry of the reactant containers or vessels, temperature, pH, and the presence of impurities are the main factors that influence the formation of Liesegang rings [60]. The role of the gel during the formation of Liesegang rings is essentially passive, i.e., to prevent convection of solutions and sedimentation of the precipitate. The dynamics of the banding are very complex, involving the coupling of diffusion and precipitation processes in a nonequilibrium regime.

Theoretical models explaining Liesegang patterns fall into two broad cate-

Figure 2.4: Disc and helical Liesegang rings of calcium phosphate in silica gel.

gories. The first one, called the prenucleation model, is based on the classical feedback cycle of supersaturation, precipitation, and depletion as originally proposed by Ostwald [61]. In the second theory, the so-called postnucleation or competitive particle growth model, it is assumed that competition between growing particles can, by itself, produce periodic precipitation structures, even in the absence of strong external gradients. It is worth mentioning that all the theories share the assumption that the precipitate appears as the system passes through some nucleation or coagulation thresholds. However, the theories differ in their pre- or postnucleation assumptions. The main unresolved problem in all these theories is the understanding of the mechanism behind the transformation of the diffusive reagents A and B into an immobile coagulant. George and Varghese proposed a new model [57, 62-65] based on the prime assumption that the boundary that separates the outer ions and the inner electrolyte virtually migrates in the positive direction of the advancement of the type A ions. Izsk and Lagzi [66] proposed a univer-

sal law, which is also valid in the case of various transport dynamics (purely diffusive, purely advective, and diffusion advection cases). The mechanism responsible for these structures is not yet fully understood. The interest in precipitate patterning phenomena is growing because of the suitability of their underlying dynamics for modeling manyself-organization processes [67-68].

Bibliography

[1] BucWey, H. E., **Crystal Growth**, John Wiley and Sons, Inc. NY, 1951.

[2] Laudire, R. A., **The Growth of Single Crystals**, kentice Hall, Inc., NJ, 1970.

[3] Pamplin, B. R. (Ed.), **Crystal Growth**, Pergamen Press, Oxford, 1975.

[4] Brice, J. C., **Crystal Growth Process**, John Wiley and Sons, New York, 1986.

[5] K. Byrappa, H. Klapper, T. Ohachi, and R. Fornari Eds., **Crystal Growth of Technologically Important Electronic Materials**, Allied Publishers PVT. Limited, New Delhi, 2003.

[6] Aggarwal, M.D.; Gebre, T.; Batra, A.K.; et al., Crystal Materials for Nonlinear Optical Devices and Microgravity Science, **4813** pp. 52-65, 2002.

[7] Aggarwal, M.D.; Wang, W.S.; Bhat, K.; Penn, P.G.; and Frazier, D.O., **Handbook of Advanced Electronic and Photonic Materials and Devices**, H. S. Nalwa. Ed., Academic Press, New York, NY, Vol. 9, pp. 193-228, 2001.

[8] Barrat, C. S. and Massalski, T. B., **Structure of Metals**, McGraw-Hills, New York, 3rd edn., 1966.

[9] D.T.J. Hurle (Ed.): **Handbook of Crystal Growth**, North Holland, Amsterdam 1994.

[10] G. Stringfellow: **Organometallic Vapor-Phase Epitaxy: Theory and Practice**, 2nd edn. Academic, New York 1998.

[11] A. Verneuil, C. R. Paris, **135**, 791-794(1902).

[12] Dash, W. C., J. Appl. Phys., **30**(1959), 459.

[13] Howe, S. and Elbaum, C., Phil. Mag., **6**(1961), 1227.

[14] Furukawa, Y., Sato, M., Nitanda, F. and Ito, K., J. Cryst. Growth, **99**(1990), 832.

[15] Bridgman, P. W., Proc. Am. Acad. Arts. Sci.. **60**(1925), 305.

[16] Shah, P. C., Ind. J. Phys., **67A**(1993), 467.

[17] Bhatt, V. P., Gireesan, K. and Pandya, G. R., J . Cryst. Growth, **96**(1989), 649.

[18] Berry, C., West, W. and Moser, F., **The Art and Science of Growing Crystals**, Gilman, J. J., Ed., Wiley, New York, 1963.

[19] Stockbarger, C., Rev. Sci. Instr., **7**(1938), 133.

[20] Czochralski, J., Z. Phys. Chem., **92**(1971), 219.

[21] Sasaki, T., J. Cryst. Growth, **99**(1990), 820.

[22] Skrtic, D., Vincekovic, N. F., MilhofeM, J. Cryst. Growth, **114**(1991), 118.

[23] Bahadur, S. A., Ramakrishnan, V. and Rajaram, R. K., Bull. Mater. Sci., **13**(1990), 161.

[24] Chaoyang, T. U., Zundu, L., Chen, G. and Wang, G., Cryst. Res. Tech., **29**(1994), K47.

[25] Yokotani, A. Sasaki, T., Fujioka, K., Nakai, S. and Chiyoe, Y., J. Cryst. Growth, **99**(1990), 815.

[26] R. A. Laudise, J. Am. Chem. Soc. **81**, 562(1959).

[27] Ellwell, D. and Scheel, H. J., **Crystal Growth from High Temperature Solutions**, Academic Press, London, 1975.

[28] H. K. Henisch, **Crystal Growth in Gels**, The Pennsylvania State Univ. Press, University Park 1973.

[29] R. E. Liesegang, Uber einige Eigenschaften von Gallerten, Naturwiss. Wochenschr. **11**, 353-1896, in German 362.

[30] H. K. Henisch, **Crystals in Gels and Liesegang Rings**, Cambridge Univ. Press, Cambridge 1988.

[31] S. K. Arora, A review, Prog. Cryst. Growth Charact. **4**, 345-378 (1981).

[32] A. R. Patel, A. Venkateswara Rao, Bull. Mater. Sci. **4**, 527-548 (1982).

[33] F. Lefaucheux, M.C. Robert, **Handbook of Crystal Growth**, ed. by D. T. J. Hurle, Elsevier Science, Amsterdam, 1994.

[34] B. Brezina, M. Havrankova, Mater. Res. Bull. **6**, 537-543(1971).

[35] E. Banks, R. Chinanelli, F. Pintchovsky, J. Cryst. Growth, **18**, 185-190 (1973).

[36] B. Brezina, M. Havrankova, K. Dusek, J. Cryst. Growth, **34**, 248-252 (1976).

[37] S. Narayana Kalkura, V. K. Vaidyan, M. Kanakavel, P. Ramasamy, J. Cryst. Growth, **132**, 617-620 (1993).

[38] E. K. Girija, S. Narayana Kalkura, P. Ramasamy, J. Mater. Sci. Mater. Med. **6**, 617-619 (1995).

[39] S. Narayana Kalkura, S. Devanarayanan, J. Cryst. Growth, **110**, 265-269 (1991).

[40] S. Narayana Kalkura, S. Devanarayanan, J. Cryst. Growth, **94**, 810-813 (1989).

[41] S. Narayana Kalkura, S. Devanarayanan, J. Mater. Sci. Lett. **7**, 827-829 (1988).

[42] M. T. George, V. K. Vaidyan, J. Cryst. Growth, **53**, 300-304 (1981).

[43] M. Muzikar, V. Komanicky, W.R. Fawcett, J. Cryst. Growth, **290**, 615-620 (2006).

[44] M. Muzikar, P. Polkov, J. C. Fettinger, W.R. Fawcett, Cryst. Growth Des. **6**, 1956-1960 (2006).

[45] K. V. Saban, T. Jini, G. Varghese, J. Magn. Magn. Mater. **265**, 296-304 (2003).

[46] M. H. Rahimkutty, K. R. Babu, K. S. Pillai, M. R. S. Kumar, C. M. K. Nai, Bull. Mater. Sci. **24**, 249-252 (2001).

[47] N. M. Sundaram, M. Ashok, S. Narayana Kalkura, Acta Cryst. D **58**, 1711-1714 (2002).

[48] N. M. Sundaram, Investigations on the cholesterol, cholesteryl acetate, hydroxyaptite and lysozyme crystallization and the influence of magnetic field on the nucleation process. **Ph.D. Thesis**, Anna University, Chennai (2004).

[49] A. R. Patel, A. V. Rao, J. Cryst. Growth **47**, 213-218 (1979).

[50] A. R. Patel, A. V. Rao, Indian J. Pure Appl. Phys. **16**, 544-545 (1978).

[51] B. Sis, T. Canda, O. Harmancioglu, Turk. J. Med. Sci. **34**, 191-193(2004).

[52] T. Antal, M. Droz, J. Magnin, Z. Racz, M. Zrinyl, J. Chem. Phys. **21**, 9479-9486 (1998).

[53] Z. Racz, Physica A **274**, 50-59 (1999).

[54] D. S. Chernavskii, A. A. Polezhaev, S. C. Muller, Physica D **54**, 160-170 (1991).

[55] J. H. E. Cartwright, J. M. Garcia-Ruiz, A. I. Villacampa, Comput. Phys. Commun. **21**, 411-413 (1999).

[56] G. Venzl, J. Ross, J. Chem. Phys. **77**, 1308-1313 (1982).

[57] J. George, G. Varghese, J. Mater. Sci. **40**, 5557-5559 (2005).

[58] T. Terada, S. Yamabi, H. Imai, J. Cryst. Growth **253**, 435-444 (2003).

[59] R. V. Suganthi, E. K. Girija, S. Narayana Kalkura, H. K. Varma, A. Rajaram, J. Mater. Sci. Mater. Med. (2008) DOI 10.1007/s10856-008- 3495-1.

[60] J. M. Garcia-Ruiz, D. Rondon, A. Garcia-Romero, F. Otalora, J. Phys. Chem. **100**, 8854-8860 (1996).

[61] W. Ostwald, Z. J. Phys. Chem. **23**,365 (1897).

[62] J. George, G. Varghese, Chem. Phys. Lett. **362**, 8-12 (2002).

[63] J. George, G. Varghese, Colloid Polym. Sci. **280**, 1131-1136 (2002).

[64] J. George, S. Nair, G. Varghese, J. Mater. Sci. Lett. **39**, 311-331 (2004).

[65] J. George, I. Paul, P.A. Varughese, G. Varghese, Pramana J. Phys. **60**, 1259-1271 (2003).

[66] F. Izsak, I. Lagzi, J. Chem. Phys. **122**, 184707-1-184707-6 (2005).

[67] B.A. Grzybowski, K.J.M. Bishop, C.J. Campbell, M. Fiallkowski, S.K. Smoukov, Soft Matter **1**, 114-128 (2005).

[68] A. Volford, F. Izsk, M. Ripszm, I. Lagzi, J. Phys. Chem. B **110**, 4535-4537 (2006).

Chapter 3

Experimental Techniques in Characterization of Materials

3.1 Introduction

The solids are characterized by nearly perfect periodicity of atomic structure. The geometric regularity of atomic structure provides a simple picture of a crystal and helps a lot in gaining the knowledge of the physical properties of the solid [1, 2]. In a crystalline solid, the atoms are arranged in a regular manner, i.e. the atomic array is periodic. Each atom is at regular intervals along arrays in all directions of the crystal. The crystalline solid has directional properties, which are also called isotropic or anisotropic substances accordingly [3-5].

The characterisation and the studies of the properties of crystals of materials are very important, in the context of technological applications. It is almost impossible to understand the properties of a material and, consequently, its proper application, if we do not understand its composition, structure, and

morphology. Characterization of crystals has become an integral part of crystal growth and process development. These studies reveal the perfection of the crystals, influence of the methods on the growth of materials and identity of the grown material. Study of the crystal habit forms an important part as it influences the physical properties.

The golden rule of material characterization is to apply numerous methods, since only one methodology normally does not bring about a complete understanding of the material. In order to properly characterize a material, various procedures are applied [6-7]. Among them include x-ray diffraction (XRD) [8-10], Mossbauer spectrometry [11], transmission electron microscopy (TEM) [12], scanning electron microscopy (SEM) [13], impedance spectroscopy [14], infrared (IR) and Raman spectroscopy [15-16], nuclear magnetic resonance (NMR), [17-18], x-ray fluorescence (XRF) [19], and energy-dispersive x-ray analysis (EDAX) [13]. To supplement these characterization methodologies, thermal methods are also usually applied [20-23], for example, differential thermal analysis (DTA) [21], thermal gravimetric analysis (TGA) [21], differential scanning calorimetry (DSC) [22], temperature-programmed reduction (TPR) [23], temperature-programmed desorption (TPD) [24], dielectric analysis methods, such as thermodielectric analysis (TDA) and dielectric spectrometry (DS). DS is an alternative impedance spectroscopy used in the study of solid electrolytes like anionic and cationic conductors) [20], and adsorption methods [25-26].

All these methods provide almost direct observation of properties of the crystals. Their merit is limited by the resolution achievable and their versatility. Choice of a suitable technique will depend on several factors, such

as:

- The shape and size of the crystal under investigation.
- Cleaving, cutting, and polishing possibilities.
- Ability to use destructive techniques, and above all.
- The extent of the details required.

In this chapter only some of the main characterization techniques have been described. These include Microscopy Techniques, X-rays Diffraction, Energy Dispersive Analysis of X-rays and Thermal Methods of Analysis.

3.2 Microscopy Techniques

3.2.1 Light Microscope

The simplest microscope is the light microscope; it consists of an objective lens and an eyepiece. Microscope objectives and eyepieces usually consist of complex lens systems of two or more lenses to correct for lens aberrations (Figure 3.1). The objective lens forms a real intermediate image, which is then magnified by the eyepiece. The objective lens and eyepiece are maintained at a fixed distance and focusing is achieved by moving the whole assembly, up and down, in relation to the sample (see Figure 3.1). High magnification requires very bright illumination of the sample, and a condenser lens is usually placed between the light source and the sample stage to focus light onto the sample.

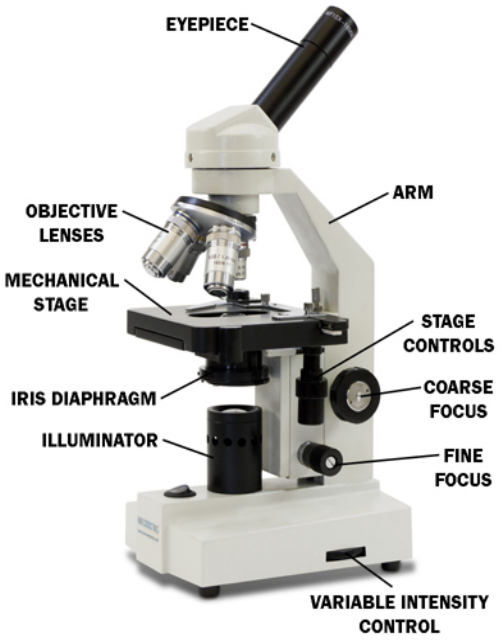

Figure 3.1: Diagram of the main parts of a light microscope.

Resolution is the smallest separation of two points that are visible as distinct entities. The resolving limit of the human eye is $0.1mm$; on the other hand, the resolving limit of the light microscope is $0.2\mu m$.

We used a polarising light microscope to do the optical studies of the grown sample. The apparatus is available at the Department of Physics, University of Kashmir, Srinagar.

3.2.2 Transmission Electron Microscope

Transmission electron microscopy (TEM) is a microscopy technique whereby a beam of electrons is transmitted through an ultra thin specimen, interacting with the specimen as it passes through. An image is formed from the interaction of the electrons transmitted through the specimen; the image is

magnified and focused onto an imaging device, such as a fluorescent screen, on a layer of photographic film, or to be detected by a sensor such as a CCD camera.

TEMs are capable of imaging at a significantly higher resolution than light microscopes, owing to the small de Broglie wavelength of electrons. This enables the instrument's user to examine fine detaileven as small as a single column of atoms, which is tens of thousands times smaller than the smallest resolvable object in a light microscope. TEM forms a major analysis method in a range of scientific fields, in both physical and biological sciences. TEMs find application in cancer research, virology, materials science as well as pollution, nanotechnology, and semiconductor research. At smaller magnifications TEM image contrast is due to absorption of electrons in the material, due to the thickness and composition of the material. At higher magnifications complex wave interactions modulate the intensity of the image, requiring expert analysis of observed images. Alternate modes of use allow for the TEM to observe modulations in chemical identity, crystal orientation, electronic structure and sample induced electron phase shift as well as the regular absorption based imaging.

After the discovery of the wave nature of the electron by de Broglie allowed Ernst Ruska and Max Knoll invented, in 1931, the first transmission electron microscope (TEM) whose maximum resolving power is $0.2nm$. A TEM is analogous in design to a light microscope with one crucial dissimilarity; that is, as a substitute of light, the TEM uses electrons [12, 27]. The light source is replaced by a cathode filament that acts as a source of electrons. The electron source must be placed in a vacuum and its position is

reversed with respect to the position of the light source, that is, the electron source is on the upper side of the TEM. Electrons are accelerated toward a given sample by a potential difference of several thousand volts, normally 100,000 V and in some cases 1,000,000 V. A series of cylindrical magnets and metal apertures are used to focus the electron beam into a monochromatic beam (see Figure 3.2). This beam collimated by one or two condenser lenses

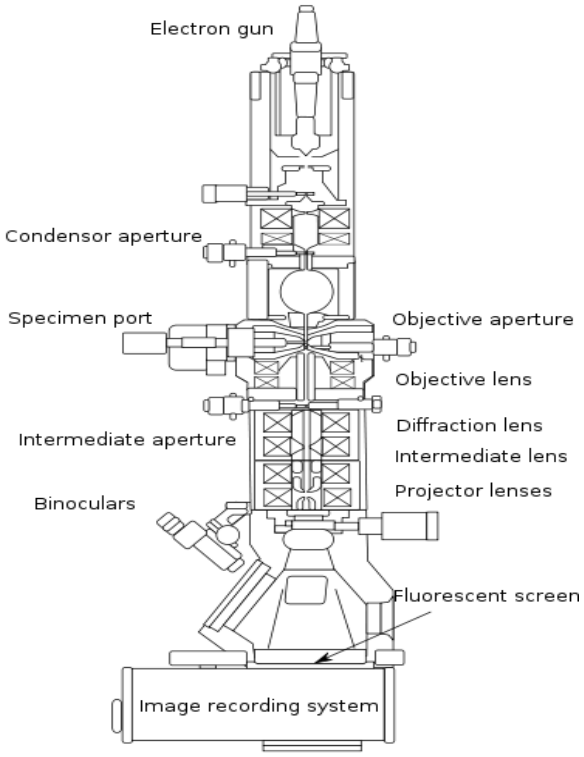

Figure 3.2: Schematic representation of a TEM.

collides with the sample and interacts with it depending on the density of the material. These interactions are greatly affected by how the specimen is prepared. Thereafter, the electron beam is focused with an objective lens, and is magnified by one intermediate magnetic lens and a projector magnetic lens. Besides, in the equipment, different apertures to help in the alignment

of the electron beam are located.

In a TEM image, the detail in the image is formed by the diffraction of electrons from the crystallographic planes of the object being tested. When a beam of electrons is passed through a sample, it is diffracted by the crystalline planes. Some electrons are diffracted and the others pass through the sample without being diffracted. Thereafter, both electron types form an image of the sample.

Electron microscopes are constructed in such a way that it is possible to project either the image of the specimen or the diffraction pattern on to a fluorescent observation screen, and then photograph it on a plate or a film.

3.2.3 Scanning Electron Microscope

A scanning electron microscope (SEM) is a type of electron microscope that images a sample by scanning it with a beam of electrons in a raster scan pattern. The electrons interact with the atoms that make up the sample producing signals that contain information about the sample's surface topography, composition, and other properties such as electrical conductivity.

The first scanning electron microscope (SEM) was constructed in 1938 by Manfred von Ardenne, by rastering the electron beam of a TEM over the surface of a sample [13, 28]. Since the original von Ardenne equipment, several design advances have been made, resulting in an improvement of the resolution from $50nm$, in 1942, to $\sim 0.7nm$, today.

In a SEM equipment, the electrons which result from the emission from a filament located in the electron gun are accelerated, with the help of a voltage ranging from 1 to 30keV (see Figure 3.3) [13, 28]. The electron

emission event takes place in a vacuum milieu ranging from 10^{-4} to 10^{-10} Torr. Then, the accelerated electrons are directed to the specimen by a series of electromagnetic lenses in the electron column [13, 28].

The resolution and depth of field of the image are established by the electron beam intensity, energy, interaction volume, and the final spot size, which are attuned with one or more condenser lenses and the objective lens [27]. The lenses are, as well, utilized to shape the electron beam in order to reduce the consequences of spherical aberration, chromatic aberration, diffraction, and astigmatism [13].

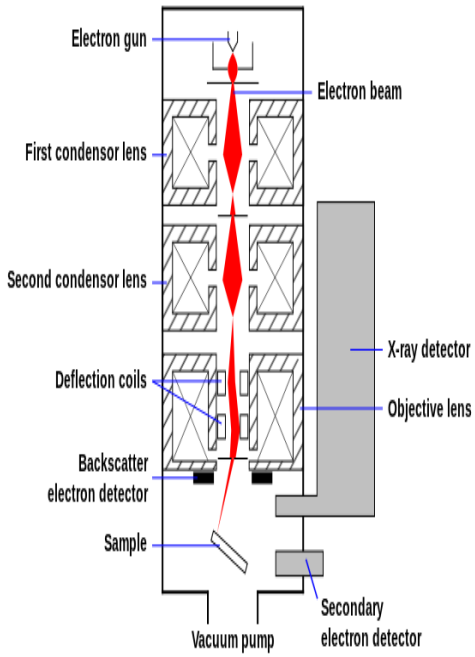

Figure 3.3: Schematic representation of the principal components of a SEM.

There are only two possible interactions between high velocity electrons and materials: the electrons can be elastically scattered, that is, energy and linear momentum are conserved, in which case, if the direction change is

more than 90^0, these electrons are elastically backscattered, or the electron could suffer an inelastic scattering process, in which case, there is a loss of energy during the process and the electron not only changes direction but also changes its energy [13, 27-28].

The mechanisms of loss of energy during an inelastic scattering process are diverse: (1) several electrons lose energy creating phonons, which heat the specimen; (2) other electrons are roduced, which create oscillations in the metals electron gas; (3) another possibility is by breaking the radiation process where the electron emits continuous x-ray radiation spectrum. Other interactions provoke the emission of secondary electrons (SEs). Finally, other electrons can trigger the emission of inner electrons of the atoms composing the test sample, and then producing the emission of a characteristic x-ray photon or an Auger electron [13, 27-28].

In Figure 3.4, the interaction of a high-energy electron beam with mate-

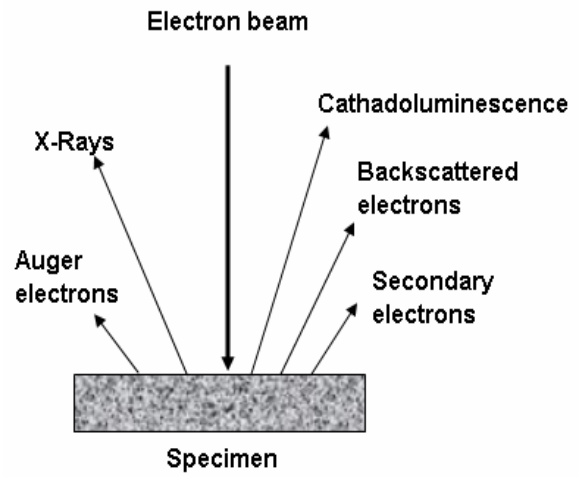

Figure 3.4: Graphic description of the principal interactions between the electron beam and the sample.

rials is represented. The electrons hitting the material surface provoke the emission of electrons from the specimen mainly as backscattered electrons (BSEs) and SEs. SEs are ordinary signals used for the study of the surface morphology of materials. SEs have low kinetic energy, that is, lower than 50eV. Therefore, those arising from the first few nanometers of the materials surface have sufficient energy to escape from the materials surface and can thus be detected.

In addition, the portion of the SEs that do not escape from the materials surface, run to ground, and can be detected with an ammeter connected between the specimen and ground [27]. This signal is usually named the specimen current. In addition, the test sample is grounded to avoid the accumulation of spatial charge, which spoils the SEM image.

SEs and BSEs are typically detected by an EverhartThornley (ET) scintillatorphotomultiplier secondary electron detector. The SEM image is shaped on a cathode ray tube screen, whose electron beam is scanned synchronously with the high-energy electron beam, so that an image of the surface of the specimen is formed [28]. The quality of this SEM image is directly related to the intensity of the secondary and/or BSE emission detected at each x- and y-point throughout the scanning of the electron beam across the surface of the material [13].

SEM is used to study material morphology by bombarding the specimen with a scanning beam of electrons, and then collecting the slow moving SEs that the specimen generates. These electrons are collected, amplified, and displayed on the picture tube of a television screen. The electron beam and the cathode ray tube scan synchronously so that an image of the surface

of the specimen is formed. The specimen preparation includes drying the sample and making it conductive to electricity, if not already. Photographs are taken at a very slow rate of scan in order to capture greater resolution. SEM is typically used to examine the external structure of objects that are as varied as biological specimens, rocks, metals, ceramics, and almost anything that can be observed under a light microscope.

Magnification

Magnification in a SEM can be controlled over a range of up to 6 orders of magnitude from about 10 to 500,000 times. Unlike optical and transmission electron microscopes, image magnification in the SEM is not a function of the power of the objective lens. SEMs may have condenser and objective lenses, but their function is to focus the beam to a spot, and not to image the specimen. Provided the electron gun can generate a beam with sufficiently small diameter, a SEM could in principle work entirely without condenser or objective lenses, although it might not be very versatile or achieve very high resolution. In a SEM, as in scanning probe microscopy, magnification results from the ratio of the dimensions of the raster on the specimen and the raster on the display device. Assuming that the display screen has a fixed size, higher magnification results from reducing the size of the raster on the specimen, and vice versa. Magnification is therefore controlled by the current supplied to the x, y scanning coils, or the voltage supplied to the x, y deflector plates, and not by objective lens power.

We used a Hitachi S-3000H electron microscope to do the SEM studies. The crystalline samples were coated with gold using a Bal-Tec SCD004 sput-

ter coating. Both apparatus are available at the University Instrumentation Centre (USIC), University of Kashmir, Srinagar.

3.3 X-ray Differaction Methods

3.3.1 General Introduction

X-ray diffraction [29-35] is the most powerful method for the study of crystalline materials. In 1912, at the University of Munich, Max von Laue and collaborators carried out one of the most important experiments of modern physics, the Laue-Knipping-Friedrich experiment, which established that x-radiation consisted of electromagnetic waves. Additionally, the experiment clearly showed that the crystals were composed of atoms arranged on a space lattice, since the electromagnetic x-ray radiation was interfering during its scattering by the crystal atoms.

An x-ray beam is generated in a vacuum tube where an electron beam, produced by a heated filament, is collimated and accelerated by an electric potential of several kilovolts, that is, from 20 to 45 kV and is then directed to a metallic anode (Figure 3.5). The electrons hitting the anode will convey a fraction of their energy to the electrons of the target material, a process resulting in the electronic excitation of the atoms composing the metallic anode. The x-ray tube has to be evacuated to allow electron movement. Finally, in order to dissipate the heat produced by this process in the metallic anode, it is normally water cooled.

The x-ray tube produces two kinds of radiations: the continuous spectrum and the characteristic spectrum (Figure 3.6). The continuous spectrum

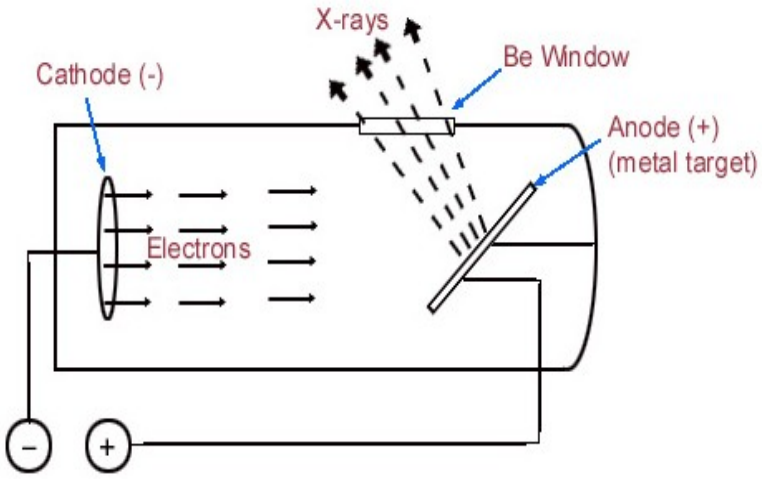

Figure 3.5: Schematic representation of an x-ray tube.

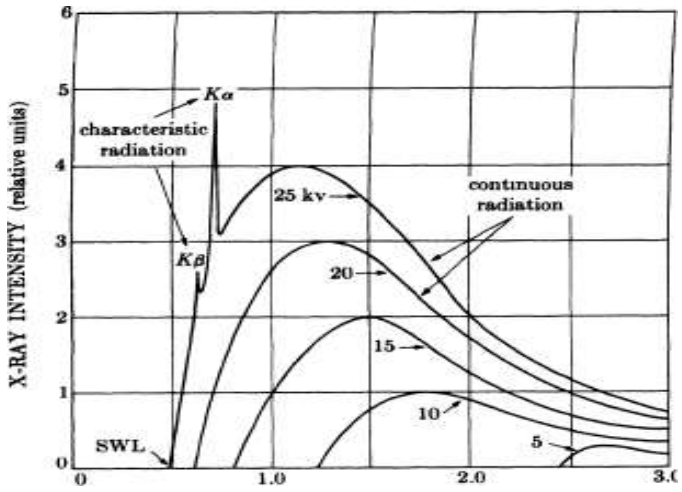

Figure 3.6: Schematic representation of a continuous and characteristic spectra.

is a plot of the intensity of the x-ray emission of the tube, which is measured in counts per second, and which is contingent on the anode material and on the high voltage imposed versus the wavelengths of the emitted x-rays. The mechanism of production of this radiation is by the deceleration of the electrons in the beam by the atoms that compose the metallic anode. Explicitly,

this is a braking radiation, in German, Bremsstrahlung, which is the name normally given to this radiation. The Bremsstrahlung is then generated when photons are emitted, when the electrons in the beam lose kinetic energy.

The second type of spectrum, called the characteristic spectrum, is produced as a result of specific electronic transitions that take place within individual atoms of the anode material. Each crystalline solid has unique atomic architecture and consequently has a unique characteristic X-ray powder pattern.These patterns can be used as fingerprints for identification of solid phases. Once the material has been identified, X-ray crystallography may be used to determine its structure, i.e. how the atoms pack together in the crystalline state and the size and the shape of the unit cell, etc.

3.3.2 Diffraction of X-rays

Crystals are regular arrays of atoms, and X-rays can be considered waves of electromagnetic radiation. Atoms scatter X-ray waves, primarily through the atoms' electrons. Just as an ocean wave striking a lighthouse produces secondary circular waves emanating from the lighthouse, so an X-ray striking an electron produces secondary spherical waves emanating from the electron. This phenomenon is known as elastic scattering, and the electron is known as the scatterer. A regular array of scatterers produces a regular array of spherical waves. Although these waves cancel one another out in most directions through destructive interference, they add constructively in a few specific directions, determined by Bragg's law:

$$2d \sin\theta = n\lambda \tag{3.1}$$

Here d is the spacing between diffracting planes, θ is the incident angle, n is any integer, and λ is the wavelength of the beam. These specific directions appear as spots on the diffraction pattern called reflections. Thus, X-ray diffraction results from an electromagnetic wave (the X-ray) impinging on a regular array of scatterers (the repeating arrangement of atoms within the crystal).

X-rays are used to produce the diffraction pattern because their wavelength λ is typically the same order of magnitude (1-100 angstroms) as the spacing d between planes in the crystal. In principle, any wave impinging on a regular array of scatterers produces diffraction. To produce significant diffraction, the spacing between the scatterers and the wavelength of the impinging wave should be similar in size. Prior to the first X-ray diffraction experiments, the spacings between lattice planes in a crystal were not known with certainty.

The basic properties of a wave significant in diffraction are wavelength, λ, that is, the distance between two adjacent peaks of the wave; wave amplitude, $|A|$, specifically, half the difference between peak and depression; intensity, $I \propto |A|^2$, and phase, ϕ, which is the location of a peak relative to other waves, measured as a fraction of the wavelength or as an angle in the range 0° to 360°.

3.3.3 Powder Differaction Method

The great majority of the applications of the x-ray diffraction methodology in material characterizations are carried out with the help of diffractometers, which use the BraggBrentano geometry. The principal characteristics of the

Bragg-Brentano geometry are shown in Figure 3.7. A specimen, located at

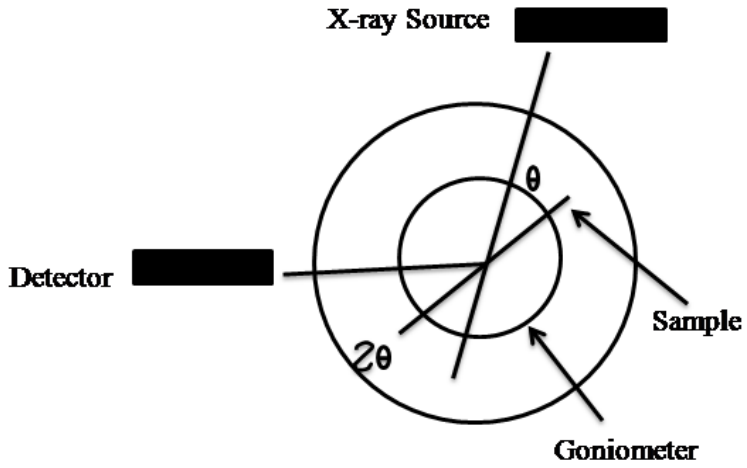

Figure 3.7: Schematic representation of Bragg-Brentano geometry.

the sample plane, is supported on a flat support bench that is free to rotate about its perpendicular axis, which is located at the origin (see Figures 3.7 and 3.8). The rotation is such that the angle of the incident x-ray beam with respect to the sample plane is θ, and the angle between the diffracted beam and the incident beam is 2θ.

The Bragg-Brentano type of diffractometer is composed of an x-ray tube with a metallic anode that supplies x-rays that are scattered from the sample and focused at the slit before hitting the detector. In some cases, a monochromator capable of yielding a monochromatic x-ray beam is added. The sample is rotated, relative to the x-ray at angles from 0° to 90° with the help of a goniometer, where the powdered sample is placed on the sample holder. Electronic equipment is used to amplify and filter signal pulses from the detector.

The powdered material sample to be tested is generally further ground in

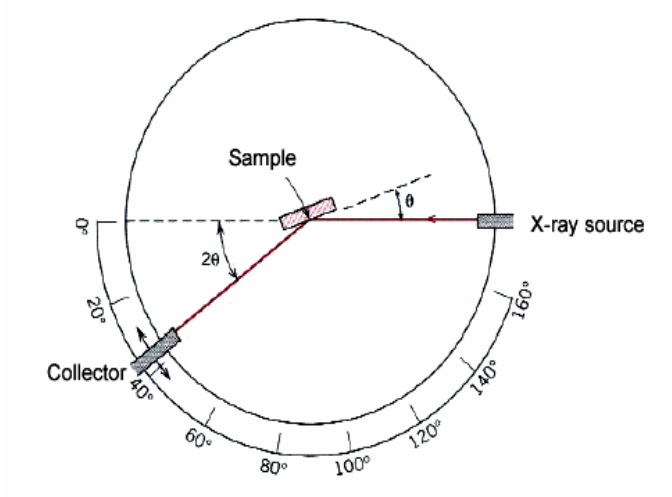

Figure 3.8: Sample irradiation in a Bragg-Brentano diffractometer.

order to get a very fine powder, where the crystalline grains have arbitrary orientations. With the help of these random grain directions, it is predicted that by rotating the sample relative to the incident x-ray (Figure 3.8), we can find all angles where diffraction take place.

The line intensity of a powder XRD pattern obtained in a Bragg-Brentano geometry diffractometer for a pure sample, comprised of three-dimensional crystallites with a parallelepiped form, is given by [8-9, 36-38]:

$$I_d(\theta) = I_0 K_e \left(\frac{1 + \cos^2(2\theta)}{\sin^2\theta \cos\theta} \right) F_{hkl}^2 m_{hkl} \left(\frac{1}{V_c} \right)^2 B_F(\theta) D(\theta) \left(\frac{v_a}{\mu} \right) \qquad (3.2)$$

where

$I_d(\theta)$ is the diffracted intensity

I_0 is the intensity of the incident beam

K_e is a constant depending on the experimental setup, in which are included: λ the wavelength of the used radiation; r the distance from sample to the detector; m and e the mass and the charge of the electron; c the velocity of light; and ϵ_0 the permittivity of free space

F^2_{hkl} is the structure factor of the reflection (hkl)

m_{hkl} is the multiplicity factor corresponding to the reflection (hkl) of the phase under study

V_c is the volume of the unit cell of the crystal

$B_F(\theta)$ is the peak profile

$D(\theta)$ is the Debye-Waller factor

υ_a is the volume fraction of the phase under test

μ is the linear absorption coefficient of the sample under test

We used Bruker AXS D8 Advance powder diffractometer using Cu K_α ($\lambda = 1.5406$ $\mathring{A}$) radiation and an applied voltage and current of 40 kV and 35 mA, respectively for the powder X-ray diffraction analysis of the samples.

3.3.4 Qualitative Identification of Phases

The simplest application of x-ray powder diffraction is the qualitative identification of phases. This application is very important, because it is the first step to understand more complex uses of the method. However, in some cases, it is enough, because of the nature of the intended application of the material under test, and the previous knowledge about the structure of the concrete material. Figure 3.9 shows an example of the use of XRD for the characterization of a material. An MCM-41 mesoporous molecular sieve (MMS), which is the hexagonal phase of the M41S family of materials, is explained as an example of XRD use. The MCM-41 MMS material shows an XRD pattern including three or more low-angle (below 10° in 2θ) peaks that can be indexed to a hexagonal lattice.

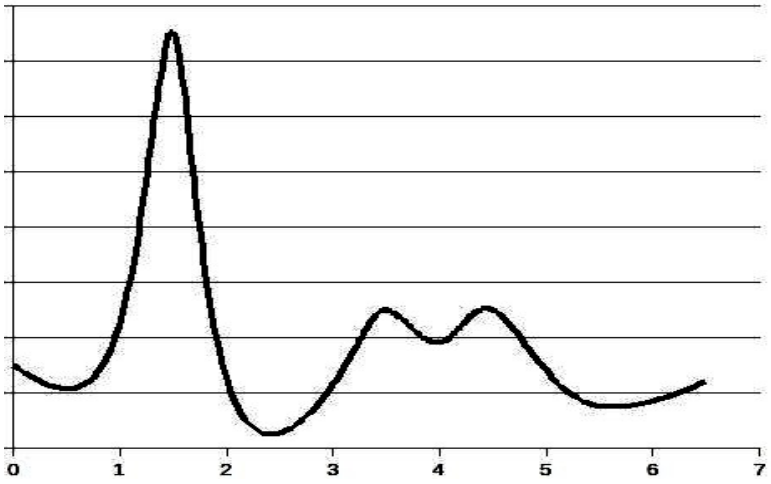

Figure 3.9: XRD pattern, counts per second (CPS) vs. 2θ of the mesoporous material MCM-41.

3.3.5 Quantitative Phase Analysis

The powder XRD analysis of the components present in a mixture was one of the first applications carried out with this methodology. In fact, in 1919, Hull was the first to apply the XRD methodology in chemical analysis [39]. However, Klug and Alexander [40] gave a big impetus to the development of the XRD phase analysis method. The absorption factor for a sample in the form of a plate located in the sample holder of a Bragg-Brentano geometry powder diffractometer is given by [9]

$$A = \frac{1}{2\mu} \tag{3.3}$$

where μ is the linear absorption coefficient. In this case, a simplified form of Equation 3.2 was proposed by Klug and Alexander to express the intensity of the ith peak of the jth phase included in the mixture under analysis [40]

$$I_{ij} = \frac{K_{ij} x_j}{\rho_j \mu^*} \tag{3.4}$$

where

K_{ij} is a constant

x_j is the weight fraction of the diffracting phase

ρ_j is the density of the diffracting phase

μ^* is the mass absorption coefficient of the mixture under analysis

Then, from Equation 3.4, the integrated intensity of the ith peak in the XRD profile of the mixture is calculated by the addition of all the contributions to this peak from all the phases present in the mixture [41-45]

$$I_i = \sum_{j=1}^{n} I_{ij} = \sum_{j=1}^{n} \frac{K_{ij} x_j}{\rho_j \mu^*} \qquad where \qquad j = 1, ..., N \tag{3.5}$$

where N is the number of crystalline phases in the mixture. Equation 3.5 forms a linear system of equations with the complementary normalization condition [41]:

$$\sum_{j=1}^{N} x_j = 1 \tag{3.6}$$

In the simplest case, this system can be solved using the method of multilinear regression [41-42, 45]. In some cases, it is necessary to experimentally determine μ^*, the mass absorption coefficient of the mixture [44-45]. To carry out this procedure, a monochromatic CuK_α radiation was used, and with the help of the following equation [44-45]

$$\mu^* = \frac{E}{M} \ln \left[\frac{I_0}{I} \right] \tag{3.7}$$

where E is a constant, characteristic of the experimental arrangement used

M is the sample mass

I_0 is the intensity measured without an absorbent

I is the intensity measured with an absorbent

it was determined that $E \approx 1.3$, with the help of a sample holder constructed to embrace a wafer of the powdered sample, and the sample holder was attached to the goniometer arm [45].

An analysis of Equations 3.4 through 3.6 reveals that the previous method could fail because of the assumption of the absence of microabsorption, when deriving Equation 3.4 [41]. The microabsorption effect for x-rays diffracted from planar granular powder specimens is caused by the presence of large particles with different absorption magnitudes in the mixture, which create bulk porosity, surface roughness, and the difference in absorption coefficient between the different phases present in the mixture. To account for the microabsorption effect, Leroux, Lennox, and Kay proposed a semiempirical correction to Equation 3.2, as follows [46]:

$$I_{ij} = \frac{K_{ij} x_j}{\rho_j (\mu^*)^{\alpha_j}} \tag{3.8}$$

where α_j are empirical parameters. Gonzales et al. [41-42, 45], applying Equation 3.8, obtained

$$I_i = \sum_{j=1}^{N} K_{ij} \left(\frac{\mu_j^*}{\mu^*} \right)^{\alpha_j} I_{ij}^0 x_j \tag{3.9}$$

with the complementary condition

$$\sum_{j=1}^{N} x_j = 1 \tag{3.10}$$

Equation 3.9 can now be interpreted as a multilinear regression equation [47]

$$I_i = \sum_{j=1}^{N} K_{ij} \left(\frac{\mu_j^*}{\mu^*} \right)^{\alpha_j} I_{ij}^0 x_j = \sum_{j=1}^{N} \beta_j I_{ij}^0 \tag{3.11}$$

with independent variables, I_{ij}^0 , which are the intensities of the peak, i, of the pure phase, j, and dependent variables, I_i, which is the intensity of the

peak, i, of the mixture. The regression coefficients, $_j$, can be determined as follows [41, 44, 47]:

$$\beta_i = \sum_{j=1}^{N} A_{ij}^{-1} B_j \tag{3.12}$$

where A_{ij}^{-1}; is the inverse matrix of the following matrix [41, 44, 47]

$$A_{ij} = \sum_{k=1}^{p} I_{ik}^{0} I_{kj}^{0} W_k \tag{3.13}$$

and

$$B_j = \sum_{k=1}^{p} I_{ik}^{0} I_k W_k \tag{3.14}$$

where [41, 42, 44, 47]

$W_k = 1/\Delta I_k$ are statistical weights

ΔI_k are the errors in the determination of the intensity of peak k

To make a complete calculation of the phase composition of the test sample, this method can take the experimentally measured value of μ^* or the mass absorption coefficient can be calculated with the help of the method of successive approximations [41, 42, 44]. However, the previously explained method is complex; therefore, it is easier to avoid the microabsorption effect by milling the test sample to get particles of about $1\mu m$ [44].

3.3.6 Lattice Parameter Determination

For different studies in materials science, it is necessary to determine the lattice parameters of the obtained or modified materials. In Table 4.3, the equations relating the interplanar distance d, the Miller indexes (hkl), and the lattice parameters for the seven crystalline systems are given [9, 36]. As evident in the cubic case, the parameter a of the cubic cell is directly related to the spacing, d_{hkl}, between planes in the (hkl) family. Then, knowing θ_{hkl},

the Bragg angle, and λ, the x-ray wavelength, it is possible to calculate the lattice parameter a with the help of the Bragg law. Consequently, it is the precision in the measurement of $\sin\theta$, not the precision in the determination of θ, that determines the precision in the determination of the cell parameter.

Table 3.1: **Relations between Interplanar Spacing, Miller Indexes, and Lattice Parameters**

Crystalline system	**Relation between, d, (hkl) and the lattice parameters**
Cubic	$\frac{1}{d^2_{hkl}} = \frac{h^2+k^2+l^2}{a^2}$
Tetragonal	$\frac{1}{d^2_{hkl}} = \frac{h^2+k^2}{a^2} + \frac{l^2}{c^2}$
Hexagonal	$\frac{1}{d^2_{hkl}} = \frac{4}{3}\left(\frac{h^2+hk+k^2}{a^2}\right) + \frac{l^2}{c^2}$
Rhombohedral	$\frac{1}{d^2_{hkl}} = \frac{(h^2+k^2+l^2)\sin^2\alpha+2[(hk+kl+hl)\cos^2\alpha-\cos\alpha]}{a^2(a-3\cos^2\alpha+2\cos^3\alpha)}$
Orthorhombic	$\frac{1}{d^2_{hkl}} = \frac{h^2}{a^2} + \frac{k^2}{b^2} + \frac{l^2}{c^2}$
Monoclinic	$\frac{1}{d^2_{hkl}} = \frac{1}{\sin^2\beta}\left(\frac{h^2}{a^2} + \frac{k^2\sin^2\beta}{b^2} + \frac{l^2}{c^2} - \frac{2hl\cos\beta}{ac}\right)$
Triclinic	$\frac{1}{d^2_{hkl}} = \frac{1}{V^2}\left(S_{11}h^2 + S_{22}k^2 + S_{33}l^2 + 2S_{12}hk + 2S_{23}kl + 2S_{13}hl\right)$

3.4 Energy-Dispersive Analysis of X-rays

SEM is also used to determine the chemical composition of the tested samples. SEMs are normally equipped with EDAX systems for quantitative chemical analysis, which allows direct information of the chemical composition of the selected crystal to be obtained. The analysis is carried out using

the x-rays emitted by the sample (Figure 3.4) tested in the SEM sample holder (Figure 3.3).

In order to generate an x-ray beam, as already disscussed above, a vacuum tube is needed, where an electron beam produced by a heated filament is collimated and accelerated by an electric potential of several kilovolts, that is, from 20 to 45kV. In a SEM (see Figures 3.3 and 3.4), this beam is directed to a sample, which acts as the anode in the x-ray tube (Figure 3.4). The electrons hitting the sample will convey a fraction of their energy to electrons of the target material, a process resulting in electronic excitation of the atoms composing the sample. The sample then produces two kinds of radiations: the continuous spectrum and the characteristic spectrum (see Figure 3.6). The second type of spectrum, called the characteristic spectra, is produced as a result of specific electronic transitions that take place within individual atoms of the anode material. If the energy of the impinging electrons is high enough, some of them will hit a K-shell electron in the anode, and, thereafter, generate an electron vacancy. When such an electron vacancy is generated, it can be quickly filled by an electron from the L-shell or the M-shell of the same atom (see Figure 3.10).

XRF spectra were broadly studied by H.G.J. Moseley who confirmed, in 1913-1914, the relationship between the wavelength of characteristic radiation and the atomic number, Z, of the radiation of the emitting anode material. Moseley found experimentally that the K_α lines for various anode materials exhibit the empirical relationship:

$$\lambda_{K_\alpha} \propto \left(\frac{1}{Z^2}\right) \quad or \quad v_{K_\alpha} \propto Z^2 \quad where \quad \lambda_{K_\alpha} = \frac{c}{v_{K_\alpha}} \tag{3.15}$$

Moseleys empirical relationship reveals a behavior that is in agreement with

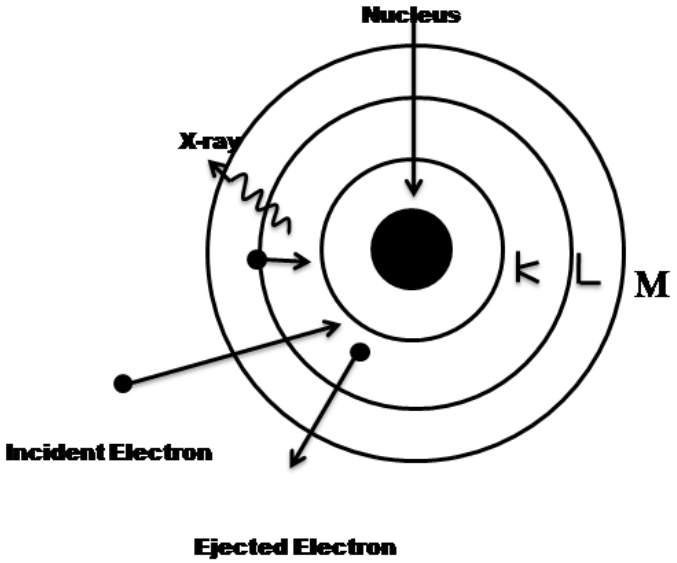

Figure 3.10: Electronic transitions during characteristic x-ray emission.

the Rydberg-Bohr equation, because the energy levels linked with the outer electron transitions are significantly affected by the screening effect of the inner electrons. The screening effect of the deepest electrons on the nuclear charge is explained by an effective nuclear charge (Z-1) in the case of the K_α transition, that is, the K-L transition, and, consequently, the Rydberg-Bohr equation assumes the form

$$v_{K_\alpha} = \frac{c}{\lambda_{K_\alpha}} = cR(Z-1)^2\left(\frac{1}{1^2} - \frac{1}{2^2}\right) = \frac{3cR(Z-1)^2}{4} \tag{3.16}$$

When a sample is bombarded with a particle beam in a SEM, the specimen liberates some of the absorbed energy as x-rays. Then, since each element has its individual exclusive collection of energy levels, the emitted photons are indicative of the element that produced them. Analyzer detectors are then used to characterize the x-ray photons for their energy and abundance to determine the elemental composition of the tested sample. The detectors

used in the EDAX analysis are, in general, semiconductor detectors.

For elemental analysis of gel grown crystals, we made the use of JEOL, JED-2300 apparatus which is attached with the SEM.

3.5 Thermal Methods of Analysis

The development of thermal analysis methods in materials research has led to a plethora of new methodologies since the elaboration of the first thermal method by by Le Chatelier and Robert-Austen [21,48]. Thermal analysis consists of a group of techniques in which a physical property of a material is measured as a function of temperature at the same time when the substance is subjected to a controlled increase, or in some cases, decrease of temperature. Temperature-programmed techniques, such as DTA [49-51], TGA [49], DSC [52, 53], TPR [54, 55], and TPD [56-59], contribute to perform a more complete characterization of materials.

3.5.1 Differential Thermal Analysis

In differential thermal analysis (DTA), the temperature difference that develops between a sample and an inert reference material is measured, when both materials are subjected to an identical heat treatment [49]. The related technique of DSA relies on differences in the energy required to maintain the sample and reference at an identical temperature.

DTA is a technique for recording the difference in temperature between a substance and a reference material. The specimens are subjected to identical temperature regimes in an environment heated or cooled at a controlled rate.

Therefore, DTA involves heating or cooling a test sample and an inert reference in the same conditions, and at the same time recording any temperature change between the sample and reference. This differential temperature is plotted against temperature and, then, changes in the sample which lead to the absorption or evolution of heat can be detected relative to the inert reference [49, 50].

The main characteristics of a DTA equipment are the following:

1. Sample holder comprising thermocouples, sample containers, and a ceramic or metallic block.

2. Furnace.

3. Temperature programmer.

4. Recording system.

The important requisites of the furnace are that it should have a stable and sufficiently large hot zone, and must be able to respond rapidly to commands from the temperature programmer. A temperature programmer is necessary in order to get stable heating rates. The recording system must have a low inertia to accurately reproduce variations. The sample holder assemblage consists of a thermocouple, each for the sample and reference, surrounded by a block to guarantee smooth heat dissemination.

The sample is contained in a small crucible designed with a cut in the base to be accomodated in the thermocouple. The thermocouples should not be placed in direct contact with the sample to avoid contamination and degradation. The crucible may be made of materials such as silica, alumina, zirconia, nickel, or platinum, depending on the temperature and nature of the tests involved.

3.5.2 Thermal Gravimetric Analysis

Thermal gravimetric analysis (TGA) is a simple analytical technique that measures the weight loss or gain of a material as a function of temperature during controlled heating. As the materials are heated, they lose weight due to different processes such as water desorption, or from chemical reactions that release gases. In contrast, some materials can gain weight by reacting with the surrounding atmosphere in the test environment. During the TGA testing process, a sample of the analyzed material is placed into, for example, an alumina cup, which is supported on, or suspended from, an analytical balance located outside the furnace chamber. The sample cup is heated according to a predetermined thermal cycle and the balance sends the weight signal to the computer for storage, along with the sample temperature and the elapsed time. The TGA curve plots the TGA signal, converted to percent weight change on the y-axis against the reference material temperature on the x-axis. Therefore, the results of the test is a graph of the TGA signal, that is, weight loss or gain converted to percent weight loss on the y-axis plotted versus the sample temperature in degree Celsius on the x-axis.

Examples of weight loss or weight gain processes are water desorption, structural water release, structural decomposition, carbonate decomposition, gas evolution, sulfur oxidation, fluoride oxidation, rehydration, and other transformations.

3.5.3 Differential Scanning Calorimetry

Differential scanning calorimetry (DSC) is a method for measuring the energy required to establish a nearly zero temperature difference between a

substance and an inert reference material, as both samples are subjected to the same temperature regimes in an environment heated or cooled at a controlled rate [22]. In one of the possible DSC arrangements, the sample and the reference are enclosed in the same furnace, and a highly sensitive sensor is used to measure the difference between the heat flows to the sample and reference crucibles based on the Boersma or heat flux principle [53].

The difference in energy required to maintain them at a nearly identical temperature is provided by the heat changes in the sample. Any excess energy is conducted between the sample and reference through the connecting metallic disc, a feature absent in DTA. In a DSC test, the thermocouples are not embedded in either of the specimens, and the small temperature difference that may develop between the sample and the inert reference is proportional to the heat flow between the two. The fact that the temperature difference is small is important to ensure that both containers are exposed to essentially the same temperature program.

3.5.4 Temperature-programmed Reduction

Temperature-programmed reduction (TPR) is normally used in the characterization of catalysts [23, 54-56]. In general, to carry out a TPR experiment, a reducing gas mixture, typically 5% hydrogen in nitrogen, flows continuously over the sample [55]. The gas flow rate can be varied precisely using either built-in controls or an optional mass flow controller accessory.

A specially designed high-temperature furnace and sample cell with in situ sample temperature sensing is used to heat the tested samples up to more than $1100\,^{\circ}C$. Linear heating rates are controlled by a temperature

controller. Heating rates are operator programmable for maximum flexibility. The reaction between the sample and reducing gas is monitored by a highly stable thermal conductivity detector (TCD) [23, 54, 55].

At present, this reaction rate signal is presented in real time on the computer display while the PC automatically records signal, temperature, and time. The resulting peak thus formed is a unique, characteristic fingerprint of the sample and the peak maximum represents the temperature of the maximum reaction rate. The reducing gas, or other reactive gas, thus absorbed during a TPR experiment, can be desorbed (TPD) in a separate experiment immediately following this procedure. Temperature-programmed oxidation (TPO) is performed in an analogous manner.

3.5.5 Temperature-programmed Desorption

Temperature-programmed desorption (TPD) is a very useful methodology in porous materials characterization. A basic feature of the experiment is that, it is necessary to use an appropriate adsorbate, such as CO, NH_3, or H_2O [57-59]; however, recently larger molecules have been applied as adsorbates [60].

The basic experiment is very simple, comprising [59] adsorption onto the sample at a relatively low temperature, normally $300K$. Subsequently, the sample is heated in a controlled fashion, that is, linearly in time, at rates between 0.5 and 20 K/s, and at the same time the evolution of species desorbed from the material into the gas phase are monitored.

In TPD practice, desorption rates are reported, that is, dN/dt, where N is the amount of molecules adsorbed in the material [59]. As the temperature

increases and a particular species is capable to desorb from the material, thereafter, the TPD signal will rise; but, as the temperature continues to increase, the amount of adsorbed species on the material will decrease, causing the TPD signal to decrease. This result is expressed as a peak in the TPD signal versus time, or a temperature plot. The temperature of the peak maximum and the shape of the desorption peak provide information about the binding character of the adsorbate/substrate system [59].

Pure carrier gas (typically helium) flows over the sample as the temperature is raised in order to desorb the previously adsorbed gas. Normally, thermoconducting detectors monitor this rate of desorption, producing a TPD profile, where the intensity of the desorption signal is proportional to the rate at which the surface concentration of the adsorbed species is changing. Consequently, the area under a peak is proportional to the quantity originally adsorbed. Besides, the kinetics of desorption provides information on the state of aggregation of the adsorbed species. Finally, the position of the peak temperature is related to the enthalpy of adsorption, that is, to the strength of the binding to the surface.

We made these analyses by Perkin Elmer Diamond Analyser which made it possible to know the thermal decomposition behaviour of the samples.

Bibliography

[1] K. S. Syed Ali, N. Ajeetha, R. Saravanan, Bull. Pure. And Appl. Sci. **21D**, 151(2002).

[2] M. Ali Omar (2000) **Elementary Solid State Physics-Principles and Applications** (Addison-Wesley, Harlow).

[3] A. R. Verma and O.N. Srivastava (1991) **Crystallography Applied to Solid State Physics** (Wilely Eastern Limited, New Delhi, India).

[4] S. A. Martin, H.N. Handler, J. Appl. Crystallogr. **11**, 62(1978).

[5] S. L. Sutib, P.F. Weller, J. Cryst. Growth **48**, 155(1980).

[6] E. N. Kaufmann, (editor), **Characterization of Materials, Vols. I and II**, John Wiley & Sons, New York, 2003.

[7] P. E. J. Flewitt and R.K. Wild, **Physical Methods for Materials Characterization**, Taylor & Francis LTD, London, 1994.

[8] A. Guinier, **X-Ray Diffraction in Crystals, Imperfect Crystals and Amorphous Bodies**, Dover Publications Inc., New York, 1994.

[9] B. D. Cullity and S.R. Stock, **Elements of X-Ray Diffraction**, 3rd edition, Prentice Hall, Upper Saddle River, NJ, 2001.

[10] M. M. J. Treacy and J.B. Higgins, **Collection of Simulated XRD Powder Patterns for Zeolites**, 4th edition, Elsevier, Amsterdam, the Netherlands, 2001.

[11] M. Mashlan, M. Miglierini, and P. Schaaf, (editors), **Material Research in Atomic Scale by Mossbauer Spectroscopy**, Springer-Verlag, New York, 2003.

[12] D. B. Williams and C. B. Carter, **Transmission Electron Microscopy**, Plenum Press, New York, 1996.

[13] M. Staniforth, J. Goldstein, P. Echlin, E. Lifschin, and D. Newbury, **Scanning Electron Microscopy and X-Ray Microanalysis**, Springer-Verlag, New York, 2003.

[14] M. E. Orazem and B. Tribollet, **Electrochemical Impedance Spectroscopy**, John Wiley & Sons, New York, 2008.

[15] K. Nakamoto, **Theory and Applications in Inorganic Chemistry**, John Wiley & Sons, New York, 1997.

[16] D. A. Long, **The Raman Effect**, John Wiley & Sons, New York, 2001.

[17] P. W. Atkins, **Physical Chemistry**, 6th edition, W.H. Freeman & Co., New York, 1998.

[18] P. T. Callaghan, **Principles of Nuclear Magnetic Resonance**, Clarendon Press, Oxford, 1991.

[19] R. Jenkins, (editor), **X-Ray Fluorescence Spectrometry**, John Wiley & Sons, New York, 1999.

[20] R. Roque-Malherbe, **Handbook of Surfaces and Interfaces of Materials**, Vol. 2, H.S. Nalwa, (editor), Academic Press, New York, Chapter 13, 2001, p. 509.

[21] R. F. Speyer, **Thermal Analysis of Materials**, Marcel Dekker, New York, 1993.

[22] P. Gabhot, (editor), **Principles and Applications of Thermal Analysis**, John Wiley & Sons, New York, 2008.

[23] A. Jones and B. Mac Nicol, **Temperature-Programmed Reduction for Solid Materials Characterization**, Marcel Dekker, New York, 2001.

[24] P. Malet and A. Caballero, J. Chem. Soc. Faraday Trans. **84**, 2369 (1988).

[25] F. Rouquerol, J. Rouquerol, and K. Sing, **Adsorption by Powder Porous Solids**, Academic Press, New York, 1999.

[26] R. Roque-Malherbe, **Adsorption and Diffusion in Nanoporous Materials**, CRC Press/Taylor & Francis, Boca Raton, FL, 2007.

[27] R. E. Reed-Hill and R. Abbaschian, **Physical Metallurgy Principles**, 3rd edition, International Thomson Publishing, Boston, MA, 1994.

[28] J. I. Goldstein, D. E. Newbury, P. Echlin, D. C. Joy, C. Fiori, and E. Lifshin, **Scanning Electron Microscopy and X-ray Microanalysis**, Plenum Publishing Co., New York, 1981.

[29] A. Guinier, X-Ray Diffraction in Crystals, **Imperfect Crystals and Amorphous Bodies**, Dover Publications Inc., New York, 1994.

[30] B. D. Cullity and S. R. Stock, **Elements of X-Ray Diffraction**, 3rd edition, Prentice Hall, Upper Saddle River, NJ, 2001.

[31] R. C. Reynolds, Reviews in Mineralogy, **20**, The Mineralogical Society of America, BookCrafters Inc., Chelsea, MI, 1989, p. 1.

[32] L. H. Schwartz and J. B. Cohen, **Diffraction from Materials**, 2nd edition, Springer-Verlag, New York, 1987.

[33] R. Jenkins and R. L. Snyder, **Introduction to X-Ray Powder Diffractometry**, John Wiley & Sons, New York, 1996.

[34] B. E. Warren, **X-ray Diffraction**, Addison-Wesley, Reading, MA, 1969.

[35] M. Birkholz, **Thin Film Analysis by X-Ray Scattering**, John Wiley & Sons, New York, 2006.

[36] M. Birkholz, **Thin Film Analysis by X-Ray Scattering**, John Wiley & Sons, New York, 2006.

[37] R. Jenkins and R. L. Snyder, **Introduction to X-Ray Powder Diffractometry**, John Wiley & Sons, New York, 1996.

[38] J. I. Gersten and F. W. Smith, **The Physics and Chemistry of Materials**, John Wiley & Sons, New York, 2001.

[39] A. W. Hull, J. Amer. Chem. Soc., **41**, 1168 (1919).

[40] H. P. Klug and L. E. Alexander, **X-Ray Diffraction Procedures for Crystalline and Amorphous Solids**, 2nd edition, John Wiley & Sons, New York, 1974.

[41] C. Gonzales, R. Roque-Malherbe, and E. D. Shchukin, J. Mater. Sci. Lett. **6**, 604 (1987).

[42] C. Gonzales and R. Roque-Malherbe, Acta Crystallogr. A **43**, 622 (1987).

[43] R. Roque-Malherbe, A. Dago, and C. Diaz, Rev. Cubana Fis. **3**, 105 (1983).

[44] C. R. Gonzalez and R. Roque-Malherbe, KINAM, **5**, 67 (1983).

[45] C.R. Gonzalez. PhD dissertation, Laboratory of Zeolites, National Center for Scientific Research, Havana, Cuba, 1986.

[46] J. Leroux, D. H. Lennox, and K. Kay, Anal. Chem. **25**, 740 (1953).

[47] N. R. Draper and H. Smith, **Applied Regression Analysis**, 3rd edition, John Wiley & Sons, New York, 1998.

[48] W. W. Wendlandt, Amer. Lab. **9**, 59 (1977).

[49] M. E. Brown, **Introduction to Thermal Analysis: Techniques and Applications**, 2nd edition, Springer-Verlag, New York, 2001.

[50] A. Montes, R. Roque-Malherbe, and E. D. Shchukin, J. Thermal Anal. **31**, 41 (1986).

[51] V. Lopez, F. Marquez-Linares, C. Morant, C. Domingo, E. Elizalde, F. Zamora, and R. Roque-Malherbe, **Nano Today** (submitted).

[52] R. Roque-Malherbe, W. del Valle, J. Ducong, and E. Toledo, Int. J. Environ. Pollut. **31**, 292 (2007).

[53] G. Hohne, W. F. Hemminger, and H. J. Flammersheim, **Differential Scanning Calorimetry**, 2nd edition, Springer-Verlag, New York, 2003.

[54] S. Besselmann, C. Freitag, O. Hinrichsen, and M. Muhler, Phys. Chem. Chem. Phys. **3**, 4633 (2001).

[55] C. de las Pozas, R. Lpez-Cordero, C. Daz-Aguilas, M. Cora, and R. Roque-Malherbe, J. Sol. State Chem. **114**, 108 (1995).

[56] J. L. Falconer and J. A. Schwarz, Catal. Rev. Sci. Eng. **25**, 141 (1983).

[57] R. J. Cvetanovic and Y. Amenomiya, Adv. Catal. **17**, 103 (1967).

[58] C. de las Pozas, R. Lpez-Cordero, J. A. Gonzlez-Morales, N. Travieso, and R. Roque-Malherbe, J. Mol. Catal. **83**, 145 (1993).

[59] P. Malet, Stud. Surf. Sci. Catal. **57B**, 333 (1990).

[60] R. Roque Malherbe and R. Wendelbo, Thermochim. Acta, **400**, 165 (2003).

Chapter 4

Literature Review

4.1 Introduction

"These elements, rare-earths, perplex us in our researches, baffle us in our speculations, and haunt us in our very dreams. They stretch like an unknown sea before us mocking, mystifying, and murmuring strange revelations and possibilities - Sir William Crookes."

These beautiful sentences vividly demonstrate how important rare-earth elements are. Rare-earths are the unacknowledged pillars of the world of modern technology. In recent times, the growth of rare-earth compounds have been one of the most fascinating areas of research because of their tremendous applications in almost every field of life.

The rare-earths impact nearly everyone in the world. All of the people living in developed or developing countries utilize rare-earths in their everyday living-the car that one drives (gasoline is refined from oil using rare-earth catalysts and catalytic converters reduce the polluting emissions from the automotive exhaust), watching the news on TV (the red and green colors

in TV screens), the telephones and computers we use to communicate (the permanent magnets in speakers and disc drives), just to name a few examples. So can one think of living in present world without these rare earths. As has been rightly pointed out by Karl Gschnedner, Jr. (Ames Laboratory, U.S. Department of Energy) the only way one can avoid the rare-earths is to grab your sleeping bag and go into the deep forests or caves in the desert far from civilization without your cell phone or even lighter flints (which are made of iron and cerium-rich rare-earths). In addition to the impact on our personal lives, the military security of the USA (and the rest of the world, likewise) is very dependent on the rare earths (permanent magnets in electric motors, computers, and guidance systems): this is also the case for our energy security (electric motors, batteries, wind turbines, petroleum refining, and fluorescent lighting).

4.2 Brief Overview of Rare Earth Compounds

Rare-Earth Elements (REE) are essential components of modern technology and have numerous applications such as data storage devices, lasers, phosphors for advanced displays, catalysts, permanent magnets, and petroleum refining [1-5]. Rare-earth Elements have contributed to the digital revolution and have enabled a variety of emerging technologies, including hybrid electric vehicles and miniaturized devices and electronics.

Several types of lanthanide complexes have successfully been developed as functional molecular devices in the fields of chemistry, biology, medicine, and material science. For example, (a) luminescent sensors and light converters [6-9], (b) nuclear magnetic resonance (NMR) and magnetic resonance imag-

ing (MRI) probes [10-13], and (c) practical catalysts in organic and biological reactions [14-15] have been presented.

The photoluminescence properties of rare-earth (lanthanide) compounds have been fascinating researchers for decades [16-29]. An attractive feature of luminescent lanthanide compounds is their line-like emission, which results in a high color purity of the emitted light. The important thing to be noted is that the emission color depends on the lanthanide ion but is largely independent of the environment of a given lanthanide ion. So lanthanide complexes can be used as promising light-emitting materials. For example, blue emitting devices based on Tm complexes [30], reddish-orange emitting devices based on Sm complexes [31-32], white emitting devices based on Dy complexes [33], and near-infrared emitting devices based on Er [34], Nd [35], and Yb [36] complexes have been fabricated. In fact, some inorganic luminescent materials, for example $BaMgAl_{10}O_{17} : Eu^{2+}$ and $GdMgB_5O_{10} : Ce^{3+}$, Tb^{3+}, have been commercially utilized for blue and green luminescent lamps, respectively. Their unique functionalities, as said, are attributed to the narrow emission and high colour purity generated from the rare-earth ions. Researchers have also shown good interest in organic luminescent materials because of their applications in organic light emitting diodes (OLEDs) in which a thin film of a luminescent organic material needs to be incorporated between two conductors for such electronic devices [37-39]. Some of Electroluminescent devices exhibited behaviors among the best reported for devices incorporating a europium complex as the red emitter [40]. In 1990, Kido et al [41] first reported the europium complex tris(thienyltrifluoro-acetonato) europium $[Eu(TTA)_3]$, based OLED in which the complex was molecularly

dispersed in hole transporting poly(methylphenylsilane) (PMPS). Luminescence started at 12V, and a maximum intensity of 0.3 cdm^{-2} at 18V was achieved when the device was operated in continuous DC mode. These inorganic and organic luminescent materials have been extensively explored and realized for their diverse functionalities and applications in lighting, display, sensing, and optical devices [42-46]. Moreover, Yamase and co-workers constructed a dispersion type of electroluminescence (EL) cell with a highly photo luminescent $[EuW_{10}O_{36}]^{9-}$ system. With AC excitation to the device consisting of the doublet structure of emissive $[EuW_{10}O_{36}]^{9-}$ and insulating Mylar film layers, the $[EuW_{10}O_{36}]^{9-}$ layer exhibits EL that matches the photoluminescence spectrum of the solid [47].

Rare-earth coordination complexes were expected to afford some new properties, for the functional materials, compared to those simple traditional rare-earth materials. For example, some complexes containing Eu or other rare earth ions can absorb excitation energies with the coordinated ligands, and the following energy transfer process will excite rare earth ions to give the anticipated luminescence emission [48]. And it has been found that the luminescence in the visible domain is the result of an energy transfer between the ligand and the rare earth ion [49]. The two rare-earth complexes namely, $[Eu_2(C_2O_4)_3(H_2O)_6.12H_2O]_\infty$ and $[Tb_2(C_2O_4)_3(H_2O)_6.12H_2O]_\infty$ exhibits intense visible luminescence under UV irradiation ($\lambda_{exc} = 266nm$) [50]. In 2002 Wang et al. reported a dinuclear luminescent terbium complex with formula $[Tb(acac - azain)_3]_2$ [acac-azain=1-(N-7-azaindolyl)-1,3-butanedionato] [51].Recent studies on near-infrared (NIR) luminescence from lanthanide ions have been highly influenced by two significant applications,

including the development of optical fibers for telecommunications and imaging for biomedical assays [52-61].

The structural, electrical, and magnetic properties of these materials are very sensitive to preparation condition such as sintering temperature, time, and type of additives. Due to the addition of small amount of larger ions such as rare earth, an important modification of both structural and magnetic properties can be obtained. This is because rare-earth ions play an important role in determining the magneto-crystalline anisotropy in 4f-3d intermetallic compounds [62]. The effect of small amount of rare-earth ions on the structural magnetic and electrical properties of Mn-Zn ferrite was studied by Ahmed et al [63]. They have found an important modification in Curie temperature, electrical resistivity, lattice constant, magnetic moment, and grain size. Rezlescu et al [64] have reported on the effect of rare-earth oxides on physical properties of Li-Zn ferrite and observed shift of Curie temperature to lower temperature as well as increase in electrical resistivity. Gadkari et al have studied the influence of rare-earth ions addition on structural and magnetic properties of $CdFe_2O_4$ ferrite prepared by oxalate co-precipitation method. The addition of R ions altered its structure and decreases the crystalline size, lattice constant, and grain size. The magnetic properties such as saturation magnetization, remanent magnetization, and magnetic moment have also been increased [65].

There has been a recent resurgence of research activities in developing lanthanide-based molecular magnetic materials stimulated by the large magnetic anisotropy of lanthanide ions, in particular toward the search for single-molecule magnets (SMM) [66]. For example, the trinuclear Dy(III) hydrox-

ide complexes has been shown to exhibit SMM-like slow relaxation behavior within its excited states, even though it possesses an almost diamagnetic ground spin state [67-69]. Furthermore, depending on the nature of the lanthanide ions, magnetic properties ranging from ferromagnetic, ferromagnetic, to antiferromagnetic couplings have been observed for a series of structurally closely related 3d4f heterometallic complexes [70]. These promising results portend a bright future in the development of novel lanthanide hydroxide based molecular magnetic materials.

Rare-earth (RE) mixed oxides constitute a wide and very important class of materials, as their technological significance is huge in several fields, for optical [71-75] and superconductive applications [76], as well as for solid oxide fuel cells [77,78]. Heavy fermion (HF) lanthanide and actinide superconducting compounds were the first that were supposed to have unconventional SC pair states mediated by low energy spin fluctuations [79]. More recently, magnetization measurements of the ultrapure f-electron-based superconductor $-YbAlB_4$ [80] demonstrate zero field quantum criticality without tuning external parameters such as high magnetic fields and pressures in a metal [81].

Rare-earth-containing thermoelectrics not only have the benefit of potential valence instabilities, but they can form complex structures and have high atomic masses, both of which contribute to a significant reduction in thermal conductivity, which can improve performance as a thermoelectric. Substitution of the isovalent, but much higher atomic mass Yb for Ca in $Ca_{14}MnSb_{11}$ led to $Yb_{14}MnSb_{11}$ [82]. $Yb_{14}MnSb_{11}$ is a complex Zintl intermetallic material with a high thermoelectric power factor at elevated temperatures and a

low room temperature lattice thermal conductivity of $\sim 0.45 W/m{-}K$, partly due to the high average atomic mass of the material. Optimized $Yb_{14}MnSb_{11}$ is the highest performing elevated temperature p-type thermoelectric material to date, with a $ZT > 1$ at 1,200 K [83]. Rare earths can be used to tune the electronic structure of a material. The Co_4Sb_{12} skutterudite is a small bandgap semiconductor with a large thermoelectric power factor. The thermal conductivity of Co_4Sb_{12} is far too high for thermoelectric applications ($> 10 W/m - K$), but the skutterudite structure contains voids large enough for rare earth atoms to reside. Rare-earth ions act as both charge donors to modify electronic properties and phonon scattering centers to significantly reduce thermal conductivity. Iron can then be substituted for Co to return the compound to a semiconducting state. The filled skutterudite $Ce(Co, Fe)_4Sb_{12}$ has a large thermoelectric power factor, partly due to f- and d-electron hybridization, and a greatly reduced thermal conductivity, leading to $ZT \sim 1$ at room temperature [84].

Another very important class of material, the rare-earth transition metal indides have not only attracted interest in the chemists community, but also the physicists have intensively investigated such materials, mainly with respect to the largely varying magnetic and electrical properties. The primary interest concerns ferromagnetic, intermediate-valent, and heavy fermion materials. Prominent examples are the 22 K ferromagnet EuRhIn (Pttgen et al., 1999c)[85], mixed-valent CeRhIn (Adroja et al., 1989),[86], valence-fluctuating CeNiIn (Fujii et al., 1989) [87], Kurisu et al., 1990 [88] or the intermediate heavy-fermion system $Ce_5Ni_6In_{11}$ (Tang et al., 1995) [89]. Gadolinium based indides are currently under investigation due to their potential

technological applications for magnetic refrigeration (Canepa et al., 2002b [90]. Finally, it is worthwhile to mention the very recent investigations on the new heavy fermion materials Ce_2TIn_8 and $CeTIn_5$ (T = Co, Rh, Ir). These indides have been thoroughly investigated in the last few years (Hegger et al., 2000) [91], Moshopoulou et al., 2001 [92].

The Endohedral Metallofullerenes (EMFs) form another very important class of material as far as advanced technology is concerned. Alloys containing both the target rare earth metal and nickel, such as YNi_2 and $GdNi_2$, are commonly used for production of EMFs with pure metals [93,94]. Bio-distributions of EMFs were investigated by using holmium-containing metallofullerenes as radiotracers [95,96]. Fullerenes and EMFs are good candidates to be inserted inside carbon nanotubes (CNTs); strong interactions between the inserted EMF molecules and the CNT walls were evidenced from many experimental results. For example, the Raman spectra of $La_2@C_{80}$@CNT differ significantly from those of the empty nanotubes and some absorptions indicate a charge-transfer between them [97]. More supportive proof has been reported by Lee et al. After insertion of $Gd@C_{82}$, the bandgap of CNTs was narrowed down from about 0.5 to 0.1 eV at sites where the EMF molecules locate [98]. Such materials are particularly suitable for quantum computing, which is expected to be the technological mainstay for the next generation of computers.

The carbene derivative La@C_{82}(Ad) can form nanorods during single-crystal growth, which shows an unusual FET (field effect transistor) property. Because thin films or whiskers of empty fullerenes and solids of EMFs are well known to show n-type semiconductivity, the nanorods are p-type [99],

which will surely find applications in such fields as nanoelectronics. Moreover, metallofullerenes have shown interesting magnetic [100] and nonlinear optical properties [101] and are expected to support applications in related fields.

The two-photon sensitization of lanthanide complexes is an emerging field of research. As two-photon microscopy (TPM) greatly reduces UV-treatment problems and provides deeper penetration (hundreds of microns) and low photodamage and photobleaching outside of the focal plane [102, 103]. For example, Wang and coworkers reported a tripyridine-sensitized Eu(III) complex Eu-71 with a significant two-photon absorption cross-section value of 185 GM(GM=GoeppertMayer, where $1GM = 10^{-50}cm^4sphoton^1$) at 735 nm, however, Eu-71 is only stable in non-aqueous solvents [104]. Maury and co-workers reported a tricationic complex Eu-72 with a two-photon antenna effect produced by an alkyloxyphenylacetylene functionalized pyridine dicarboxamide ligand [105].

Not only have this, rare-earth complexes started showing its power in the field of medicine also. Liu et al. has reported that the complex $[TbAs_4W_{40}O_{140}]^{25-}$ displays inhibitory action to HL60 (leukaemia), B16 (melanoma), H22 (liver cancer cell) cancers, and rectum cancer vivicells as well as breast cancer vivicells [106]. Yamamoto et al. have reported that $K_{13}[Ce(SiW_{11}O_{39})_2]$ shows inhibitory action to the human immunodeficiency virus (HIV) and the simian immunodeficiency virus [107]. Inouye et al. have reported $[NH_4]_{12}H_2$ $[Eu_4(MoO_4)(H_2O)_{16}(Mo_7O_{24})_4].13H_2O$ displays potent anti-HIV-1 activity [108].

A significantly increased relaxivity over the clinically utilized Gd(III) contrast reagent has been achieved [109]. The potential use of high-nuclearity

lanthanide hydroxide complexes as new paradigms for radiographic imaging has also been envisioned [110]. The key roadblock to further development appears to be the stability (or lack thereof) of the currently available complexes. The first gadolinium-based MRI CA was gadopentetate dimeglumine (gadolinium diethylenetriaminepentaacetatic acid, Gd-DTPA), which was introduced into patients in 1983 and approved for clinical use in 1988 [111]. Time-resolved luminescence bioassay techniques using luminescent lanthanide complexes as probes have been exploited in various fields, especially immunoassays and high-throughput screenings, since the first application was reported in 1983 [112-114]. In 2005, Yuan and co-workers demonstrated a Eu(III) complex Eu-69 as a sensitive and selective time-resolved luminescence probe for singlet oxygen (O_2^1) [115,116]. O_2^1 probably plays an important role in the cell signalling cascade and in the induction of gene expression [117]. Lanthanide complexes have great applications in molecular recognition and chirality sensing of biological substrates [118].

Lanthanide hydroxide complexes have been found to catalyze the hydrolytic cleavage of DNA and RNA analogs, mimicking the function of natural nucleases [119-121]. In 1992, the authors found that various lanthanide(III) salts are active for the hydrolysis of phosphodiester linkages in DNA (Matsumoto and Komiyama, 1992) [122]. Interestingly, the activity of $Ce(NH_4)_2 -(NO_3)_6$ for DNA hydrolysis is substantially enhanced when $PrCl_3$ is added to the mixture (Takeda et al., 1996) [123].

Till now one must be having no confusion as far as importance and applications of rare-earth materials is concern. Such a tremendous applicability of rare-earths is because of their unique positions in the periodic Table,

which correspond to the first period of f-block elements from lanthanum to lutetium, and their trivalent cations possess characteristic $4f^n$ open shell configurations (n: 0-14) [124-127]. They have a varying valence character while reacting with different elements because of which compounds of different modifications are obtained. It has been found that The use of rare-earth materials in the various areas such as luminescent, magnetic, and catalytic materials, is because of their unique properties originating from their 4f electron configurations [128-132].

4.3 An Overview of Rare Earth Molybdates

The present research deals with a very important class of rare earth compounds, known as rare earth molybdates. At the end of 60th there was a great interest to the rare earth molybdates family $R_2(MoO_4)_3$ (R= Pr, Nd, Sm, Eu, Gd, Tb and Dy) because these compounds exhibited the phenomena of ferroelectricity and ferroelasticity [133]. There ferroelectric properties was theoretically predicted by Levanyuk and Sannikov in 1968 [134]. Analogous result was obtained for TMO from neutron scattering experiments in 1970s [135-136]. Their Ferroelasticity was established in 1969 by Aizu [137]. These properties, ferroelectricity and ferroelasticity, as investigated for GMO were found to be temperature dependent [138-139]. Subsequent investigations of the dielectric, optical, and mechanical behaviour of these materials have revealed several unique and potentially useful properties [140]. Pure and mixed rare earth molybdates are important for use in optical equipment and electronic and acoustic studies [141-142]. Many complex molybdate crystals are noncentrosymmetric and they show potentials for nonlinear optical ef-

fects [143-148]. For several recently discovered binary molybdates, the large levels of nonlinear optical susceptibility $\chi^{(2)}$ are reported and these crystals are of great attention for the design of new nonlinear optical materials [149-151]. Because of their potential optical application, rare-earth molybdate compounds have been studied extensively [152-158]. For example, the $MRE(MoO_4)_2$, (M=alkali metal, RE=rare earths) single crystals, which is with a scheelite structure, can be used as self-doubling solid-state laser host materials. Photo-active rare-earth ions, such as Nd^{3+}, Yb^{3+}, Ho^{3+}, and Er^{3+} have been used to activate these kinds of host materials and their optical properties or laser performance have been widely investigated [159-163]. Thallium-containing rare-earth molybdates show diverse crystal structures and properties due to the strong distortion of coordination polyhedra. A presence of stereo-active lone electron pair and high effective radius of Tl^{+} ion seems to be the key factors providing the noncentrosymmetric crystal structure [143,151,164,165]. The low-symmetry positions are observed for Ln^{3+} ions with benefits for the creation of new effective laser mediums [166-168]. Other properties, besides crystal structure, remain to be unknown for many Tl^{+}- and Ln^{3+}- containing molybdates.

In the fields of phosphor materials, $MRE(MoO_4)_2$ materials doping Eu^{3+} or Tb^{3+} also present excellent properties [169,170]. Wang et al [170] reports, it is interesting that no concentration quenching of Eu^{3+} can be observed in the samples of $NaRE_{1-x}Eu_x(MoO_4)_2$ and $LiEu(MoO_4)_2$systems, both of which exhibit the strongest red emission under 395 nm light excitation and appropriate CIE chromaticity coordinates (0.66, 0.34) close to the NTSC standard values. Not only the research on the optical properties of scheelite

type $MRE(MoO_4)_2$ is the hot topic but also the research on their microstructure attracts many scientists [171,172].

Molybdate and tungstate materials comprise a large class of inorganic compounds that exhibit interesting physical properties and thus have technological applications in the fields of catalysis and quantum electronics [173]. Intensive research efforts have been focused on rare-earth molybdate compounds due to their unique catalytic, and magnetic properties [174,175]. Magnetic properties of a single crystal and single domain spherical sample of GMO were investigated in papers [176-180]. Magnetic properties and heat capacity of $Gd_2(Mo0_4)$ and $Tb_2(Mo0_4)_3$ at liquid helium temperatures for magnetic fields up to 90kOe have been investigated [181-185]. It was shown that triply positive-charged rare earth ions were responsible for the magnetic properties of these substances. Also it was shown that $Gd_2(MoO_4)_3$ and $Tb_2(Mo0_4)_3$ were antiferromagnets with Neel temperatures $T_N = 0.3$ and 0.45 K respectively.

The compounds existing in $R_2O_3MoO_3$ (R = rare earth) systems, known as higher rare-earth molybdates, can be grown in the form of single crystals and find various practical applications [186-189]. At the same time, molybdenum is known to exhibit a wide variety of oxidation states in oxides. The MoO system is characterized by extremely complex phase relations [190-193]. Along with 6+, the oxidation state 4+ is rather stable. Molybdenum (IV) oxide, MoO_2, can be obtained readily by reacting MoO_3 and powder Mo in an evacuated silica tube at $1000\,^{\circ}C$ and is stable in air up to $440\,^{\circ}C$ [186,187]. Compounds in which the oxidation state of molybdenum is lower than 6+ (lower rare-earth molybdates) have been investigated less extensively, but

they are also of practical interest. Low-valent molybdenum compounds are known to exhibit catalytic properties [194-198]. Lower rare-earth molybdates possess semi-conducting [199] and metallic [200] properties and are, therefore, of scientific interest from the viewpoint of the metalinsulator transition. In addition, they have anomalous magnetic properties [201]. Mixed-valent molybdenum bronze-like phases are potentially attractive as cathodes for electrochemical cells.

The following applications of rare earth molybdates with non-zero orbital moments of triply charged rare earth ions as discussed in [202] are possible.

(i) Threshold sensor devices for measuring a DC magnetic field. These devices should generate a jump in electrical voltage when the magnetic field under test reaches a certain value.

(ii) Small displacements (of the order of $10^{-5}cm$) can be generated on the basis of rare earth molybdates with non-zero orbital moment. The displacements are due to the influence of the magnetic field on the crystal distortions related to the ferro-electric arrangement.

(iii) Optical shutters, phase shifters and relays with fine magnetic regulation of their parameters.

(iv) New types of current-less engine based upon the magneto-electric interactions.

(v) Producing low temperatures by means of adiabatic demagnetization is possible using rare earth molybdates independently of the angular momentum value.

Keeping in view the importance and interesting properties of rare earth molybdates, lot of work has been carried out on their growth in last few

decades. Several investigators have reported their growth using different growth techniques. They have been grown using solid state reaction methods [203]. High quality single crystals of $R_2(MoO_4)_3$ type, using Czochralski procedure were first time grown in 1971 which give rise to scattering the light of a laser beam passed through the crystal [204]. Using rotation less pulling technique, crystals could be obtained scattering free for laser investigation [205]. Mixed crystals of neodymium hyptamolybdate were grown in silica gel [206]. Also erbium-doped photonic materials and structures have been grown by sol-gel, in the form of hafnium based optical planar wave guides and 1D photonic band gap structures consisting of alternating silica and titanium layers [207]. Praseodymium molybdate crystals have been grown by silica gel method [208,209].The growth of pure Gd- and Gd-Ba- molybdate crystals, bearing the stoichiometric composition $Gd_2Mo_7O_2 : H_2O$ and $Gd_2Ba_{24}Mo_{42}O_{153}$ has been achieved by the gel technique [210]. Tetragonal molybdate micro crystallites with delicate morphologies have been successfully prepared via a very simple alkalescent aqueous mineralization method. The products were characterized by x-ray powder diffraction, field emission scanning electron microscopy [211]. Growth and spectroscopic investigations of Yb^{3+}- doped $NaGa(MoO_4)_2$ and $NaLa(MoO_4)_2$ has been done by Czochralski method and was found as active media of solid state lasers [212,213]. $Nd^{3+} : BaGa_2(MoO_4)_4$ crystals with dimensions 20mmx28mm have been grown by the CZ method [214]. A 3D flowerlike europium doped lanthanum molybdate $[La_2(MoO_4)_3 : Eu]$ micro-architectures that exhibit efficient photoluminescence have been successfully synthesized via a facial hydrothermal process [215]. Transparent and nearly colorless ferroelectric

$Tb_2(MoO_4)_3$ (TMO) single crystal have been grown by Czochralski method. The single crystal was investigated by XRD method and was shown to be a single crystal [216].

So lot of work has already been done for the growth and characterization of rare earth molybdates using different methods and techniques. Keeping in view the importance of these materials it is worthwhile to grow crystals of known rare earth compounds as well as to explore the possibilities of the growth of new materials of rare earth compounds for various scientific investigations by an inexpensive and simple technique called the gel technique. A large number of crystals have been grown at ambient temperature by this technique, which may be classified as a low temperature solution technique. The growth at lower temperatures is expected to yield crystals with minimum defects. Although the gel technique of growing crystals proves to be less expensive and advantageous, this method cannot yield crystals of a large size. If one is able to obtain a crystal of optimum size suitable for a particular scientific study, the purpose is served. The gel method is the most acceptable one, and one has only to attempt to grow crystals of a size that may be optimum for characterization by a particular probe. On the other hand, high temperature techniques are usually expensive and may not be within the reach of every laboratory. Furthermore, high growth temperatures become sources of increased thermal stress, as a result of which the crystals may contain more defects.

It is an established fact that the physical and chemical properties of these materials are very sensitive to preparation condition such as sintering temperature, time, and type of additives. They may positive or negative effects

on the properties of these compounds. But, the present work is performed in order to study the changes that are brought about in the physical and chemical properties of pure rare earth molybdates by differrent factors such as concentration of upper and lower reactants, gel pH etc. The present work also include different characteristics such as morpholgy, thermal behaviour etc. after they are grown in pure form.

4.4 Overview of Spherulites

Spherulites are ubiquitous in solids formed under highly non-equilibrium conditions [217]. They are observed in a wide range of metallurgical alloys, in pure Se [218,219], in oxide and metallic glasses [220], mineral aggregates and volcanic rocks [221,222], polymers [217], liquid crystals [223], simple organic liquids [224], and diverse biological molecules [225]. Many everyday materials, ranging from plastic grocery bags to airplane wings and cast iron supporting beams for highway bridges, are fabricated by freezing liquids into polycrystalline solids containing these structures. The properties and failure characteristics of these materials depend strongly on their microstructure, but the factors that determine this microstructure remain poorly understood [217].

4.4.1 Habit and Morphology

While the term spherulite suggests a nearly spherical shape, but it is used in a broader sense of densely branched, polycrystalline solidification patterns [218,223,226-231]. Spherulitic patterns exhibit a diversity of forms and rep-

resentative patterns are shown in Fig. 4.1 [226-230].

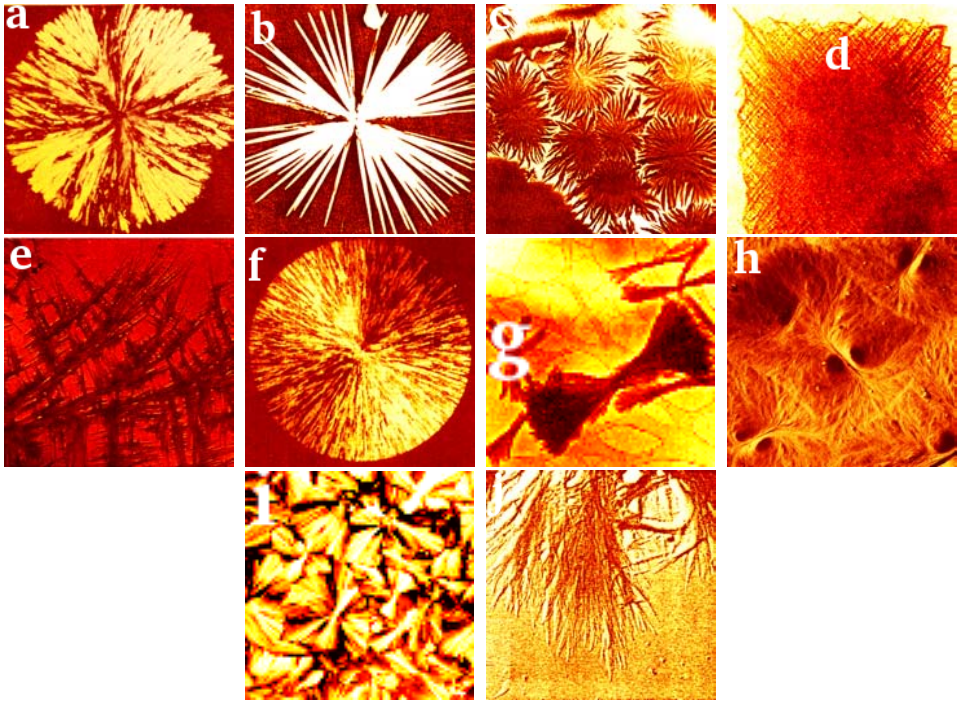

Figure 4.1: Various spherulitic morphologies. (a) Densely branched spherulite formed in a blend of isotactic and atactic polypropylene. (b) Spiky spherulite grown in malonamide-d-tartatic acid mixture. (c) Arboresque spherulites forming in polypropylene film, (d) and (e) Quadrites formed by nearly rectangular branching in isotactic polypropylene. (f) Spherulite formed in pure Se. (g) Crystal sheaves in pyromellitic dianhydrite-oxydianilin poly(imid) layer. (h) Spherulites (a thin film of polybutene) with two eyes on the sides of the nucleus. (i) Multi-sheave / early spherulite structure formed in dilute long n-alkane blend. (j) Arboresque growth form in polyglycine. To improve the contrast/visibility of the experimental pictures, false colors were applied. The linear size of the panels are (a) 220 m, (b) 960 m, (c) 2.4 mm, (d) 2.5 m, (e) 7.6 m, (f) 550 m, (g) 2.5 m, (h) 20 m, (i) 250 m, and (j) 1.7 m, respectively.

Individual crystallites that assemble as spherulites in the aggregate are often needle-like but other habits are observed. Plank-like crystallites (flattened needles) are not infrequent; plate-like crystallites are rare. The predom-

inance of structures with exaggerated aspect ratios is a consequence of the fact that a high crystallographic driving force is a precondition of spherulitic growth.

The morphology of subindividuals is generally similar to the morphology of the parent crystal. Blocks beget blocks, needles beget needles. Thin polymer lamellae branch to give equally thin descendants (5-20 nm), a dimension dictated by material properties and growth conditions [232]. The needle-like fibers are typically straight, and plate-, and plank-like crystallites are typically straight and flat. However, bending, twisting, and scrolling of fibrils and lamellae further confounds spherulite morphology.

Spherulites can also be classified by their fiber density. Compact, massive, or closed spherulites do not contain free space between individual fibers or crystallites, in contrast to open or spiky [233] spherulites. Outer surfaces of compact spherulites are often smooth; coarse spherulites typically form rough interfaces [234,235].

4.4.2 Growth of Spherulites

Spherulites form in distinct environments. As crystallization conditions intimately control spherulite growth, melts, solid phases, and solutions have their own idiosyncrasies. Spherulites are formed via noncrystallographic branching, distinguishing them from dendrites and diffusion-limited aggregates [233]. They are more commonly grown from the melt where they display compact morphologies. Solution-grown spherulites are rare and usually exhibit open morphologies. On the other hand, there is no fundamental difference between multicomponent melts and solutions; all spherulites, whatever

the growth environment, seem to be triggered by comparable processes.

Spherulitic growth requires a high crystallization driving forces (typical values of supersaturation or supercooling expressed as differences of chemical potential are $\Delta\mu/RT > 0.5$) with interface control of growth. This is the most important prerequisite for spherulitic growth. Spherulitic growth is comparatively slow. For high supercooling and/or supersaturation at the growth front, slow growth necessitates a comparatively small kinetic coefficient, . This is consistent with low melt crystallization temperature. For solution grown crystals, small s are consistent with higher probabilities of spherulites among slightly soluble compounds.

A viscous medium is not a prerequisite for spherulitic growth. Melt growth tends to give more well-formed spherulites grown at lower temperatures (higher melt viscosity), but spherulites can be formed near the melting point of nonviscous liquids. For solution grown crystals, experiments are often conducted in a viscous gels since such conditions often facilitate the monitoring of crystallization. On the other hand, in many cases, spherulites of the same compounds can be obtained from freely flowing solutions [236]. Impurities encourage spherulite formation. For melt grown crystals, the thickness of spherulite fibers decreases as supercooling increases (temperature decreases). Qualitatively it appears that higher supersaturation results in thinner fibers.

In 1963, Keith and Padden [233] concluded that spherulite formation required growth of crystals with a fibrous habit and noncrystallographic small-angle branching. The fibrous habit, while common, is not requisite, but noncrystallographic branching lies at the heart of the spherulite growth mechanism.

4.4.3 Properties of Spherulites

Spherulites are polycrystalline aggregates composed by highly anisometric crystallites with an outer spherical envelope. The original single crystal undergoes noncrystallographic branching or splitting and turns into an ensemble of new crystallites or individuals that grow independently of their progenitor. The misorientations typically vary between 0 and 15 and relationships between directions of growth of the primary and secondary crystallites are not crystallographic; in other words, the relative orientations are not fixed by crystal structure or symmetry. Noncrystallographic branching distinguishes spherulites from other branched crystals and polycrystalline aggregates possessing round forms. The apparent properties of spherulites are frequently averages of many imperfectly oriented fibrils [237,238].

An ideal, well-developed spherulite is spherical. During its evolution from a single crystal nucleus, it passes through a series of intermediate dumbbell and sheaf-like morphologies. Although, formally, objects with such intermediate morphologies are not spherulites, in that they are not yet spherical, their formation is controlled by the same mechanisms. They are on their way to becoming spherulites, and thus are generally counted as spherulites.

An ideal spherulite consists of one phase. However, there are also pseudo-spherulites [239] composed by subindividuals of two or more phases [240,241] often formed in the course of eutectic crystallization. Sometimes radial growth and concentric sedimentation are concomitant, forming two- and polyphase spherulites with punctuated amounts of a crystalline phase [242,243].

The size of spherulites varies in a wide range, from micrometers up to 1 centimeter [244] and is controlled by the nucleation. Strong supercooling or

intentional addition of crystallization seeds results in relatively large number of nucleation sites; then spherulites are numerous and small and interact with each other upon growth. In case of fewer nucleation sites and slow cooling, a few larger spherulites are created [245].

Formation of spherulites affects many properties of the polymer material; in particular, crystallinity, tensile strength and Young's modulus of polymers increase during spherulization. Changes in mechanical properties of polymers upon formation of spherulites however strongly depend on the size and density of the spherulites.

when spherulites are viewed between crossed polarizers in an optical microscope, results in birefringence producing a variety of colored patterns. From the birefringence point of view, spherulites can be positive or negative. This distinction depends not on the orientation of the molecules (parallel or perpendicular to the radial direction) but to the orientation of the major refractive index of the molecule relative to the radial vector. The spherulite polarity depends on the constituent molecules, but it can also change with temperature [244].

Bibliography

[1] T. J. Kane and R. L. Byer, Optics Letters, **10**, 65(1985).

[2] C. R. Ronda, T. Jstel and J. Nikol, J. Alloys Compd. **275**, 669(1998).

[3] R. J. H. Voorhoeve, J. P. Remeika, P. E. Freeland and B. T. Matthias, Science **177**, 353(1972).

[4] M. Sagawa, S. Fujimura, N. Togawa, H. Yamamoto and Y. Matsuura, J. Appl. Phys. **55**, 2083(1984).

[5] M. E. Kitto, D. L. Anderson, G. E. Gordon and I. Olmex, Environ. Sci. Technol. **26**, 1368(1992).

[6] W. Horrocks, Jr. DeW. and D. R. Sudnick, Acc. Chem. Res. **14**, 384(1981).

[7] G. E. Buono-Core and H. Li, Coord. Chem. Rev. **99**, 55(1990).

[8] N. Sabbatini and M. Guardigli, Coord. Chem. Rev. **93**, 201(1993).

[9] D. Parker, Coord. Chem. Rev. **205**, 109(2000).

[10] T. J. Wezel, **NMR Shift Reagents**; CRC Press: Raton, FL, 1987.

[11] D. Parker, Chem. Rev. **91**, 1441(1991).

[12] S. Aime, M. Botta, M. Fasano and E. Terreno, Chem. Soc. Rev. **27**, 19(1998).

[13] P. Caravan, J. J. Ellison, T. J. McMurry and R. B. Lauffer, Chem. Rev. **99**, 2293(1981).

[14] T. Imamoto, **Lanthanides in Organic Synthesis**; Academic Press: London, 1994.

[15] M. Komiyama, N. Takeda and H. Shigekawa, Chem. Commun (**Feature Article**), 1443(1999).

[16] J. C. G. Bunzli, **Lanthanide Probes in Life, Chemical and Earth Sciences: Theory and Practice**; Elsevier: Amsterdam, 1989.

[17] A. J. Kenyon, Prog. Quantum Electron. **26**, 225(2002).

[18] G. Blasse and B. C. Grabmaier, **Luminescent Materials**; Spinger-Verlag: Berlin, 1994.

[19] G. Blasse, Prog. Solid State Chem. **18**, 79(1998).

[20] M. Elbanowski and B. Makowsaka, J. Photochem. Photobiol. A, **99**, 85(1996).

[21] J. C. G. Bunzli, Acc. Chem. Res. **39**, 53(2006).

[22] J. C. G. Bunzli and C. Piguet, Chem. Soc. ReV. **34**, 1048(2005).

[23] Y. Hasegawa, Y. Wada and S. Yanagida, J. Photochem. Photobiol. C, **5**, 183(2004).

[24] B. M. Tissue, Chem. Mater. **10**, 2837(1998).

[25] W. T. Carnall, J. V. Beitz, H. Crosswhite, K. Rajnak, J. B. Mann, **Systematics and the Properties of Lanthanides**; S. P. Sinha, Ed.; D. Reidel Publishing Company: Dordrecht, The Netherlands, 389(1983).

[26] W. T. Carnall, **Handbook on the Physics and Chemistry of Rare Earths**; K. A. Gschneidner, L. Eyring, Eds.; Elsevier: Amsterdam, Vol. 3, Chapter 24, 171(1979).

[27] J. Blasse, **Handbook on the Physics and Chemistry of Rare Earths**; K. A. Gschneidner, L. Eyring, Eds.; Elsevier: Amsterdam, Vol. 4, Chapter 34, 237(1979).

[28] M. J. Weber, **Handbook on the Physics and Chemistry of Rare Earths**; K. A. Gschneidner, L. Eyring, Eds.; Elsevier: Amsterdam, Vol. 4, Chapter 35, 275(1979).

[29] C. A. Morrison and R. P.Leavitt, **Handbook on the Physics and Chemistry of Rare Earths**; K. A. Gschneidner, L. Eyring, Eds.; Elsevier: Amsterdam, Vol. 5, Chapter 46, 461(1982).

[30] J. B. Yu, L. Zhou, H. J. Zhang, et al. Inorgnic Chemistry, **44**, 1611(2005).

[31] Z. R. Hong, W. L. Li, D. X. Zhao, et al. Synthetic Metals, **104**, 165(1999).

[32] Z. Kin, H. Kajii, Y. Hasegawa, et al. Thin Solid Films, **516**, 2735(2008).

[33] Z. R. Hong, W. L. Li, D. X. Zhao, et al. **111**, 43(2000).

[34] R. G. Sun, Y. Z. Wang, B. Q. Zheng, et al. J. Appl. Phy. **87**, 7589(2000).

[35] Y. Kawamura, Y. Wada, Y. Hasegawa, et al. Appl. Phy. Lett. **74**, 3245(1999).

[36] Z. R. Hong, C. J. Liang, R. G. Li, et al. Thin Solid Films, **391**, 122(2001).

[37] S. C. Lo & P. L. Burn, Chem. Rev. **107**, 1097(2007).

[38] A. C. Grimsdale, K. Leok Chan, R. E. Martin, P. G. Jokisz, & A. B. Holmes, Chem. Rev. **109**, 897(2009).

[39] J. G. C. Veinot, T. J. Marks, Acc. Chem. Res. **38**, 632(2005).

[40] P. P. Sun, J. P. Duan, J. J. Lih and C. H. Cheng, Adv. Func. Mat. **13**, 683(2003).

[41] J. Kido, K. Nagai and Y. Okamoto, Chemis. Lett. **235**, 1267(1991).

[42] S. V. Eliseeva, J. C. G. Bunzli, Chem. Soc. Rev. **39**, 189(2010).

[43] K. Binnemans, Chem. Rev. **109**, 4283(2009).

[44] S. H. Hwang, C. N. Moorefield & G. R. Newkome, Chem. Soc. Rev. **37**, 2543(2008).

[45] L. D. Carlos, R. A. S. Ferreira, V. de Zea Bermudez, B. Julian Lopez & P. Escribano, Chem. Soc. Rev. **40**, 536(2011).

[46] J. Kido, and Y. Okamoto, Chem. Rev. **102**, 2357(2002).

[47] T. Yamase, Chem. Rev. **98**, 307325(1998).

[48] N. Sabbatini, M. Guardigli & J. M. Lehn, Coord. Chem. Rev. **123**, 201(1993).

[49] M. Elhabiri, R. Scopelliti, J. C. G. Bunzli & C. Piguet, J. Am. Chem. Soc. **121**, 10747(1999).

[50] D. Kustaryono, N. Kerbellec, G. Calvez, S. Freslon, C. Daiguebonne and O. Guillou, cryst. growth and design **10**, 780(2010).

[51] R. Y. Wang, D. T. Song, C. Seward, et al. Inorg. Chem. **41**, 5187(2002).

[52] J. C. G. Bunzli, S. Comby, A. S. Chauvin and C. D. B. Vandevyver, J. Rare Earths, **25**, 257(2007).

[53] Y. Hasegawa, Y. Wada and S. Yanagida, J. Photochemistry and Photobiology C: Photochemis. Rev. **5**, 183(2004).

[54] J. Kido and Y. Okamoto, Chem. Rev. **102**, 2357(2002).

[55] S. Faulkner, S.J.A. Pope and B.P. Burton-Pye, Appl. Spectroscopy Rev. **40**, 1(2005).

[56] T. Gunnlaugsson and F. Stomeo, Organic and Biomolecular Chemistry, **5**, 1999(2007).

[57] H. Tsukube, S. Shinoda and H. Tamiaki, Coord. Chem. Rev. **226**, 227(2002).

[58] S. Kaizaki, Coord. Chem. Rev. **250**, 1804(2006).

[59] C. M. G. dos Santos, A. J. Harte, S. J. Quinn and T. Gunnlaugsson, Coord. Chem. Rev. **252**, 2512(2008).

[60] A. Dossing, European J. Inorg. Chem. 1425(2005).

[61] A. de Bettencourt-Dias, **Lanthanide-based emitting materials in light emitting diodes**, Dalton Transactions, 2229(2007).

[62] M. A. Ahmed, E. Ateia, S. I. El-Dek, and F.M Salem, J. Mater. Sci., **38**, 1087(2003).

[63] M. A Ahmed, N. Okasha and M.M. El-Sayed, Ceram. Int. **33**, 49(2007).

[64] N. Rezlescu, E. Rezlescu, P. D Popa and L. Rezlescu, J. Alloys Compd. **657**, 275(1998).

[65] A. Gadkari, T. Shinde and P. Vasambekar, Rare Metals, **29**, 168(2010).

[66] C. Benelli, and D. Gatteschi, Chem. Rev. **102**, 2369(2002).

[67] J. Tang, I. Hewitt, N. T. Madhu, G. Chastanet, W. Wernsdorfer, C. E. Anson, et al. Angewandte Chemie International Edition, **45**, 1729(2006).

[68] J. P. Costes, F. Dahan and F. Nicodeme, Inorg. Chem. **40**, 5285(2001).

[69] W. J. Evans, M. A. Greci and J. W. Ziller, J. Chem. Society, **Dalton Transactions**, 3035-3039(1997).

[70] X. Kong, Y. Ren, L. Long, Z. Zheng, G. Nichols, R. Huang, et al. Inorg. Chem. **47**, 2728(2008).

[71] J. C. G. Bunzli, S. Comby, A. S. Chauvin and C. D. B. Vandevyver, J. Rare Earth, **25**, 257(2007).

[72] J. Blanusa, N. Jovic, T. Dzomic, B. AnticB, A. Kremenovic, M. Mitric and V. Spasojevic, Opt. Mater. **30**, 1153(2008).

[73] T. Biljan, A. Gajovic, Z. Meic and E. Mestrovic, J. Alloy. Compd. **431**,217(2007).

[74] J. L. Ferrari, A. M. Pires and M. R. Davolos, Mater. Chem. Phys. **113**, 587(2009).

[75] M. S'roda, J. Therm. Anal. Calorim. **97**, 239(2009).

[76] P. Mele, C. Artini, R. Masini, G. A. Costa, A. Hu, N. Chikumoto and M. Murakami, Physica C. **391**, 49(2003).

[77] C. Peng and Z. Zhang, Ceram. Int. **33**, 1133(2007).

[78] D. Y. Chung and E. H. Lee, J. Alloy. Compd. **374**, 69(2004).

[79] K. A. Gschneidner, Jr. J. C. G. Bunzli and V. K. Pecharsky(editors), **Handbook on the Physics and Chemistry of Rare Earths**, volume 34, pp 139, Elsevier, 2004

[80] R. T. Macaluso, S. Nakatsuji, K. Kuga, E.L. Thomas, Y. Machida, Y. Maeno, Z. Fisk and J. Y. Chan, Chem. Mater. **19**, 1918(2007).

[81] Y. Matsumoto, S. Nakatsuji, K. Kuga, Y. Karaki, N. Horie, Y. Shimura, T. Sakakibara, A. H. Nevidomskyy and P. Coleman, Science, **331**, 316(2011).

[82] J. Y. Chan, M. M. Olmstead, S. M. Kauzlarich and D. J. Webb, Chem. Mater. **10**, 3583(1998).

[83] S. R. Brown, S. M. Kauzlarich, F. Gascoin and G. J. Snyder, Chem. Mater. **18**, 1873(2006).

[84] G. S. Nolas, D. T. Morelli and T. M. Tritt, Annu. Rev. Mater. Sci. **29**, 89(1999).

[85] R. Pottgen, R. D. Hoffmann, M. H. Moller, G. Kotzyba, B. Kunnen, C. Rosenhahn and B. D. Mosel, J. Solid State Chem. **145**, 174(1999).

[86] D. T. Adroja, S. K. Malik, B. D. Padalia and R. Vijayaraghavan, Phys. Rev. B, **39**, 4831(1989).

[87] H. Fujii, T. Inoue, Y. Andoh, T. Takabatake, K. Satoh, Y. Maeno, T. Fujita, J. Sakurai and Y. Yamaguchi, Phys. Rev. B, **39**, 6840(1989).

[88] M. Kurisu, T. Takabatake and H. Fujii, J. Magn. Magn. Mater. **90**, 469(1990).

[89] J. Tang, Jr. K. A. Gschneidner, S. J. White, M. R. Roser, T. J. Goodwin and L. R. Corruccini, Phys. Rev. B **52**, 7328(1995).

[90] F. Canepa, M. Napoletano, M. L. Fornasini and F. Merlo, J. Alloys Compd. **345**, 42(2002).

[91] H. Hegger, C. Petrovic, E. G. Moshopoulou, M. F. Hundley, J. L. Sarrao, Z. Fisk and J. D. Thompson, Phys. Rev. Lett. **84**, 4986(2002).

[92] E. G. Moshopoulou, Z. Fisk, J. L. Sarrao and J. D. Thompson, J. Solid State Chem. **158**, 25(2001).

[93] Y. F. Lian, Z. J. Shi, X. H. Zhou, et al. Chinese Chemical Letters, **10**, 425(1999).

[94] X. Lu, Z. J. Shi, B. Y. Sun, et al. Fullerenes, Nanotubes, Carbon Nanostructures, **13**, 13(2005).

[95] D. W. Cagle, S. J. Kennel, S. Mirzadeh, et al. Proceedings of the National Academy of Sciences of the United States of America, **96**, 5182(1999).

[96] D. W. Cagle, T. P. Thrash, M. Alford, et al. J. Am. Chem. Society, **118**, 8043(1996).

[97] A. Debarre, R. Jaffiol, C. Julien, et al. Phys. Rev. Lett. **91**, 085501(2003).

[98] J. Lee, H. Kim, S. J. Kahng, et al. Nature, **415**, 1005(2002).

[99] T. Tsuchiya, R. Kumashiro, K. Tanigaki, et al. J. Am. Chem. Society, **130**, 450(2008).

[100] Y. Ito, W. Fujita, T. Okazaki, et al. Chem. phys. chem. **8**, 1019(2007).

[101] J. R. Heflin, D. Marciu, C. Figura, et al. Appl. Phys. Lett. **72**, 2788(1998).

[102] W. Denk, J. H. Strickler and W. W. Webb, Science, **248**, 73(1990).

[103] M. Rubart, Circulation Research, **95**, 1154(2004).

[104] L. M. Fu, X. F. Wen, X. C. Ai, et al. Angewandte Chemie International Edition, **44**, 747(2005).

[105] A. Picot, P. L. Baldeck, A. Grichine, et al. J. Am. Chem. Society, **130**, 1532(2008).

[106] J. F. Liu, Y. G. Chen, L. Meng, et al. Polyhedron, **17**, 1541(1998).

[107] N. Yamamoto, D. Schols, E. DeClercq, et al. Molecular Pharmacology, **42**, 1109(1992).

[108] Y. Inouye, Y. Tokutake, T. Yoshida, et al. Antiviral Research, **20**, 317(1993).

[109] L. Messerle, D. Nolting, L. Bolinger, A.H. Stolpen, B.F. Mullan, D. Swenson, et al. Academic Radiology, **12**, S46(2005).

[110] S. B. Yu and A. D. Watson, Chem. Rev. **99**, 2353(1999).

[111] M. Laniado, H. J. Weinmann, W. Schorner, et al. Physiological Chemistry and Physics and Medical Nuclear Magnetic Resonance, **16**, 157(1984).

[112] H. Siitari, I. Hemmila, E. Soini, et al. Nature, **301**, 258(1983).

[113] S. Sueda, J. L. Yuan and K. Matsumoto, Bioconjugate Chemistry, **11**, 827(2000).

[114] S. Sueda, J. L. Yuan and K. Matsumoto, Bioconjugate Chemistry, **13**, 200(2002).

[115] S. W. Ryter and R. M. Tyrrell, Free Radical Biology and Medicine, **24**, 1520(1998).

[116] B. Song, G. L. Wang and J. L. Yuan, **Chemical Communications**, 3553(2005).

[117] B. Song, G. L. Wang, M. Q. Tan and J. L. Yuan, New J. Chemistry, **29**, 1431(2005).

[118] H. Tsukube and S. Shinoda, Chem. Rev. **102**, 2389(2002).

[119] E. R. Farquhar, J. P. Richard and J. R. Morrow, Inorganic Chemistry, **46**, 7169(2007).

[120] S. J. Franklin, Current Opinion in Chemical Biology, **5**, 201(2001).

[121] M. Komiyama, N. Takeda and H. Shigekawa, **Chemical Communications**, 1443(1999).

[122] Y. Matsumoto and M. Komiyama, Symp. Ser. **27**, 33(1992).

[123] N. Takeda, T. Imai, M. Irisawa, et al. Chem. Lett. **25**, 599(1996).

[124] F. S. Richardson, Chem. Rev. **82**, 541(1982).

[125] V. Alexander, Chem. Rev. **95**, 273(1995).

[126] C. Piguet and J. C. G. Bunzli, Chem. Soc. Rev. **28**, 347(1999).

[127] N. Kaltsoyannis, **Oxford Chemistry Primers 76**; Oxford University Press: Oxford, 1999.

[128] A. Trovarelli, Catal. Rev. Sci. Eng. **38**, 439(1996).

[129] J. C. G. Bunzli, Acc. Chem. Res. **39**, 53(2006).

[130] J. C. G. Bunzli and C. Piguet, Chem. Soc. Rev. **34**, 1048(2005).

[131] E. G. Moore, A. P. S. Samuel and K. N. Raymond, Acc. Chem. Res. **42**, 542(2009).

[132] J. M. D. Coey, M. Viret and S. von Molnar, Adv. Phys. **48**, 167(1999).

[133] L. H. Brixner , J. R. Barkley and W. Jeitschko, **Handbook on the Physics and Chemistry of Rare Earths**, edited by K.A.Gschneidner, Jr. and L.Eyring. (North-Holland Publishing Company, 1979), Chapter 30, pp. 610-655.

[134] A. P. Levanyuk and D. G. Sannikov, JETP, **55**, 256(1968).

[135] J. D. Axe, B. Dorner and G. Shirane, Phys. Rev. Let. **26**, 519(1971).

[136] B. Dorner, J. D. Axe and G. Shirane, Phys. Rev. B, **6**, 1950(1972).

[137] K. Aizu, J. Phys. Soc. Japan, **27**, 387(1969).

[138] E. Savaguchi and L. E. Cross, J. Appl. Phys., **44**, 2541(1973).

[139] L. E. Cross, A. Fouskova and S.T. Cummins, Phys. Rev. Letters, **28**, 812(1968).

[140] A. W. Smith and G. Burns, Phys. Lett. **28A**, 501(1969).

[141] J. R. Barkley, L. H. Brixner, E. M. Hogan and R. K. Waring, J. Ferroelectr. **3**, 191(1972).

[142] J. Sapriel and R. Vacher, J. Appl. Phys. **48**, 1191(1977).

[143] P. S. Halasyamani and K. R. Poeppelmeier, Chem. Mater. **10**, 2753(1998).

[144] D. Xue, K. Betzler, H. Hesse and D. Lammers, J. Phys. Chem. Solids **63** 359(2002).

[145] V. V. Atuchin, B.I. Kidyarov and N.V. Pervukhina, Comput. Mater. Sci. **30**, 411(2004).

[146] E. T. Khobrakova, V. A. Morozov, et al. Solid State Sci. **7**, 1397(2005).

[147] Z. A. Solodovnikova and S. F. Solodovnikov, Acta Cryst. C, **62**, 153(2006).

[148] B. I. Kidyarov and V. V. Atuchin, Ferroelectrics **360**, 104(2007).

[149] R. E. Sykora, K. Min Ok, P. S. Halasyamani and T. E. Albrecht-Schmitt, J. Am. Chem. Soc. **124**, 1951(2002).

[150] W. Zhang, X. Tao, C. Zhang, H. Zhang and M. Jiang, Cryst. Growth Des. **9**, 2633(2009).

[151] H. Y. Chang, S. W. Kim and P. S. Halasyamani, Chem. Mater. **22**, 3241(2010).

[152] X. Mateos, M. C. Pujol, F. Guell, R. Sole , J. Gavalda, M. Aguilo, F. Diaz and J. Massons, Phys. Rev. B, **66**, 214104112 (2002).

[153] B. Z. Malkin, A. A. Kaminskii, N. R. Agamalyan, L. A. Bumagina, and T. I. Butaeva, Phys. Status Solidi B, **110**, 417(1982).

[154] J. Huang, J. Loriers, P. Porcher, G. T. De Sagey, P. Caro, and C. Levy-Clement, J. Less-Common Met. **94**, 251(1983).

[155] E. Antic-Fidancev, C. Cascales, M. Lematre-Blaise and P. Porcher, J. Alloys Compd., **207-208**, 178(1994).

[156] V. S. Mironov and L. E. Li, J. Alloys Compd. **279**, 83(1998).

[157] Z. Wang, H. B. Liang, M. L. Gong and Q. Su, J. Alloys Compd. **432**, 308(2007).

[158] C. Guo, S. Wang, T. Chen, L. Luan and Y. Xu, Appl. Phys. A, **94**, 365(2009).

[159] L. Macalik, J. Hanuza, J. Sokolnicki and J. Legendziewicz, Spectrochim. Acta A, **55**, 251(1999).

[160] C. Cascales, A. M. Blas, M. Rico, V. Volkov and C. Zaldo, Opt. Mater. **27**, 1672(2005).

[161] X. Z. Li, Z. B. Lin, L. Z. Zhang and G. F. Wang, J. Cryst. Growth, **290**, 670(2006).

[162] X. Z. Li and G. F. Wang, Chin. J. Struct. Chem. **25**, 392(2006).

[163] Y. K. Voronko, K. A. Subbotin, V. E. Shukshin, D. A. Lis, S. N. Ushakov, A. V. Popov and E. V. Zharikov, Opt. Mater. **29**, 246(2006).

[164] S. V. Krivovichev, A. J. Locock and P. C. Burns, Z. Kristallogr. **220**, 10(2005).

[165] T. Sivakumar, H. Y. Chang, J. Baek and P. S. Halasyamani, Chem. Mater. **19**, 4710(2007).

[166] O. M. Basovich, E. G. Khaikina and S. F. Solodovnikov, Russ. J. Inorg. Chem. **45**, 1586(2000).

[167] E. T. Khobrakova, V. A. Morozov, A. A. Belik, B. I. Lazoryak, E. G. Khaikina and O. M. Basovich, Russ. J. Inorg. Chem. **49**, 444(2004).

[168] V. G. Grossman, B. G. Bazarov, R. F. Klevtsova, S. F. Solodovnikov, L. A. Glinskaya, K. N. Fedorov, Z. G. Bazarova, Russ. J. Inorg. Chem. **53**, 1660(2008).

[169] S. Neeraj, N. Kijima and A. K. Cheetham, Chem. Phys. Lett. **387**, 2(2004).

[170] Z. L. Wang, H. B. Liang, M. L. Gong, and Q. Su, Opt. Mater. **29**, 896(2007).

[171] M. Maczka, J. Hanuza, and A. Pietraszko, J. Solid State Chem. **154**, 498(2000).

[172] V. A. Morozov, A. V. Arakcheeva, G. Chapuis, N. Guiblin, M. D. Rossell and G. V. Tendeloo, Chem. Mater. **18**, 4075(2006).

[173] T. Ano, N. Ogata, Y. Miyaro, J. Catal. **161**, 78(1996).

[174] F. D. Smet, R. Ruiz, B. Delmon and M. Devillers, J. Phys. Chem. B, **105**, 12355(2001).

[175] V. A. Pashchenko, A. G. M. Jansen, M. I. Kobets, E. N. Khatsko and P. Wyder, Phys. ReV. B, **62**, 1197(2000).

[176] R. A. Fisher, E. W. Hornung, G. E. Brodale and W. F. Giauque, J. Chem. Phys. **56**, 193(1972).

[177] E. W. Hornung, G. E. Brodale, R. A. Fisher and W. F. Giauque, J. Chem. Phys. **56**, 5007(1992).

[178] G. E. Brodale, R. A. Fisher, E. W. Hornung and W. F. Giauque, J. Chem. Phys. **56**, 6118(1972).

[179] R. A. Fisher, E. W. Hornung, G. E. Brodale and W. F. Giauque. J. Chem. Phys. **59,**, 5796(1973).

[180] R. A. Fisher, E. W. Hornung, G. E. Brodale and W. F. Giauque, J. Chem. Phys. **69**, 2892(1978).

[181] R. A. Fisher, E. W. Homung, G. E. Brodaie and W. F. Giauque, I. J. Chem. Phys. **56**, 193(1972).

[182] E. W. Homung, G. E. Brodale, R. A. Fisher and W. F. Giauque, J. Chem. Phys. **56**, 5007(1972).

[183] G. E. Brodale, R. A. Fisher, E. W. Homung and W. F. Giauque, J. Chem Phys. **56**, 6118(1972).

[184] R. A. Fisher, E. W. Hornung, G. E. Brodale and W. F. Giauque, N.J . Chem. phys. **59**, 5796(1973).

[185] R. A. Fisher, E. W. Homung, G. E. Brodale and W. F. Giauque, I. J. Chem. Phys. **63**, 1296(1975).

[186] M. V. Mokhosoev and Z. G. Bazarova, Slozhnye oksidy molibdena i volframa s elementami IIV grupp (Mixed Oxides of Molybdenum and Tungsten with Group IIV Elements), Moscow: Nauka, 1990.

[187] A. A. Evdokimov, V. A. Efremov, V. K. Trunov, et al. Khimiya redkikh elementov. Soedineniya RZE: Molibdaty i volframaty (Chemistry of Rare Elements: Rare-Earth Molybdates and Tungstates), Moscow: Nauka, 1991.

[188] K.I Petrov, M. E. Poloznikova, K. T. Sharipov and V. V. Fomichev, Kolebatelnye spektry molibdatov i volframatov (Vibrational Spectra of Molybdates and Tungstates), Tashkent: FAN, 1990.

[189] V. N. Kurlov, Crystal Growth of Rare-Earth Molybdates, **Cand. Sci. (Technol.) Dissertation**, Chernogolovka: Inst.of Solid State Physics, Russ. Acad. Sci., 1992.

[190] Gmelin Handbook, Mo Supplement: Compounds with Oxygen, 1983, pp. 3443.

[191] Gmelin Handbook, Mo Supplement: Compounds with Oxygen, 1991, vol. B8, chapter 3.3, pp. 14.

[192] R. L. Smith and G. S. Rohrer, J. Solid State Chem. **124**, 104(1996).

[193] E. Broclawik and D. R. Salahub, Int. J. Quantum Chem. **26**, 393(1992).

[194] J. C. Edwards and P. D. Ellis, Solid-State, **7**, 2117(1991).

[195] Z. Sojka, K. Dyrek, P. C. Roberge and M. Che, Pol. J. Chem. **65**, 643(1991).

[196] S. O. Daminova, Synthesis, Properties, and Structure of Rare-Earth Molybdates, **Cand. Sci. (Chem.) Dissertation**, Moscow: Russ. Univ. of Peoples Friendship, 1999.

[197] J. C. Volta and J. L. Portefaix, Appl. Catal. **18**, 1(1985).

[198] R. L. Smith and S. R. Gregory, J. Catal. **184**, 49(1999).

[199] G. V. Bazuev and G. P. Shveikin, **Slozhnye oksidy elementovs dostraivayushchimisya d- i f-obolochkami** (Mixed Oxides of Elements with Partially Filled d and f Shells), Moscow: Nauka, 1985.

[200] W. H. McCarroll, M. Borgia, K. V. Ramanujachary, et al. J. Solid State Chem. **138**, 7(1998).

[201] K. V. Ramanujachary, M. Greenblatt, W. H. McCarroll and J. B. Goodenough, Phys. Rev. B, **66**, 2141041(2002).

[202] B. K. Ponomarev, V. D. Negrii, B. S. Red'kin and Yu. F. Popov, J. Phys. D: Appl. Phys. **27**, 1995(1994)

[203] Springer Handbook of crystal Growth, 1667(2010).

[204] L.H. Brixner, J. Cryst. Growth, **18**, 297(1973).

[205] B. joukoff and G. Grimouille, J. Crys. Growth, **43**, 719(1978).

[206] S. Bhat, P.N. Kotru and M.L. Koul, Mat. Sci. and Eng. B, **34**, 138(1995).

[207] B. R. Pumplin, Crystal Growth, (Pergamon Press Oxford), 1980.

[208] S. Pandita, V. Hangloo, K. K. Bamzai, P. N. Kotru and N. Shani, int. J. inorg. Mat. **3**, 675(2001).

[209] S. Pandita, V. Hangloo, K. K. Bamzai, P. N. Kotru and Neera Shani, Bull. Mat. Sci. **24**, 435(2001).

[210] S. Pandita, V. Hangloo, K. K. Bamzai, P. N. Kotru and N. Shani, Cryst. Growth and Design, **3**, 753(2003).

[211] K. Tang, F. Li, Cryst. Growth & Design, 2006, (ACS Publications).

[212] W. Koechner, Solid State Laser Engineering, 2006.

[213] Y. K. Voronko & K. A. Subbotine, Optical Materials, **29**, 246(2006).

[214] D. Zhoa, Z. Lin, L. Zhang & G. Wang, J. Phys. D: Appl. Phys. **40**, 1018(2007).

[215] N. Zhang, W. Bu, Y. Xu, D. Jiang & J. Shi, J. Phys. Chem C, **111**, 5014(2007).

[216] G. Cai, J. Wang & H. Zhang, Cryst. Res. & tech. **44**, 1001(2009).

[217] J. H. Magill, J. Mater. Sci. **36**, 3143 (2001).

[218] G. Ryschenkow, G. Faivre, J. Non-Cryst. Solids, **87**, 221(1988).

[219] J. Bisault, G. Ryschenkow, G. Faivre, J. Cryst. Growth, **110**, 889 (1991).

[220] P. F. James, **Advances in Ceramics**, Vol. 4, eds. J. H. Simmons, D. R. Uhlmann and G. H. Beagle (American Ceramic Society, Westerville, 1982) pp. 1.

[221] H. W. Morse, C. H. Warren, and J. D. H. Donnay, Am. J. Sc. **23**, 421 (1932).

[222] H. W. Morse, J. D. H. Donnay, Am. J. Sci., **23**, 440(1932).

[223] J. L. Hutter, J. Bechhoefer, Phys. Rev. E **59**, 4342 (1999).

[224] J. H. Magill, D. J. Plazek, J. Chem. Phys. **46**, 3757 (1967).

[225] P. J. Phillips, **Handbook of Crystal Growth**, Vol. 2 (Elsevier, Amsterdam, 1993) Chapter 18.

[226] H. D. Keith, F. J. Padden, J. Appl. Phys. **35**, 1270 (1964).

[227] H. D. Keith, F. J. Padden, J. Appl. Phys. **34**, 2409 (1963).

[228] F. Khoury, J. Res. Nat. Bur. Stand. A **70**, 29 (1966).

[229] J. R. Ojeda, D. C. Martin, Macromol. **26**, 6557 (1993).

[230] I. L. Hosier, D. C. Bassett, A. S. Vaughan, Macromol. 33, 8781 (2000).

[231] D. R. Norton, A. Keller, Polymer, **26**, 704 (1985).

[232] D. C. Bassett, **Principles of Polymer Morphology**; Cambridge University Press: Cambridge, UK, 1981.

[233] H. D. Keith and F. J. Padden, J. Appl. Phys. **34**, 2409(1963).

[234] Y. G. Lei, C. M. Chan, Y. Wang, K. M. Ng, Y. Jiang and L. Lin, Polymer, **44**, 4673(2003).

[235] L. Li, C. m. Chan, K. L. Yeung, J. X. Li, K. M. Ng and Y. Lei, Macromolecules, **34**, 316(2001).

[236] H. W. Morse, C. H. Warren and J. D. H. Donnay, Am. J. Sci. **223**, 421(1932).

[237] H. W. Morse and J. D. H. Donnay, Am. J. Sci. **223**, 440(1932).

[238] H. W. Morse and J. D. H. Donnay, Am. Mineral. **21**, 391(1936).

[239] N. I. Krasnova and T. G. Petrov, **Genesis of Mineral Individuals and Aggregates**; Nevskii Kurier: St. Petersburg, Russia, 1997 (in Russian).

[240] A. D. Fowler, B. Berger, M. Shore, M. I. Jones and J. Ropchan, Precambr. Res. **115**, 311(2002).

[241] R. K. Smith, R. L. Tremallo and G. E. Lofgren, Am. Mineral. **86**, 589(2001).

[242] K. Iwamoto, S. I. Mitomo, M. Seno, J. Colloid Interface Sci. **102**, 477(1984).

[243] K. Iwamoto, S. I. Mitomo, J. I. Fukide, T. Shigemoto and M. Seno, Bull. Chem. Soc. Jpn. **55**, 709(1982).

[244] C. Vasile (2000). **Handbook of polyolefins**, CRC Press. p. 183.

[245] L. C. Sawyer, D. T. Grubb, G. F. Meyers (2008). **Polymer microscopy**, Springer. p. 5.

Chapter 5

Growth and Characterization of Holmium Molybdate crystals

5.1 Introduction

A large number of crystals have been grown at ambient temperature by the gel diffusion technique (as already discussed in previous chapter), which may be classified as a low temperature solution technique. The growth at lower temperatures is expected to yield crystals with minimum defects. Although the gel technique of growing crystals proves to be less expensive and advantageous, this method cannot yield crystals of a large size. If one is able to obtain a crystal of optimum size suitable for a particular scientific study, the purpose is served. The gel method is the most acceptable one, and one has only to attempt to grow crystals of size that may be optimum for characterization by a particular probe. On the other hand, high temperature techniques are usually expensive and may not be within the reach of every laboratory. Furthermore, high growth temperatures become sources of increased thermal stress, as a result of which the crystals may contain more

defects.

Keeping in view the versatility of the gel technique in obtaining a large number of crystals, it was thought worthwhile to grow the crystals of holmium molybdate by this method for scientific investigations. It is an established fact that the physical and chemical properties of materials are very sensitive to preparation condition such as sintering temperature, time, and type of additives. But, the aim of present work is to perform an in-depth study of the changes that are brought about in the physical and chemical properties of pure holmium molybdate crystals by different growth parameters. So, it was thought worthwhile to grow them in pure form.

5.2 Experimental Procedure for Growth of Holmium Molybdate Crystals

The experiments were conducted to grow pure crystals of Holmium molybdates using a simple technique, known as gel diffusion technique. The crystals were grown in a crystallizer consisting of a single glass tube of length 15 cm and diameter 2.5 cm. The glass tube was filled three-fourth of its volume by one type of reactant, called lower reactant (LR), encapsulated in the gel network and one-fourth of its volume was filled up with other reactant, called upper reactant (UR).

The experiments were conducted in two types of gels: silica gel and agar-agar gel. The silica gel is an inorganic gel, while as agar-agar gel is an organic gel. The experiments conducted in agar-agar gel did not yield any fruitful result, so most of the work was conducted in silica gel. The silica

gel was prepared by thoroughly mixing the solution of sodium metasilicate (Na_2SiO_3) of desired molarity with a solution of ammonium molybdate. The ammonium molybdate solution was prepared by dissolving equal amounts of ammonium molybdate ($(NH_4)_6Mo_7O_{24}$) and ammonium nitrate (NH_4NO_3) each of 5 g (say) in distilled water. To this solution, 15 mL of concentrated nitric acid (HNO_3) was slowly added. Finally, distilled water was added to this solution until the whole volume become 250 mL. The gel of desired pH so prepared was then allowed to set in the crystallizer and aged for desired time. The concentrated nitric acid was added to fix the pH of the gel to a desired value. The gelling reaction is based on the hydrolytic process given by the following reaction

$$Na_2SiO_3 + 3H_2O \rightarrow Na_4SiO_4 + 2NaOH$$

that must be acidified to produce a gel.

After the gel was properly set and aged, the upper reactant holmium nitrate ($HoNO_3$) of desired molarity was poured drop by drop along the sides into the crystallizer. The upper reactant was slowly added to prevent the gel breakage. The crystallizer was then left for a desired period (known as growth period) at a particular temperature. The experiments were conducted at room temperature and at $45\,^{\circ}C$. The higher temperature was achieved by using a temperature controlled water bath.

5.3 Effect of Various Growth Parameters

Series of experiments were conducted with an aim to grow good quality crystals suitable for characterization and to observe the effects of various

factors on the nucleation as well as on growth of holmium molybdate crystals. The experiments were conducted for different gel age, gel pH, temperature and concentration of upper and lower reactants. It was observed that the holmium molybdate crystals invariably grow in the form of spherulites under all conditions of growth. But, these factors affected both nucleation process and growth of the crystals. The effects of these factors and hence the results as observed from the experiments are discussed below.

5.3.1 Effect of Gel Age

The gel age is a period for which the gel in a crystallizer is left undisturbed before adding upper reactant to it. The experiments were conducted for the gel age of 2 days, 5 days, 10 days, 15 days and 30 days. It was observed that with the increase in gel age the nucleation density of holmium molybdate crystals decreases. This may be because the gel age affects the strength of gel, as higher gel age results in hard gel, while as lower gel age results in weak gel. Due to which there is a gel breakage and fast diffusion in case of weak gel and slow diffusion in case of hard gel. Thus affected the nucleation density of the holmium molybdate crystals.

5.3.2 Effect of Gel pH

Gel pH plays a very important role as for as growth of crystals in silica gel is concerned. The experiments were conducted at various gel pH and the results are given in table 5.1. It was observed that at lower pH (< 4.5) there was either no precipitation or very slow precipitation which results mostly in the formation of Liesegang rings. On the other hand at higher pH (> 5.4)

Table 5.1: Effect of gel pH on growth of holmium molybdate crystals.*

Serial No.	Gel pH	Upper Reactant (in moles)	Results
1	4	0.05	No ppt. no crystals formed
		0.1	Only Liesegang Rings were observed
		0.2	Only Liesegang Rings were observed
		0.5	Only fast ppt. no crystal growth
		1.0	Only fast ppt. no crystal growth
2	4.5	0.05	No ppt. no crystals formed
		0.1	Only Liesegang Rings were observed
		0.2	Only Liesegang Rings were observed
		0.5	Only fast ppt. no crystal growth
		1.0	Only fast ppt. no crystal growth
3	5	0.05	No ppt. no crystals formed
		0.1	Tiny spherulites were observed
		0.2	Normal size ($\sim 2mm$) spherulites were obsersed
		0.5	Only fast ppt. no crystal growth
		1.0	Only fast ppt. no crystal growth
4	5.2	0.05	No ppt. no crystals formed
		0.1	Normal size ($\sim 2mm$) spherulites were observed
		0.2	Normal size ($\sim 2mm$) spherulites were observed
		0.5	Only fast ppt. no crystal growth
		1.0	Only fast ppt. no crystal growth
5	5.4	0.05	No ppt. no crystals formed
		0.1	Only fast ppt. no crystal growth
		0.2	Only fast ppt. no crystal growth
		0.5	Only fast ppt. no crystal growth
		1.0	Only fast ppt. no crystal growth

*Mean temperature of growth = $45\,^{\circ}C$, Age of gel = 2 days,
Lower reactant = ammonium molybdate (0.16 M), Upper reactant = holmium nitrate

the precipitation was very fast and there was neither crystals nor Liesegang rings. So, It was concluded that the gel pH in the range of 4.5 and 5.4 was very conducive for the growth of holmium molybdate crystals. In the pH range 4.5 to 5.4 a few to large number of crystals were observed to grow inside the gel.

5.3.3 Effect of Temperature

The temperature is another very important factor for the growth of crystals as well as for gel setting. Its effect on nucleation density is profound which is clear from the figure 5.1, which shows the nucleation density of holmium molybdate crystals at two different temperature.

It is reported that the free energy of formation of a critical nucleus increases with the increase in temperature, but the degree of supersaturation decreases [1,2]. In the present case it was observed that at temperature near to $0\,^{\circ}C$ the gel was hardly able to set and was weak. Also for high temperatures above $50\,^{\circ}C$, the gel was observed to be weak. The feasible temperature for good strength gel, found to be around room temperature. As for as the growth of crystals is concerned, it was observed that at lower temperature ($\sim 10\,^{\circ}C$) the diffusion rate was very slow, there were few nucleation sites and it takes longer time for holmium molybdate crystals to grow. But at higher temperature ($\sim 45\,^{\circ}C$) the diffusion rate was observed to be fast, and as such there were large number of nucleation sites and the crystals were observed to grow in 3 to 4 days.

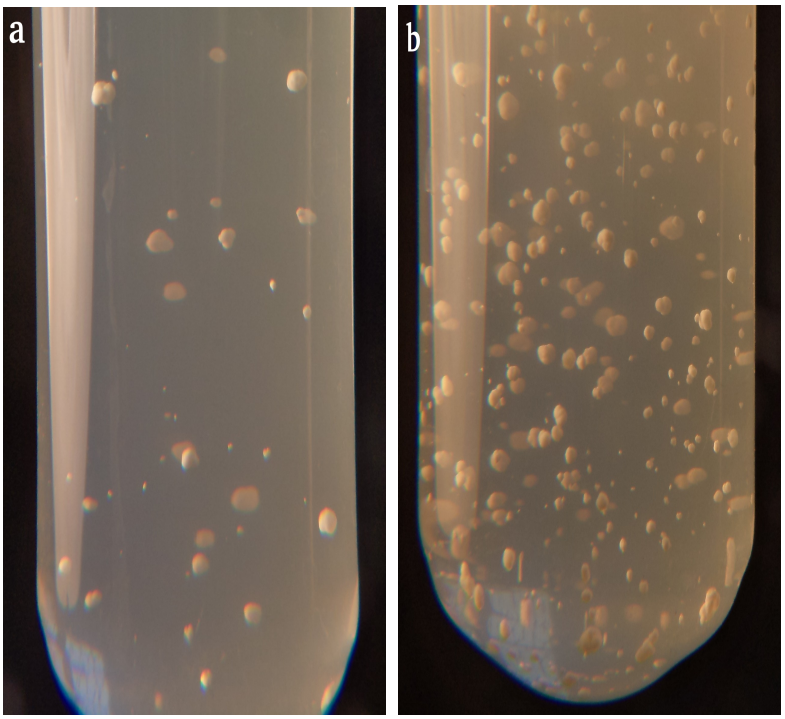

Figure 5.1: Effect of temperature on nucleation density of holmium molybdate crystals: (a) at lower temperature (b) at higher temperature.

5.3.4 Effect of Change in Concentration of Upper Reactant

In order to study the effect of variation of upper reactant ($HoNO_3$) concentration on the nucleation and growth process of holmium molybdate crystals, the upper reactant of different concentrations was used. It was observed that the variation in concentration of upper reactant has a profound effect on the overall crystallization process, though the morphology remains same, that is spherulitic. The results obtained due to the variation in the concentration of upper reactant are shown in table 5.2.

It was observed that within few hours of pouring of upper reactant, there

Table 5.2: Effec of upper reactant conc. on growth of holmium molybdate.*

Serial No.	Upper Reactant (in moles)	Gel pH	Results
1	0.05	4.0	No ppt. no crystals formed
		4.5	No ppt. no crystals formed
		5.0	No ppt. no crystals formed
		5.2	No ppt. no crystals formed
		5.4	No ppt. no crystals formed
2	0.1	4.0	Only Liesegang Rings were observed
		4.5	Only Liesegang Rings were observed
		5.0	Tiny spherulites were observed
		5.2	Normal size ($\sim 2mm$) spherulites were found
		5.4	Only fast ppt. no crystal growth
3	0.2	4.0	Only Liesegang Rings were observed
		4.5	Only Liesegang Rings were observed
		5.0	Normal size ($\sim 2mm$) spherulites were found
		5.2	Normal size ($\sim 2mm$) spherulites were found
		5.4	Only fast ppt. no crystal growth
4	0.5	4.0	Only fast ppt. no crystal growth
		4.5	Only fast ppt. no crystal growth
		5.0	Only fast ppt. no crystal growth
		5.2	Only fast ppt. no crystal growth
		5.4	Very fast ppt. no crystal growth
5	1.0	4.0	Only fast ppt. no crystal growth
		4.5	Only fast ppt. no crystal growth
		5.0	Only fast ppt. no crystal growth
		5.2	Only fast ppt. no crystal growth
		5.4	Very fast ppt. no crystal growth

*Mean temperature of growth = $45\,^{\circ}C$, Age of gel = 2 days,
Lower reactant = ammonium molybdate (0.16 M), Upper reactant = holmium nitrate

appeared a white precipitation at the gel-upper reactant interface. This is the spurious nucleation and the actual crystallization takes at much longer time. This precipitate vanishes into the gel column with the passage of time, leaving behind a transparent region just below the gel-upper reactant interface where nucleation occurs.

Gels possess the property of adsorption, which is different for different gels. At the gel-upper reactant interface where the upper and the lower reactants come in immediate and direct contact leading to higher rate of reaction, holmium molybdate did not get enough time for regular growth into crystals initially and so particles get readily adsorbed by the gel which gives rise to a column of creamish white colloidal precipitate. This reaction generates acid. The reaction proceeds further as the upper reactant diffuses further into the gel, liberating more and more acid. The liberation of acid decreases the effective pH around reaction site, which in turn decreases the force of adsorption.

As the reaction proceeds, a stage is reached when the number of holmium ions reacting with the lower reactant per unit time get reduced which eventually results into decreased liberation of acid, thus leading to decreased variation of pH. The precipitate now becomes stationary. At this stage, the pH of the gel is reduced to a value where the force of adsorption among the colloidal particles decrease to minimum, rendering colloidal particles free so that they can diffuse to the growth sites. Every colloidal particle can act as a nucleation site for the growth of a crystal. By probability, a few nuclei can grow gradually. The smaller crystals dissolve more easily than the large ones because of the large volume of surface to volume ratio and this assists

the large ones to grow. That the crystal grows at the expense of the colloidally dispersed particles becomes clear from the experimental observation of complete disappearance of the white precipitate column. The formation of crystals out of the colloidal precipitate has also been explained by Abdul Kadar [3] and Kotru [4-6] for other crystals.

It is clear from the table 5.2 that there is no diffusion and hence no crystal growth for concentration of upper reactant below 0.1M. For concentration of upper reactant equal and above 0.1M there is a diffusion of upper reactant into the gel. It was observed that for upper reactant concentration between 0.1 and 0.5M crystal formation takes place, provided the gel pH is between 4.5 and 5.4. Very fast precipitation and no crystal formation were observed for upper reactant concentrations 0.5M or more. So the upper reactant concentration conducive for the crystal formation is between 0.1 and 0.5M.

5.3.5 Effect of Change in Concentration of Lower Reactant

The concentration of lower reactant also plays a very significant role in nucleation as well as in growth process. It was observed that higher concentration of lower reactant results in fast reaction, while as lower concentration of lower reactant results in slow reaction. However, change in lower reactant concentration does not change the morphology of the crystals, but does affect the nucleation density and size of crystals. It is observed that whatever may be the concentration of lower reactant the crystallization starts only for solutions of pH higher than 4.

5.3.6 Liesegang Ring Formation

The Liesegang ring formation was another very important effect observed during the experimentation process. It was observed that the ring formation was very much visible for gel with pH below 5. For the gel with pH higher than 5, there was fast precipitation and no ring formation. The change in concentration of upper reactant also affects the ring formation. It was observed that the ring formation takes place for the upper reactant concentration between 0.1 and 1M. For upper reactant concentration below 0.1M as well as for above 1M there is no ring formation. The Liesegang ring formation is a common process in gels during the growth process, as has been reported by many authors [7-10].

5.4 Characterization of Holmium Molybdate Crystals

The solids are characterized by nearly perfect periodicity of atomic structure. The geometric regularity of atomic structure provides a simple picture of a crystal and helps a lot in gaining the knowledge of the physical properties of the solid [11,12]. In a crystalline solid, the atoms are arranged in a regular manner, i.e. the atomic array is periodic. Each atom is at regular intervals along arrays in all directions of the crystal. The crystalline solid has directional properties, which are also called isotropic or anisotropic substances accordingly [13-15]. The characterisation and the studies of the properties of crystals of materials are very important, in the context of technological applications. Characterization of crystals has become an integral part of crystal

growth and process development. These studies reveal the perfection of the crystals, influence of the methods on the growth of materials and identity of the grown material. Study of the crystal habit forms an important part as it influences the physical properties.

The laboratory-grown crystals of holmium molybdate were characterized by different physio-chemical techniques of characterization. These were characterized by scanning electron microscopy (SEM), powder X-ray diffraction (XRD), Energy-Dispersive Analysis of X-rays (EDAX) and Thermal methods (TGA/DTA).

5.4.1 Energy Dispersive Analysis of X-rays (EDAX)

In order to confirm the presence of heavy elements, like holmium (Ho) and molybdenum (Mo) in the grown sample which is assumed to be holmium molybdate, the crystals were characterized by EDAX. In the present work elemental analysis of gel grown crystals, was carried out by using JEOL, JED-2300 energy dispersive spectrometer, attached to a scanning electron microscope JEOL JSM-6390LV. Figure 5.2 shows EDAX spectrum of the sample and Table 5.3 shows the values of its main elemental content as measured by the EDAX technique. The EDAX pattern shows the presence of holmium and molybdenum in the sample. So it confirms the laboratory-grown sample to be holmium molybdate.

On the basis of experimental quantitative estimation of elements done by EDAX (table 5.3), it is suggested that the chemical formula of the grown crystals may be $NH_4Ho(Mo_8O_{26}).nH_2O$ which is an octamolybdate rare earth compound. From this molecular formula, considering n=7 i.e. the

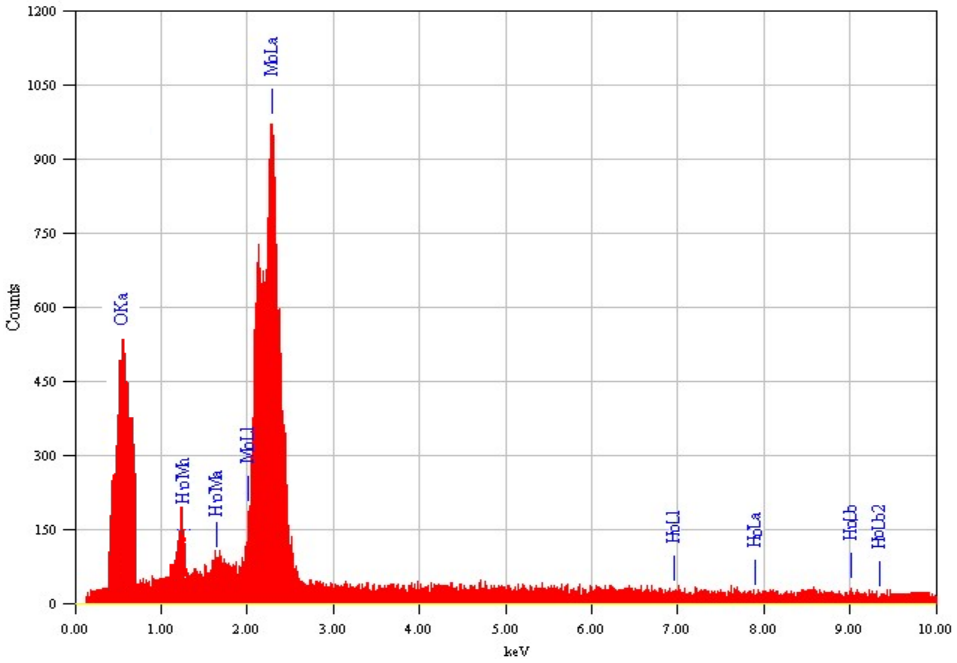

Figure 5.2: EDAX pattern of holmium molybdate crystals.

Table 5.3: Elemental analysis of holmium molybdate crystals.

Element	Energy (KeV)	Mass %age	Atomic %age
Oxygen	0.525	36.27	78.28
Molybdenum	2.293	55.63	20.02
Holmium	1.347	8.09	1.69

number of water molecules attached as seven, the values (mass %age) of oxygen, molybdenum and holmium are 36.15% , 52.56% and 11.29% respectively. These values are close with the values measured by EDAX (table 5.3). The growth of β-octamolybdate supported rare earth metal complexes, $[NH_4]_2[\{Gd(DMF)_7\}_2(\beta{-}Mo_8O_{26})][\beta{-}Mo_8O_{26}]$ and $[NH_4][La(DMF)_7(\beta{-}$

$Mo_8O_{26})$], has been reported in [16], which supports the laboratory-grown crystals could be $NH_4Ho(Mo_8O_{26}).7H_2O$.

5.4.2 SEM Studies

The holmium molybdate crystals were analyzed under polarizing optical microscope. Figure 5.3 shows the external morphology of the lab-grown crystals. The morphology was observed to be that of spherulites, which are polycrystalline in nature.

Figure 5.3: Spherulites of holmium molybdate crystals.

The in-depth external morphology of holmium molybdate crystals was studied by using scanning electron microscope (SEM). The morphological studies were made by using the Hitachi S-3000H electron microscope. The crystalline samples were coated with gold, in order to enhance its conductivity, using a Bal-Tec SCD004 sputter coating unit. Both apparatus are available at the University Instrumentation Centre (USIC), University of Kashmir, Srinagar.

The SEM micrographs, obtained from the characterization of holmium molybdate crystals, grown at room temperature, are shown in Fig. 5.4(a-e). It is evident from the SEM pictures that the material has grown as well developed spheres. As already discussed in previous chapter, a well developed spherulite to be of spherical shape is considered as an ideal case, but this work has shown that ideal things are not far from reality. Figure 5.4(a) shows the shape of spherulites at a magnification of 210x, figure 5.4(b) shows at 800x, figure 5.4(c) shows at 1500x, figure 5.4(d) shows at 4700x and figure 5.4(e) shows at 25000x. It is clear from the pictures that these spherulites are not single units, but are composed of crystallites. Generaly, crystallites that assemble as spherulites in the aggregate are often needle-like, but other habits are also observed. Plank-like crystallites (flattened needles) are not infrequent and plate-like crystallites are very rare. But in the present case, as is evident from the SEM-micrographs, the crystallites that form the surface of the spherulites are plate-like with an average thickness of about 20 nm. Thus the spherulites grown at room temperature were observed to be composed of nano-plates.

The spherulites that were grown at elevated temperature of $45\,^{\circ}C$ (keeping other factors same), were observed to be of different morphology. The crystallites that form the surface of spherulites are quite different from what is observed for spherulites grown at room temperature. Figure 5.5(a-b) shows the SEM micrographs of holmium molybdate crystals that were grown at a temperature of $45\,^{\circ}C$. Figure 5.5(a) shows the shape of spherulites at a magnification of 10000x and figure 5.5(b) shows at a magnification of 20000x. The crystallites that form the surface of the spherulites in this case are not

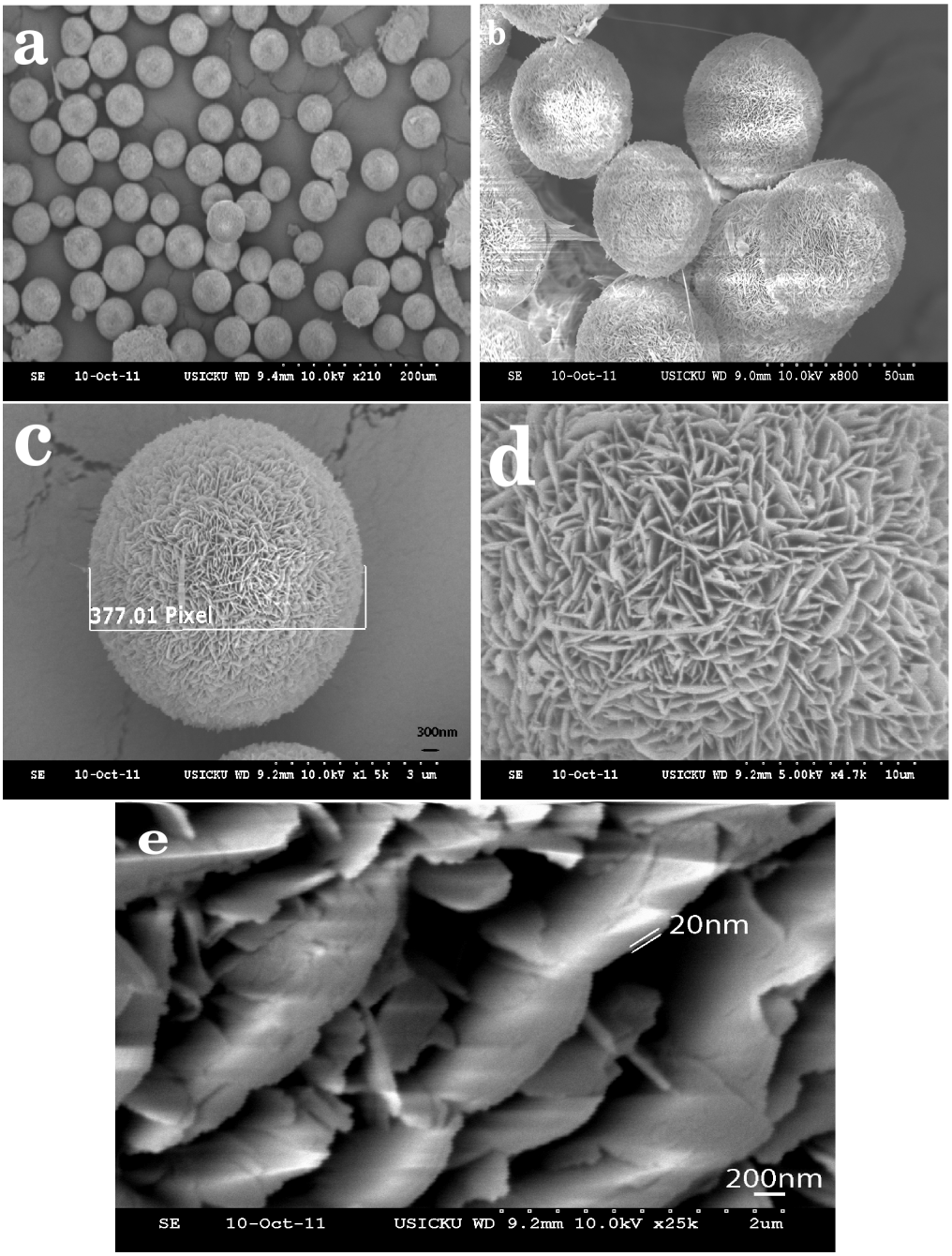

Figure 5.4: SEM images of holmium molybdate, grown at room temperature, at a magnification of: (a) 210x, (b) 800x, (c) 1500x, (d) 4700x and (e) 25000x.

plate-like, but rod shaped. Thus the spherulites grown at higher temperature were observed to be composed of nano-rods with an average diameter of 80 nm and an average transverse length of about 300 nm.

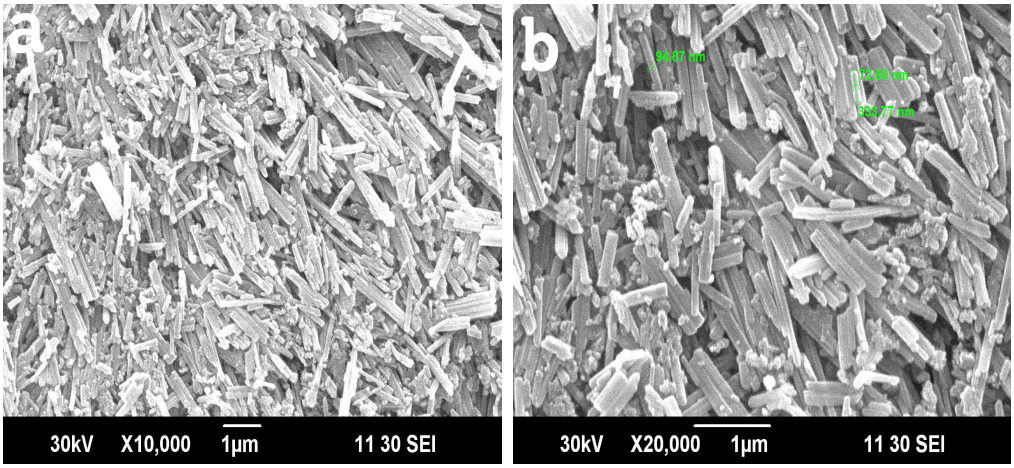

Figure 5.5: SEM images of holmium molybdate crystals, grown at higher temperature, at a magnification of: (a) 10000x and (b) 20000x.

Rare-earth nanocrystals with controllable shapes and sizes have received intense research attention during the past few years [17-28] because of their potential applications in optics [17-19], optoelectronics, biological labeling [20,21], catalysis fields [22] etc. It is expected that with reduced dimensionalities, the movement of electrons and photons in rare-earth nanocrystals would be confined in two and/or all directions and then lead to enhanced optical and magnetic properties in a manner similar to that of typical systems such as II-VI semiconductor nanocrystals [29-33]. This is particularly important for the exploration of new research and application fields on the basis of the novel properties of rare-earth nanocrystals. However, there still remains much to be carefully addressed in the rare-earth nanocrystal system, especially for the general principle in shape and size control, which may provide

possibilities for systematically investigating the size- and shape-dependent properties on the nanoscale.

To obtain desired nanocrystals of rare earth compounds, the methods such as sol-gel method [34,35,36], hydrothermal synthesis [37,38], combustion [39], coprecipitation [40], and the Pechini method [41,42], at a relatively low temperature, have been extensively adopted. In comparsion to these methods, the gel diffusion method of crystal growth, used in the present work, is very simple and inexpensive. This method, though needs further research in order to have control over the size and shape of crystals, could be a very efficient method for the growth of nanocrystals.

5.4.3 X-ray Diffraction Studies

The most widespread use of powder diffraction is the identification and characterization of crystalline solids, each of which produces a distinctive diffraction pattern. Both the positions (corresponding to lattice spacings) and the relative intensity of the lines are indicative of a particular phase and material, providing a "fingerprint" for comparison.

X-ray powder diffraction data of the present sample were collected at room temperature and under ambient conditions with Bruker AXS D8 Advance powder diffractometer using Cu K_α ($\lambda = 1.5406$ $\mathring{A}$) radiation and an applied voltage and current of 40 kV and 35 mA, respectively. The data were recorded in the range of $3^0 \leq 2\theta \leq 80^0$ with a stepped scan rate of 0.020^0 per step and a count time of 31.2 seconds per step. The X-ray diffraction pattern of the sample is shown in figure 5.6. The series of sharp peaks present in the pattern clearly shows the crystalline nature of the material.

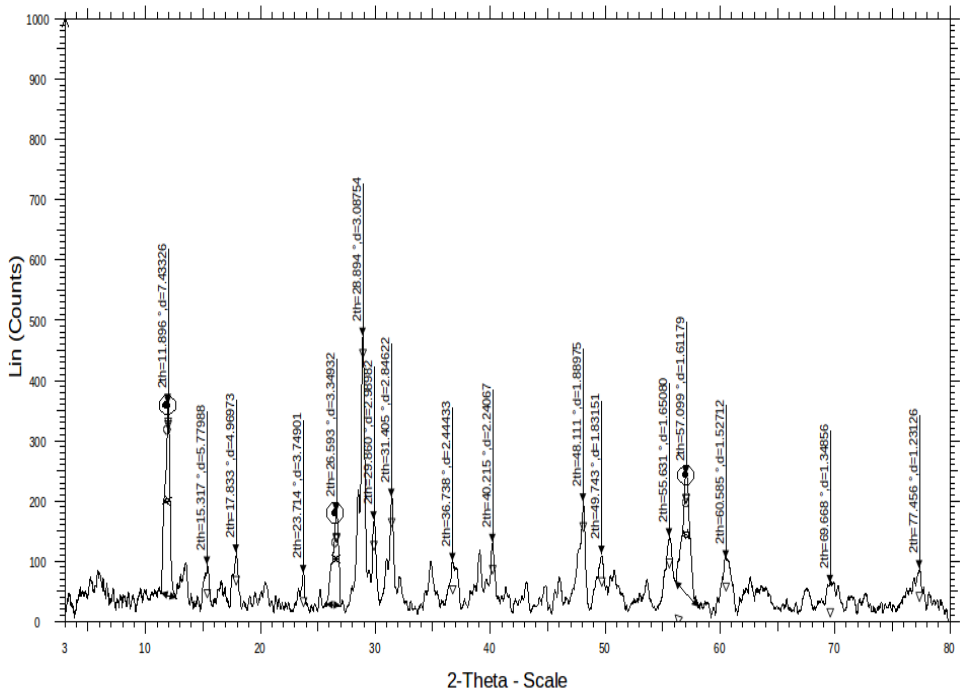

Figure 5.6: Powder XRD pattern of holmium molybdate crystals.

The position of a diffraction peak is independent of the atomic positions within the cell and entirely determined by the size and shape of the unit cell of the crystalline phase. Each peak represents a certain lattice plane and can therefore be characterized by a Miller index. The observed 'd' values for different 2θ with hkl indices of the corresponding planes for the crystal are given in Table 5.4. From the powdered X-ray data, the various planes of reflections were indexed using Crysfire program [43] and the lattice parameters were evaluated. The data revealed that the structure of the as-grown holmium molybdate crystals is triclinic belonging to the space group of P1 with a = 7.80 $\mathring{A}$, b = 9.01 $\mathring{A}$, c = 13.54 $\mathring{A}$, $\alpha = 76.39^0$, $\beta = 131.38^0$ and $\gamma = 76.73^0$ as cell parameters.

Table 5.4: X-ray powder diffraction data (indexed) of holmium molybdate crystals.

$2\theta(deg)$	d values	hkl indices
11.896	7.43326	0 -1 0
15.317	5.7798	-1 -1 0
17.833	4.96973	1 0 0
23.714	3.74901	1 2 1
26.593	3.34932	1 0 1
28.894	3.08754	-1 -2 2
29.860	2.98982	-1 2 4
36.462	2.84622	-2 -3 2
36.738	2.44433	0 1 4
40.216	2.24067	-2 1 6
48.111	1.88975	1 2 4
49.743	1.83151	-4 0 4
55.631	1.65080	-3 -4 4
57.099	1.61179	-2 -3 5
60.585	1.52712	-1 -4 3
69.668	1.34856	1 5 6
77.455	1.23126	1 4 7

5.4.4 Calculation of Size of Crystallites

The approximate value of the size of the crystallites can be calculated from Scherrer equation [44] which correlates the size of sub-micrometre particles, or crystallites, in a solid to the broadening of a peak in a diffraction pattern.

In the Scherrer equation,

$$\tau = \frac{K\lambda}{\beta \cos\theta} \tag{5.1}$$

where K is the shape factor, λ is the x-ray wavelength, β is the line broadening at half the maximum intensity (FWHM) in radians, and θ is the Bragg angle; τ is the mean size of the ordered (crystalline) domains, which may be smaller or equal to the grain size. The dimensionless shape factor has a typical value of about 0.9, but varies with the actual shape of the crystallite. The Scherrer equation is limited to nano-scale particles. It is not applicable to grains larger than about 0.1 μm, which precludes those observed in most metallographic and ceramographic microstructures.

From the diffraction pattern of holmium molybdate crystals, we have the averages of

$\theta = 31.8607$ deg $= 0.5563$ rad

$\beta = 0.5713$ deg $= 0.0099$ rad

$\lambda = 1.5406$ $\mathring{A} = 0.15406$ nm

K $= 0.9$

Substituting the above values in equation 5.1, the mean size of the crystallites, $\tau =$ 16.3643 nm.

So, the crystallites that assemble as spherulites in the aggregate are of nano range which confirms the information already revealed by the SEM images of the sample.

5.4.5 Thermal Gravimetric Analysis

Thermogravimetric analysis (TGA) and differential thermal analysis (DTA) are very important to throw light on the thermal stability of the substances.

These are utilized for the characterization of decomposition behaviour of the material. TGA/DTA of holmium molybdate crystals ($NH_4Ho(Mo_8O_{26}).nH_2O$) are recorded by Perkin Elmer Diamond Analyser using the Nitrogen atmosphere.

The thermogravimetric analysis (TGA), derivative TG (DTG) and differential thermal analysis (DTA) curves of the sample are depicted in figure 5.7, figure 5.8 and figure 5.9 respectively. A powdered sample weighing 11.214 mg was used for the analysis. The analysis was carried out at a heating rate of $10\,^{\circ}C/$ minute for a temperature range of $40 - 1050\,^{\circ}C$. The TGA curve shows that it is a multi-step decomposition process. It is clear from the TGA curve that the material starts decomposing at around $50\,^{\circ}C$ and continues even after reaching the maximum temperature of $1000\,^{\circ}C$.

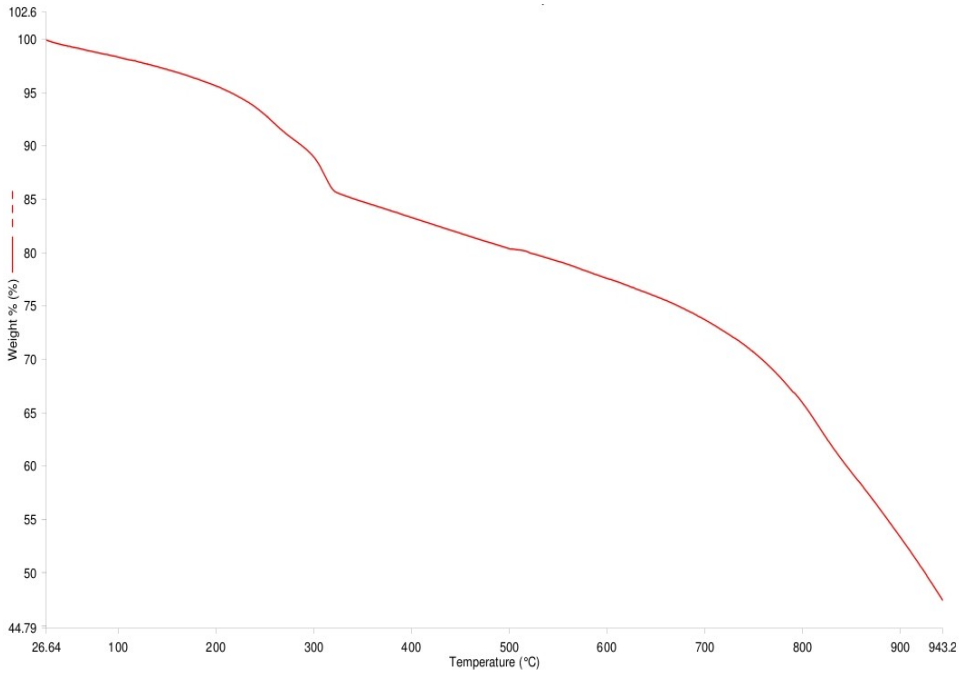

Figure 5.7: TGA curve of holmium molybdate crystals.

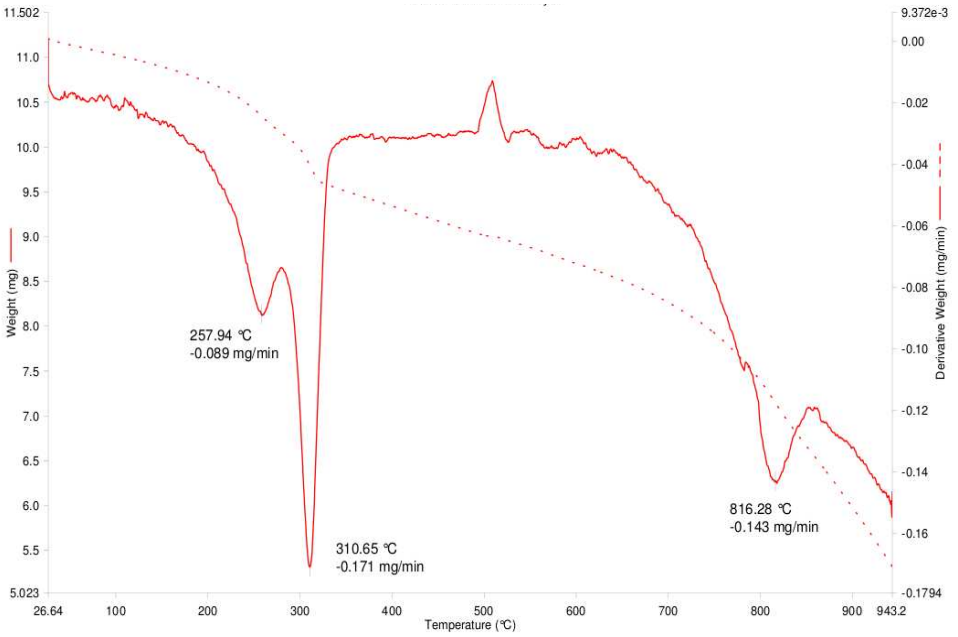

Figure 5.8: DTG curve of holmium molybdate crystals.

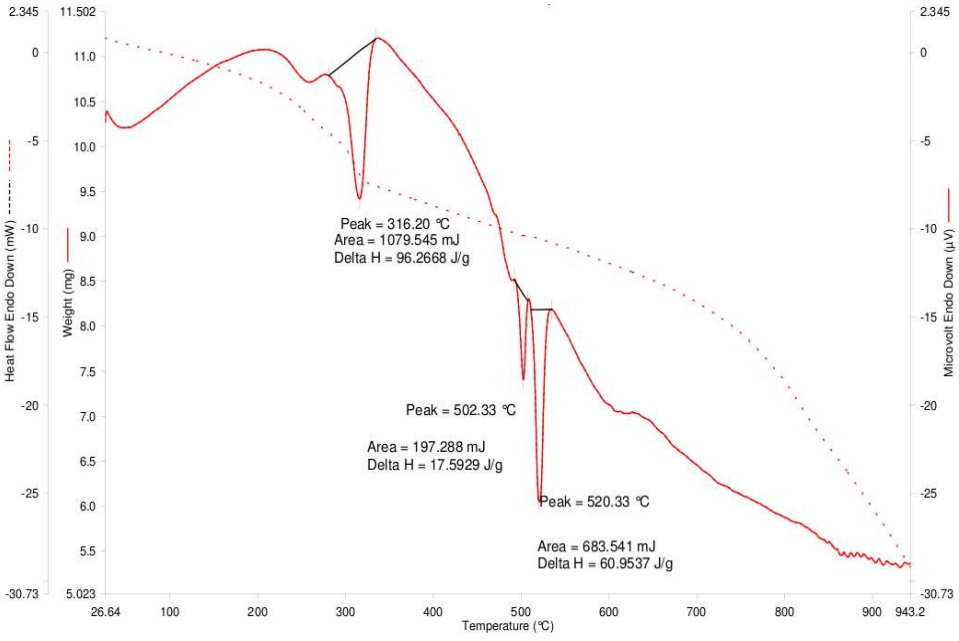

Figure 5.9: DTA curve of holmium molybdate crystals.

There are three derivative peaks in the DTG curve which corresponding to three mass losses in the TGA curve. The first peak is at about 257.94 $^{\circ}C$, and the percentage mass loss is about 5%. The second peak is at about 310.65 $^{\circ}C$ and the percentage mass loss is about 10%. The third peak is at about 816.28 $^{\circ}C$ and the percentage mass loss is about 30%. The first and second step may be due to the removal of water (H_2O) molecules. A number of compounds crystallizing with water of hydration and losing water from somewhere at 40 $^{\circ}C$ onwards has been reported in the literature [45-48]. The gel grown rare earth tartrates or molybdates leading to crystals associated with water of hydration is reported in the literature, eventhough different systems have been used [49-52].

The DTA curve (figure 5.9) shows three sharp endothermic peaks at 316.20 $^{\circ}C$, 502.33 $^{\circ}C$ and 520.33 $^{\circ}C$ and the corresponding enthalpy changes are 96.2668 J/g, 17.5929 J/g and 60.9537 J/g respectively. The TGA curve is nearly flat, i.e. no weight loss between 400 $^{\circ}C$ and 600 $^{\circ}C$, but the DTA curve shows a large endothermic peak at 520.33 $^{\circ}C$ with corresponding enthalpy change of 60.9537 J/g. The occurence of a DTA peak at about 520.33 $^{\circ}C$ may be suggested to be due to the phase transition occuring in the material under study. The ferroelectric phase transition in rare earth molybdate compounds have been reported by several authors [53,54]. During the measurement of the specific heat of terbium molybdate, two anomalies have been observed [14]. One at 430 K corresponds to the ferroelectric phase transition. The anomaly at 270 K has been observed as a small broad maximum, and the origin is not known. Therefore, it may be suggested that the peak at 520.33 $^{\circ}C$ corresponds to ferroelectric phase transition in holmium molyb-

date.

5.5 Conclusion

The growth of spherulitic crystals of holmium molybdate was accomplished by gel method, using holmium nitrate ($HoNO_3$) as upper reactants and ammonium molybdate ($(NH_4)_6Mo_7O_{24}$) as lower reactant. The pH of the gel medium was found to have a profound effect on the crystallization process of holmium molybdate crystals. The factors such as gel age, surrounding temperature, growth period and concentration of upper and lower reactant were also observed to affect the overall crystallization process.

The qualitative and quantitative elemental analysis, employing EDAX technique, confirmed the growth of rare earth Ho-molybdate crystals from silica gel, using $HoNO_3 - (NH_4)_6Mo_7O_{24} - NH_4NO_3 - Na_2SiO_3$ system. From the EDAX data, it is suggested that the grown sample is holmium octamolybdate with molecular formula $NH_4Ho(Mo_8O_{26}).nH_2O$. The X-ray diffraction pattern showed the crystalline nature of rare earth Ho-molybdate crystals.

The optical microscopic studies revealed that the crystals of Holmium molybdate are of spherulitic shape. The in-depth studies using scanning electron microscopic revealed that the holmium molybdate spherlites, grown at room temperature, are assemblies of plate-like crystalittes with an average thickness of about 20 nm and those grown at a temperature of $45\,^{\circ}C$ are composed of nono-rods with an average diameter of about 80 nm and an average transverse length of about 300 nm.

Thermogravimetric methods have revealed that the gel grown Ho-molybdate

crystals are associated water molecules. The Thermal behaviour suggests that the Ho-molybdate ($NH_4HoMo_8O_{26}.nH_2O$) decomposes at moderate temperatures i.e. around $50\,^{\circ}C$ and continues decomposing even after reaching the maximum temperature of $1000\,^{\circ}C$. The first two peaks in DTG curve are, suggeseted, due to the removal of water molecules. DTG and DTA curves also indicate that there may be some physical transformations besides mass changes associated with the loss of water. The DTA curve also suggested a ferroelectric phase transition in holmium molybdate crystals at $520.33\,^{\circ}C$.

Bibliography

[1] A. F. Arimington and J. I. O'Connor, Mater. Res. Bull. **2**, 907(1967).

[2] H. K. Henisch, Helv. Phys. Acta,**41**, 888(1968).

[3] M. Abdulkadar and M. A. Ittyachen, Proc. Indian Acad. Sci. (Chemical Sci.), **189**, 69(1980).

[4] V. Mansotra, K. K. Raina and P. N. Kotru. Jr. Mat. Sci. Lett. **8**, 481(1989).

[5] P. N. Kotru, K. K. Raina and N. K. Gupta, Cryst. Res. Technol, **22**, 177(1987).

[6] P. N. Kotru and K. K. Raina, Jr. Mat.Sci. Lett. **5**, 760(1986).

[7] D. S. Chernavskii, A. A. Polezhaev, S. C. Muller, Physica D **54**, 160-170 (1991).

[8] J. George, G. Varghese, J. Mater. Sci. **40**, 5557-5559 (2005).

[9] T. Terada, S. Yamabi, H. Imai, J. Cryst. Growth **253**, 435-444 (2003).

[10] R. V. Suganthi, E. K. Girija, S. Narayana Kalkura, H. K. Varma, A. Rajaram, J. Mater. Sci. Mater. Med. (2008) DOI 10.1007/s10856-008- 3495-1.

[11] K.S. Syed Ali, N. Ajeetha and R. Saravanan, Bull. Pure. And Appl. Sci. **21D**, 151(2002).

[12] M. Ali Omar (2000), **Elementary Solid State Physics-Principles and Applications**, (Addison-Wesley, Harlow).

[13] A.R. Verma and O.N. Srivastava (1991), **Crystallography Applied to Solid State Physics**, (Wilely Eastern Limited, New Delhi, India).

[14] S.A. Martin and H.N. Handler, J. Appl. Crystallogr. **11**, 62(1978).

[15] S.L. Sutib and P.F. Weller, J. Cryst. Growth, **48**, 155(1980).

[16] C.-D. Wu, C.-Z. Lu, X. Lin, H.-H. Zhuang and J.-S. Huang, Inorg. Chem. Comm. **5**, 664(2002).

[17] K. Riwotzki, H. Meyssamy, H. Schnablegger, A. Kornowski and M. Haase, Angew. Chem. Int. Ed. **40**, 573(2001).

[18] S. Heer, O. Lehmann, M. Haase and H. U. Gudel, Angew. Chem. Int. Ed. **42**, 3179(2003).

[19] J. W. Stouwdam and F. C. van Veggel, J. M. Nano Lett. **2**, 733(2002).

[20] G. S. Yi and G. M. Chow, J. Mater. Chem. **15**, 4460(2005).

[21] R. X. Yan and Y. D. Li, AdV. Func. Mater. **15**, 763(2005).

[22] K. B. Zhou, X. Wang, X. M. Sun, Q. Peng and Y. D. Li, J. Catal. **229**, 206(2005).

[23] X. Wang and Y. D. Li, Angew. Chem., Int. Ed. **41**, 4790(2002).

[24] X. Wang, X. M. Sun, D. P. Yu, B. S. Zou and Y. D. Li, AdV. Mater. **15**, 1442(2003).

[25] X. Wang and Y. D. Li, Angew. Chem., Int. Ed. **42**, 3497(2003).

[26] Y. P. Fang, A. W. Xu, R. Q. Song, H. X. Zhang, L. P. You, J. C. Yu and H. Q. Liu, J. Am. Chem. Soc. **125**, 16025(2003).

[27] Y. W. Zhang, X. Sun, R. Si, L. P. You and C. H. Yan, J. Am. Chem. Soc. **127**, 3260(2005).

[28] R. Si, Y. W. Zhang, L. P. You and C. H. Yan, Angew. Chem., Int. Ed. **44**, 3256(2005).

[29] C. B. Murray, D. J. Norris and M. G. Bawendi, J. Am. Chem. Soc. **115**, 8706(1993).

[30] X. G. Peng, L. Manna, W. D. Yang, J. Wickham, E. Scher, A. Kadavanich and A. P. Alivisatos, Nature, **404**, 59(2000).

[31] C. B. Murray, C. R. Kagan and M. G. Bawendi, Science, **270**, 1335(1995).

[32] W. C. W. Chan and S. M. Nie, Science, **281**, 2016(1998).

[33] M. Bruchez, M. Moronne, P. Gin, S. Weiss and A. P. Alivisatos, Science, **281**, 2013(1998).

[34] M. Yu, J. Lin, Z. Wang, J. Fu, S. Wang, H. J. Zhang and Y. C. Han, Chem. Mater. **14**, 2224(2002).

[35] H. Guo, N. Dong, M. Yin, W. P. Zhang, L. R. Lou and S. D. Xia, J. Phys. Chem. B **108**, 19205(2004).

[36] E. Rosa-Cruz, L. A. Diaz-Torres, R. A. Rodriguez-Rojas, M. A. Meneses Nava and O. Barbosa-Garcia, Appl. Phys. Lett. **83**, 4903(2003).

[37] Y. Q. Lei, H. W. Song, L. M. Yang, L. X. Yu, Z. X. Liu, G. H. Pan, X. Bai and L. B. Fan, J. Chem. Phys. **123**, 174710(2005).

[38] J. H. Zeng, J. Su, Z. H. Li, R. X. Ya and Y. D. Li, Adv. Mater. **17**, 2119(2005).

[39] F. Vetrone, J. C. Boyer, J. A. Capobianco, A. Speghini and M. Bettinelli, Chem Mater **15**, 2737(2003).

[40] D. Matsuura, Appl. Phys. Lett. **81**, 4526(2002).

[41] W. Liu, G. C. Farrington, F. Chaput and B. Dunn, J. Electrochem. Soc. **143**, 879(1996).

[42] Y. X. Pan, Q. Su, H. F. Xu, T. H. Chen, W. K. Ge, C. L. Yang and M. M. Wu, J. Solid. State. Chem. **74**, 69(2003).

[43] R. Shirley (1999), **The CRYSFIRE System for Automatic Powder Indexing: User's Manual**, The Lattice Press, 41 Guildford Park Avenue, Guildford, Surrey GU2 5NL, England.

[44] A. Patterson, Phys. Rev. **56**, 978(1939).

[45] P.N. Kotru, K.K. Raina and M.L. Koul, J. Mater. Sci. **21**, 3933(1986b).

[46] P.N. Kotru, N.K. Gupta, K.K. Raina and I.B. Sharma, J. Mater. Sci. Lett. **21**, 83(1986a).

[47] P.N. Kotru, N.K.Gupta, K.K. Raina and M.L. Koul, Bull. Mater. Sci. Lett. **8**, 547(1986c).

[48] P.N. Kotru, K.K. Raina and M.L. Koul, Indian J. Pure and Appl. Phys. **25**, 220(1987a).

[49] S. Bhat, P.N. Kotru and M.L. Koul, cryst. Res. Technology, **31**, 78(1966).

[50] S. Bhat, P.N. Kotru and M.L. Koul, J. Mater. Sci. Technol. **11**, 455(1995).

[51] A. Jain, S. Bhat, S. Pandita, M.L. Koul and P.N. Kotru, Bull. Mater. Sci. **20**, 1089(1997).

[52] S. Pandita, K.K. Bamzai, P.N. Kotru and M.L. Koul, **Proc. XXX Nat. Sem. Crystall.**, Tirupati Univ., Tirupati (India) June 28-30, 2000; abs. no E-25, P54.

[53] B. A. Strukov, S. A. Taraskin, I. V. Shnaidshtein, A. Onodera, H. Haga and B. S. Redkin, Sov. Phys. JETP, **81**, 202 (1995).

[54] M. Roy, R. N. P. Choudhary and H. N. Acharya, Thermochim. Acta **145**, 11(1989).

Chapter 6

Growth and Characterization of Gadolnium Molybdate crystals

6.1 Introduction

Gadolnium molybdate is one of the important compounds of rare earth molybdate faimly because of its tremendous applicability. It exhibits the phenomena of ferroelectricity and ferroelasticity [1]. It is very important for use in optical equipment and electronic and acoustic studies [2,3]. It is well documented that crystals of gadolinium molybdate possessing mixed ferroelastic and ferroelectric properties have been applied in electric and mechanical field [4,5]. It is worthwhile to grow the crystals of gadolnium molybdate as well as to explore the possibilities of the growth of new materials of rare earth compounds for various scientific investigations by an inexpensive and simple technique called the gel technique. A large number of crystals have been grown at ambient temperature by this technique, which may be classified as a low temperature solution technique. Due to the various advantages

of growing crystal by gel diffusion technique as already discussed in previous chapter, the crystals of gadolnium molybdates were also grown by this method for scientific investigations. To perform an in-depth study of the changes that are brought about in the physical and chemical properties of pure gadolnium molybdate crystals by different growth parameters, it was thought worthwhile to grow them in pure form.

6.2 Experimental Procedure for Growth of Gadolnium Molybdate Crystals

The experiments were conducted to grow pure crystals of gadolnium molybdates using gel diffusion technique. The crystals of gadolnium molybdate were grown under the similar procedure as that adopted for the growth of holmium molybdate crystals. They were grown in a crystallizer consisting of a single glass tube of length 15 cm and diameter 2.5 cm. The glass tube was filled three-fourth of its volume by one type of reactant, called lower reactant (LR), encapsulated in the gel network and one-fourth of its volume filled up with other reactant, called upper reactant (UR). Here, the upper reactant used was gadolnium chloride ($GdCl_3$).

The experiments for the growth of gadolnium molybdate crystals were also conducted in two types of gels: silica gel and agar-agar gel. The experiments conducted in agar-agar gel did not yield any fruitful results, so most of the work was conducted in silica gel. The silica gel was prepared by thoroughly mixing the solution of sodium metasilicate (Na_2SiO_3) of desired molarity with a solution of ammonium molybdate. The ammonium molyb-

date solution was prepared in the same manner as discussed in previous chapter.

After the gel was properly set and aged, the upper reactant gadolnium chloride ($GdCl_3$) of desired molarity was poured drop by drop along the sides into the crystallizer. The crystallizer was then left for a desired period (known as growth period) at a particular temperature. The experiments were conducted at a temperature of $45\,^{\circ}C$. This temperature was achieved by using a temperature controlled water bath.

6.3 Effect of Various Parameters on Growth of Gadolnium Molybdate Crystals

Series of experiments were conducted with an aim to grow good quality gadolnium molybdate crystals suitable for characterization and to observe the effect of various factors on the nucleation as well as on growth process. The experiments were conducted for different gel age, gel pH, and concentration of upper and lower reactants. Gadolnium molybdate being the isomorphs of holmium molybdate, it was observed that these factors have same effect on the nucleation and growth process of gadolnium molybdate crystals as they have on the nucleation and growth process of holmium molybdate crystals that is already discussed in previous chapter. So, it was not considered worthy to discuss the effect of these factors here again.

6.4 Characterization of Gadolnium Molybdate Crystals

In order to reveal the the morphology, elemental composition, size of crystals, the thermal behaviour of the lab-grown gadolnium molybdate crystals, they were characterized by different physio-thermal techniques. These are characterized by scanning electron microscopy (SEM), powder X-ray diffraction (XRD) and Thermal methods (TGA/DTA).

6.4.1 SEM Studies of Gadolnium Molybdate Crystals

The as-grown gadolnium molybdate crystals were observed under a polarizing optical microscope. Figure 6.1 shows the external morphology of these crystals. The morphology was observed to be that of spherulites, which are polycrystalline in nature.

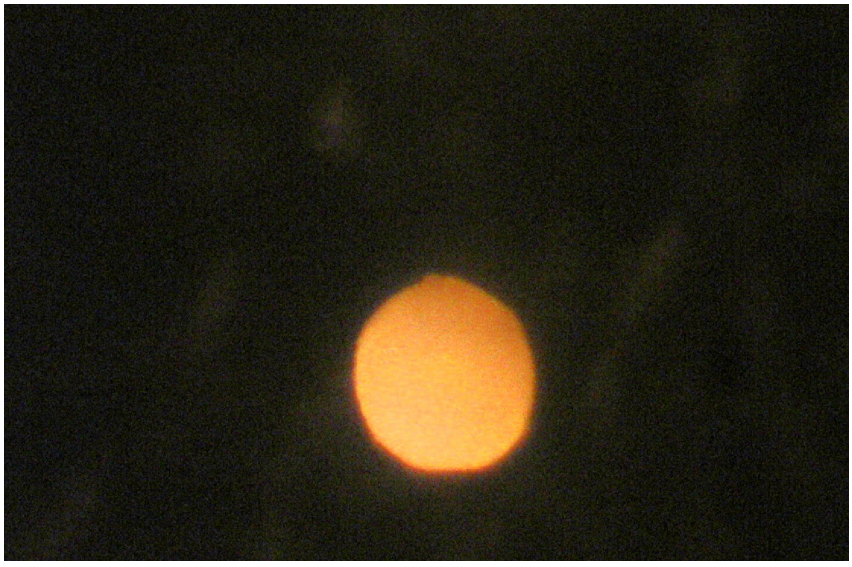

Figure 6.1: Spherulites of gadolnium molybdate crystals.

The in-depth external morphological studies of gadolnium molybdate crystals were carried out by using scanning electron microscope (SEM). The studies were performed by using the Hitachi S-3000H electron microscope. In order to enhance the conductivity of the laboratory-grown samples were coated with gold by using a Bal-Tec SCD004 sputter coating unit. Both apparatus are available at the University Instrumentation Centre (USIC), University of Kashmir, Srinagar.

The SEM micrographs, obtained from the characterization of gadolnium molybdate crystals that were grown at a temperature of $45\,^{\circ}C$, are shown in Fig. 6.2(a-b). Figure 6.2(a) shows the shape of spherulites at a magnification

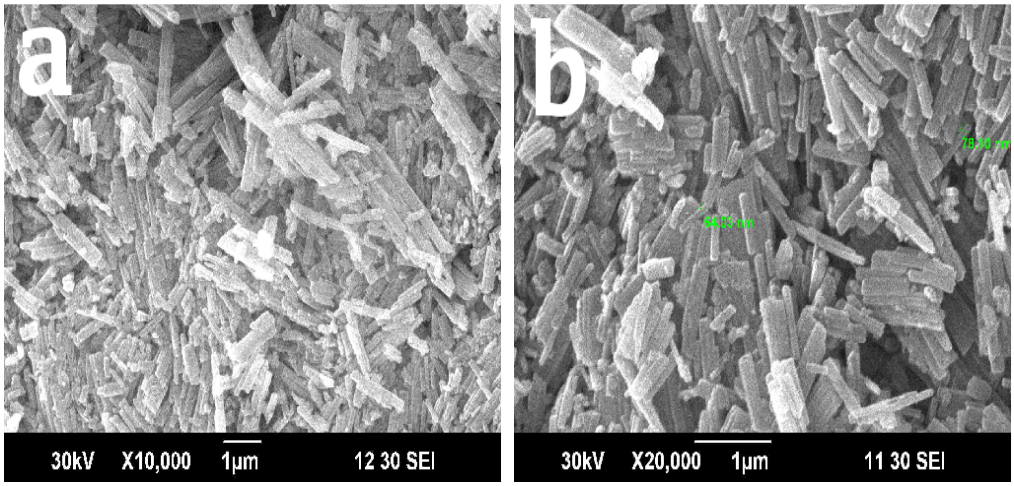

Figure 6.2: SEM images of gadolnium molybdate crystals at a magnification of: (a) 10000x and (b) 20000x.

of 10000x and figure 6.2(b) shows at 20000x. It is clear from these SEM-micrographs that these spherulites are not single units, but are composed of crystallites. These crystallites that form the surface of the spherulites are rod shaped. Thus the spherulites grown at a temperature of $45\,^{\circ}C$ are composed of nano-rods with an average diameter of 60 nm and average transverse length

of 300 nm. It is worthwhile to mention that these nanocrystals are nearly similar to the nanocrystals that form the external morphology of holmium molybdate spherulites (discussed in previous chapter) and were grown under similar conditions. Those nanocrystals were also observed to be rod-shaped with nearly same dimensions, an average diameter and transverse length of 80 nm and 300 nm respectively. These results reveal that it is possible to have controle over the shape and size of nanocrystals grown by gel diffusion technique which is very simple and inexpensive method of crystal growth. As discussed in previous chapter that rare earth nanocrystals have tremendous applicability, but the control over shape and size is a big challange in this path. The above results suggests that the gel diffusion method could be employed to grow rare earth nanocrystals with controllable shapes and sizes, but needs further research to be carried on.

6.4.2 X-ray Diffraction Studies of Gadolnium Molybdate Crystals

The most widespread use of powder diffraction is in the identification and characterization of crystalline solids, each of which produces a distinctive diffraction pattern. Both the positions (corresponding to lattice spacings) and the relative intensity of the lines are indicative of a particular phase and material, providing a "fingerprint" for comparison.

X-ray powder diffraction data of the present sample were collected at room temperature and under ambient conditions with Bruker AXS D8 Advance powder diffractometer using Cu K_α ($\lambda = 1.5406$ $\mathring{A}$) radiation and an applied voltage and current of 40 kV and 35 mA, respectively. The data were

recorded in the range of $3^0 \leq 2\theta \leq 80^0$ with a stepped scan rate of 0.020^0 per step and a count time of 31.2 seconds per step. The X-ray diffraction pattern of the sample is shown in figure 6.3. The series of sharp peaks present in the

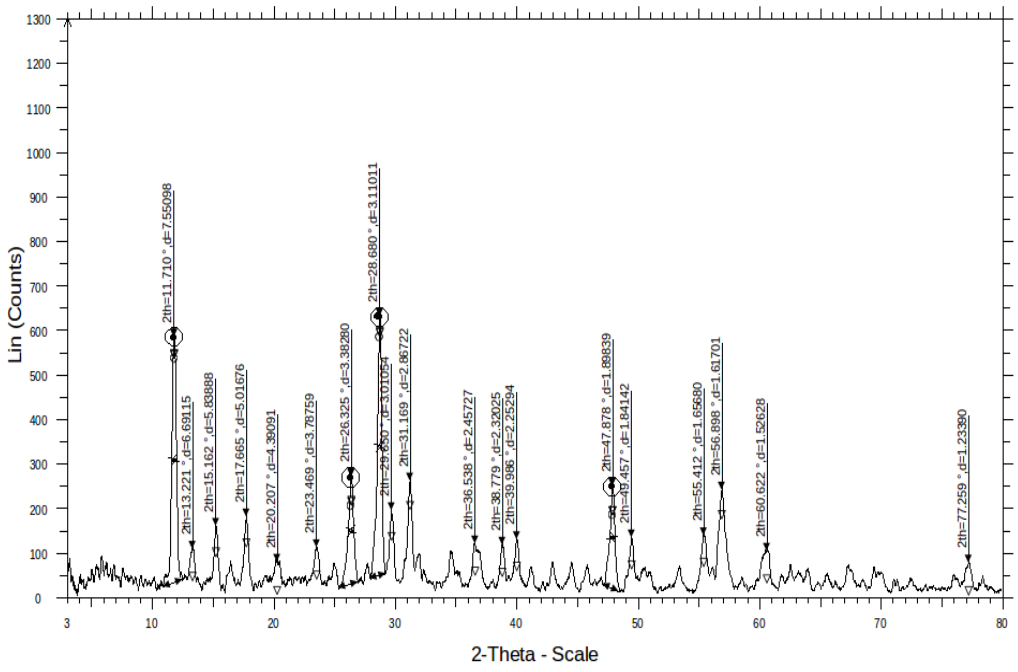

Figure 6.3: Powder XRD pattern of gadolnium molybdate crystals.

pattern clearly shows the crystalline nature of the material.

The position of a diffraction peak is independent of the atomic positions within the cell and entirely determined by the size and shape of the unit cell of the crystalline phase. Each peak represents a certain lattice plane and can therefore be characterized by a Miller index. The observed 'd' values for different 2θ with hkl indices of the corresponding planes for the crystal are given in Table 6.1. From the powdered X-ray data, the various planes of reflections were indexed using Crysfire program and the lattice parameters were evaluated. From the studies it is found that the structure of the

Table 6.1: X-ray powder diffraction data (indexed) of gadolnium molybdate crystals.

$2\theta(deg)$	d values	hkl indices
11.710	7.55098	0 0 1
13,221	6.69115	0 1 1
15.162	5.83888	1 1 0
17.665	5.01676	-1 0 0
20.207	4.39091	1 0 1
23.469	3.78759	-1 -2 0
26.325	3.38280	1 2 3
28.680	3.11011	-1 1 1
29.650	3.01054	1 3 1
31.169	2.86722	0 1 3
36.538	2.45727	2 0 1
38.779	2.32025	2 4 4
39.986	2.25294	1 4 2
47.878	1.89839	2 5 2
49.457	1.84142	3 2 4
55.412	1.65680	-1 3 3
56.898	1.61701	2 5 6
60.622	1.52628	-3 -2 2
77.259	1.23390	-3 -3 3

laboratory-grown gadolnium molybdate crystals is triclinic belonging to the space group of P1 with a = 7.1560 $\mathring{A}$, b = 10.1980 $\mathring{A}$, c = 10.1740 $\mathring{A}$, $\alpha = 48.140^0$, $\beta = 58.220^0$ and $\gamma = 44.840^0$ as cell parameters.

6.4.3 Calculation of Size of Crystallites

As already discussed, the approximate value of the size of the crystallites can be calculated from Scherrer equation which correlates the size of sub-micrometre particles, or crystallites, in a solid to the broadening of a peak in a diffraction pattern. The Scherrer equation is given by,

$$\tau = \frac{K\lambda}{\beta \cos\theta} \tag{6.1}$$

where K is the shape factor, λ is the x-ray wavelength, β is the line broadening at half the maximum intensity (FWHM) in radians, and θ is the Bragg angle; τ is the mean size of the ordered (crystalline) domains, which may be smaller or equal to the grain size. The dimensionless shape factor has a typical value of about 0.9, but varies with the actual shape of the crystallite. The Scherrer equation is limited to nano-scale particles. It is not applicable to grains larger than about 0.1 μm, which precludes those observed in most metallographic and ceramographic microstructures.

From the diffraction pattern of gadolnium molybdate crystals, we have the averages of

$\theta = 28.6487$ deg $= 0.5002$ rad

$\beta = 0.4150$ deg $= 0.0072$ rad

$\lambda = 1.5406\ \mathring{A} = 0.15406$ nm

K = 0.9

Substituting the above values in equation 6.1, the mean size of the crystallites is

$\tau = \underline{21.9434 \text{ nm}}$

So, the crysttalites which that assemble as spherulites in the aggregate are of nano range which confirms the information already revealed by the SEM-micrographs of the gadolnium molybdate crystals.

6.4.4 Thermal Studies of Gadolnium Molybdate Crystals

Thermal studies are very important to throw light on the thermal stability of the substances. These are utilized for the characterization of decomposition behaviour of the material. The thermogravemetric analysis (TGA), differential TG (DTG) and differential thermal analysis (DTA) of gadolnium molybdate crystals were recorded by Perkin Elmer Diamond TG/DTA Analyser.

The TGA, DTG and TGA curves of the gadolnium molybdate crystals are depicted in figure 6.4, figure 6.5 and figure 6.6 respectively. A powdered sample weighing 13.477 mg was used for the analyses. The analyses were carried out in the nitrogen atmosphere at a heating rate of $10\,^{\circ}C/$ minute for a temperature range of $40 - 1050\,^{\circ}C$. The TGA curve reveals that gadolnium molybdate crystals shows a multi-step decomposition process. The TGA curve also reveals that the material starts decomposing at above $50\,^{\circ}C$ and continues even after reaching the maximum temperature of $1000\,^{\circ}C$.

There are three derivative peaks in the DTG curve which corresponding to three mass losses in the TGA curve. The first peak is at about $249.72\,^{\circ}C$,

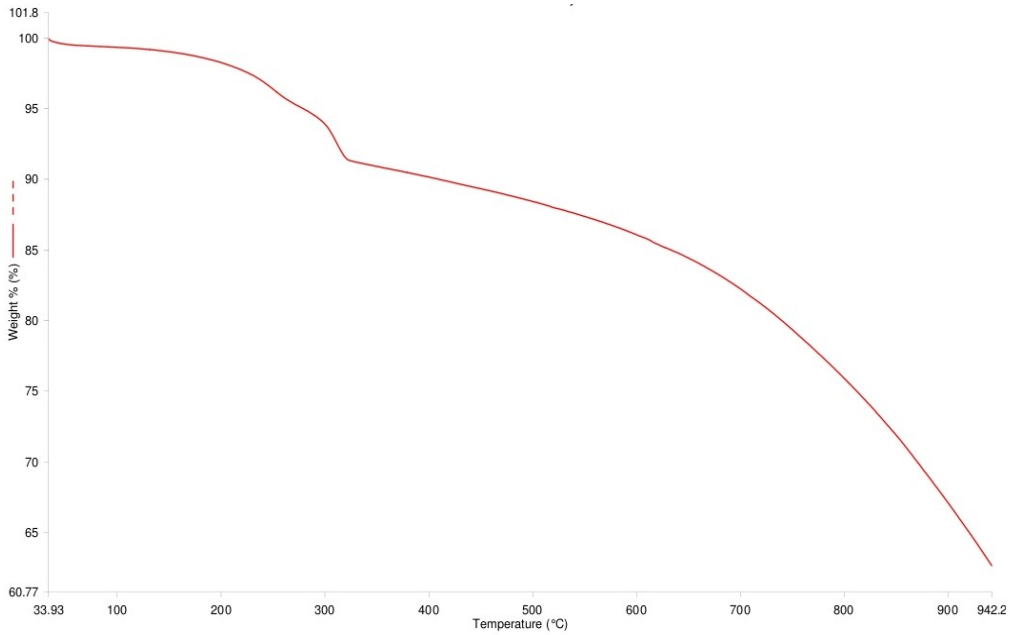

Figure 6.4: TGA curve of gadolnium molybdate crystals.

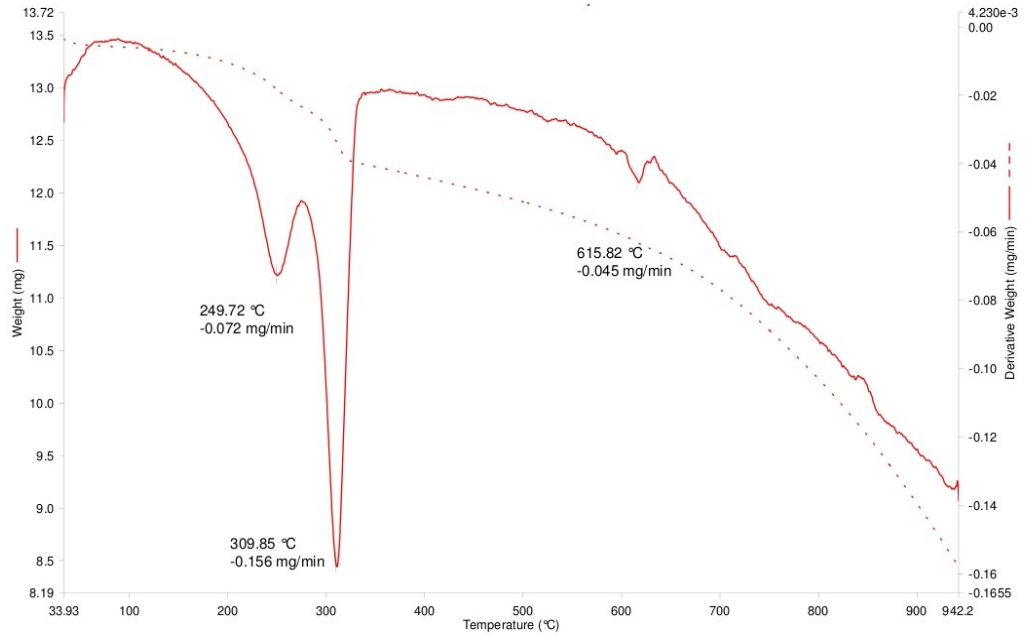

Figure 6.5: DTG curve of gadolnium molybdate crystals.

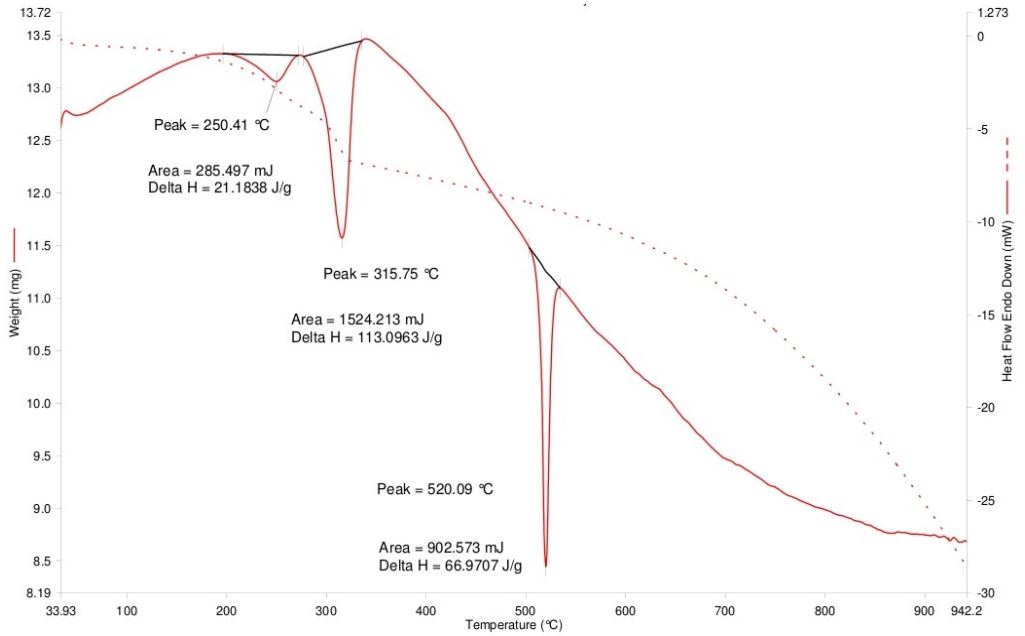

Figure 6.6: DTA curve of gadolnium molybdate crystals.

and the percentage mass loss is about 5%. The second peak is at about $309.85\,^{\circ}C$ and the percentage mass loss is about 7%. The third peak is at about $615.82\,^{\circ}C$ and the percentage mass loss is about 10%. The first and second step may be due to the removal of NH_3 gas and water (H_2O) molecules. A number of compounds crystallizing with water of hydration and losing water from somewhere at $40\,^{\circ}C$ onwards has been reported from in the literature [6-9]. The gel grown rare earth tartrates or molybdates leading to crystals associated with water of hydration is reported in the literature, eventhough different systems have been used [10-13].

The DTA curve (figure 6.6) shows three sharp endothermic peaks at $250.41\,^{\circ}C$, $315.75\,^{\circ}C$ and $520.09\,^{\circ}C$ and the corresponding enthalpy changes are 21.1838 J/g, 113.0963 J/g and 66.9707 J/g respectively. The TGA curve is nearly flat, i.e. no weight loss between $450\,^{\circ}C$ and $550\,^{\circ}C$ which is also con-

firmed by DTG curve of the sample as there is no peak in this temperature range, but the DTA curve shows a large endothermic peak at 520.09 $^{\circ}C$ with corresponding enthalpy change of 66.9707 J/g. The occurence of DTA peak at 520.09 $^{\circ}C$ may be suggested to be due to the phase transition occuring in the material under study. The phase transition in gadolnium molybdate is also reported by many authors. The temperature dependence of the spontaneous electric polarization in gadolnium molybdate was measured in [14] over the temperature range from 4.2 K up to the Curie point T_C = 432.3 K and reported a phase transition of first order at 432.3 K. Sakai et. al [15] measured the temperature dependence of the specific heat in gadolnium molybdate over a wide temperature region and they also reported a sharp anomaly appears at T_c =431.36 K which corresponds to the ferroelectric phase transition. Therefore, it may be suggested that the peak at 520.09 $^{\circ}C$ in the DTA curve of gadolnium molybdate corresponds to its ferroelectric phase transition.

It is worthwhile to mention that a careful observation of DTG/DTA of gadlonium molybdate crystals (figure 6.5 and figure 6.6) and that of holmium molybdate crystals (figure 5.8 and figure 5.9) reveals that most of the peaks in both the materials are nearly at same temperature. This suggests that the molecular structures of gadolnium molybdate crystals and holmium molybdate crystals could be similar.

6.5 Conclusion

The growth of spherulitic crystals of gadolnium molybdate is accomplished by gel method, using gadolnium chloride ($GdCl_3$) as upper reactants and

ammonium molybdate [$(NH_4)_6Mo_7O_{24}$] as lower reactant. The pH of the gel medium has a profound effect on the crystallization process. The factors such as gel age, growth period and concentration of upper and lower reactant were also observed to affect the crystallization process of gadolnium molybdate crystals.

The optical microscopic studies reveal that the crystals of gadolnium molybdate have the shape of spherulites which are polycrystalline in nature. The in-depth studies using scanning electron microscopic reveal that these spherlites are assemblies of rod-shaped crystalittes of nano-scale. So the gadolnium molybdate spherulites are composed of nano-rods with an average diameter of 80 nm and an average transverse length of 300 nm.

The sharp peaks in the X-ray diffraction pattern of gadolnium molybdate sample revealed its crystalline nature. The structure of the laboratory-grown gadolnium molybdate crystals was calculated to be triclinic belonging to the space group of P1 with a = 7.1560 $\mathring{A}$, b = 10.1980 $\mathring{A}$, c = 10.1740 $\mathring{A}$, $\alpha = 48.140^0$, $\beta = 58.220^0$ and $\gamma = 44.840^0$ as cell parameters.

Thermogravimetric methods have revealed that the gel grown Gd-molybdate crystals are associated water molecules. The Thermal behaviour suggests that the Gd-molybdate decomposes at moderate temperatures i.e. around $50\,^{\circ}C$ and continues decomposing even after reaching the maximum temperature of $1000\,^{\circ}C$. DTG and DTA curves also indicate that there may be some physical transformations besides mass changes associated with the loss of water. The DTA curve suggests a ferroelectric phase transition in gadolnium molybdate crystals at $520.09\,^{\circ}C$. Thus, the rare earth molybdates, gadolnium molybdate and holmium molybdate, exhibit the isomorphic phase

transition at about the same transition temperature, 520.09 $^{\circ}C$ and 520.33 $^{\circ}C$ respectively.

Gadolnium molybdate and holmium molybdate crystals almost shows similar behaviour in almost all characterization experiments. Both materials (grown at 45 $^{\circ}C$) have same morphology i.e. spherulite and both are composed of nano-rods and have almost same dimensions. They show similar decomposition behaviour and show ferroelectric phase transition at same temperature. X-ray diffraction patterns show that they also similar structure. Being isomorphic, it may be concluded that the lab-grown gadolnium molybdate may have the similar molecular formula as that of holmium molybdate. So it is suggested that the molecular formula of gadolnium molybdate may be $NH_4Gd(Mo_8O_{26}).nH_2O$.

Bibliography

[1] L. H. Brixner , J. R. Barkley and W. Jeitschko, **Handbook on the Physics and Chemistry of Rare Earths**, edited by K.A.Gschneidner, Jr. and L.Eyring. (North-Holland Publishing Company, 1979), Chapter 30, pp. 610-655.

[2] J. R. Barkley, L. H. Brixner, E. M. Hogan and R. K. Waring, J. Ferroelectr. **3**, 191(1972).

[3] J. Sapriel and R. Vacher, J. Appl. Phys. **48**, 1191(1977).

[4] H. J. Borchardt and P. E. Bierstedt, Appl. Phys. Lett. **8**, 50(1966).

[5] Y. V. Shur, E. V. Nikolaeva, E. I. Shishkin, I. S. Baturin, A. G. Shur, T. Utschig, T. Schlegel and D. C. Laupascu, Appl. Phys. Lett. **98**, 74106(2005).

[6] P.N. Kotru, K.K. Raina and M.L. Koul, J. Mater. Sci. **21**, 3933(1986b).

[7] P.N. Kotru, N.K. Gupta, K.K. Raina and I.B. Sharma, J. Mater. Sci. Lett. **21**, 83(1986a).

[8] P.N. Kotru, N.K.Gupta, K.K. Raina and M.L. Koul, Bull. Mater. Sci. Lett. **8**, 547(1986c).

[9] P.N. Kotru, K.K. Raina and M.L. Koul, Indian J. Pure and Appl. Phys. **25**, 220(1987a).

[10] S. Bhat, P.N. Kotru and M.L. Koul, cryst. Res. Technology, **31**, 78(1966).

[11] S. Bhat, P.N. Kotru and M.L. Koul, J. Mater. Sci. Technol. **11**, 455(1995).

[12] A. Jain, S. Bhat, S. Pandita, M.L. Koul and P.N. Kotru, Bull. Mater. Sci. **20**, 1089(1997).

[13] S. Pandita, K.K. Bamzai, P.N. Kotru and M.L. Koul, **Proc. XXX Nat. Sem. Crystall.**, Tirupati Univ., Tirupati (India) June 28-30, 2000; abs. no E-25, P54.

[14] E. Sawaguchi and L. E. Cross, J. Appl. Phys. **44**, 2541(1973).

[15] A. Sakai, K. Kodama, Y. Kawamura, A. Onodera and B. A. Strukov, J. Korean Phys. Soc. **32**, 509(1998).

Chapter 7

Summary and Future Work

7.1 Summary of the Present Work

The present work has revealed many new aspects about the gel diffusion technique and the rare earth molybdate crystals. The growth of holmium molybdate and gadolnium molybdate crystals is accompolished by gel diffusion method, using $HoNO_3 - (NH_4)_6Mo_7O_{24} - NH_4NO_3 - Na_2SiO_3$ and $GdCl_3 - (NH_4)_6Mo_7O_{24} - NH_4NO_3 - Na_2SiO_3$ systems. The crystals of holmium molybdate and gadolnium molybdate assunme spherulitic shape under all varying parameters such as gel age, surrounding temperature, growth period and concentration of upper and lower reactants. The scanning electron microscopic studies reveal that these spherulites are not single units, but are composed of nanocrystals. The spherulites of holmium molybdate, grown at room temperature are composed of nano plates with an average thickness of 20 nm and those grown at $45\,^{\circ}C$ are composed of nono-rods with an average diameter of about 80 nm and an average transverse length of about 300 nm. The spherulites of gadolnium molybdate were grown at

$45\,^{\circ}C$ only and were observed to be composed of nono-rods with an average diameter of about 60 nm and an average transverse length of about 300 nm. Thus, the size and shape of the nano crystallites composing the spherulites of holmium molybdate and gadolnium molybdate, grown at $45\,^{\circ}C$, are nearly same.

The qualitative and quantitative elemental analysis, employing EDAX technique, confirm the growth of Ho-molybdate and Gd-molybdate crystals. The X-ray diffraction patterns indicate crystallinity of these crystals. Thermogravimetric methods have established that the gel grown Ho-molybdate and Gd-molybdate material starts decomposing at above $50\,^{\circ}C$ and continues even after reaching the maximum temperature of $1000\,^{\circ}C$. The thermal analysis curves provided their thermal decomposition behaviour and revealed that the holmium molybdate and gadolnium molybdate crystals shows an isomorphic phase transion at nearly the same temperature, $520.33\,^{\circ}C$ and $520.09\,^{\circ}C$ respectively.

7.2 Future Scope

Several recommendations are being made for future research in the area of crystal growth by gel diffusion technique. Although extensive research has already been performed in the growth of holmium molybdate and gadolnium molybdate crystals, more experiments are suggested for wide range of gel age, gel pH, temperature and other growth factors to explore the possible formation of other compounds with different morphology and molecular structure. Further investigation should aim to confirm the molecular formulae of holmium molybdate and gadolnium molybdate compounds referred to

here as $NH_4Ho(Mo_8O_{26}).nH_2O$ and $NH_4Gd(Mo_8O_{26}).nH_2O$. The weight change experiments (TGA, DTA, DSC) need to be carried out upto very high temperature in order to fully investigate their thermal decomposition behaviour. Fourier transform infra-red spectroscopy should be performed in order to reveal the structure fully and to confirm the presence of water molecules in the laboratory grown samples.

Rare-earth nanocrystals with controllable shapes and sizes have received intense research attention during the past few years [1-12] because of their potential applications in optics [1-3], optoelectronics, biological labeling [4,5], catalysis fields [6] etc. It is expected that with reduced dimensionalities, the movement of electrons and photons in rare-earth nanocrystals would be confined in two and/or all directions and then lead to enhanced optical and magnetic properties in a manner similar to that of typical systems such as II-VI semiconductor nanocrystals [13-17]. This is particularly important for the exploration of new research and application fields on the basis of the novel properties of rare-earth nanocrystals. However, there still remains much to be carefully addressed in the rare-earth nanocrystal system, especially for the general principle in shape and size control, which may provide possibilities for systematically investigating the size- and shape-dependent properties on the nanoscale. To obtain desired nanocrystals of rare earth compounds, the methods such as sol-gel method [18,19,20], hydrothermal synthesis [21,22], combustion [23], coprecipitation [24], and the Pechini method [25,26], at a relatively low temperature, have been extensively adopted. In comparsion to these methods, the gel diffusion method of crystal growth, used in the present work, is very simple and inexpensive. This method, though needs further

research in order to have control over the size and shape of crystals, could be a very efficient method for the growth of nanocrystals. The present work suggests that the gel diffusion method could be employed to grow rare earth nanocrystals with controllable shapes and sizes, but needs further research to be carried on.

There is a large scope for further investigations into the thermal and dielectric characteristics of these crystals. These studies could enhance their applicability in the fields of science and technology.

In nut shell, there is a lot of scope for future research on many aspects in this field including growth (which involves size, perfection, morphology, water of crystallization and other related aspects), thermal characteristics (thermal stability, reaction kinetic parameters), dielectric characteristics (identification of ferroelctric nature), structural characteristics and mechanical characteristics of these crystals. The maximum possible extent to which one can go in respect of the above mentioned investigations and many more could only depend on the availability of a variety of sophisticated instruments for carrying out the accurate measurements and critical analysis. These investigations could ultimately lead us to better understanding of their characteristics and practical utility in various fields of science and technology.

Bibliography

[1] K. Riwotzki, H. Meyssamy, H. Schnablegger, A. Kornowski and M. Haase, Angew. Chem. Int. Ed. **40**, 573(2001).

[2] S. Heer, O. Lehmann, M. Haase and H. U. Gudel, Angew. Chem. Int. Ed. **42**, 3179(2003).

[3] J. W. Stouwdam and F. C. van Veggel, J. M. Nano Lett. **2**, 733(2002).

[4] G. S. Yi and G. M. Chow, J. Mater. Chem. **15**, 4460(2005).

[5] R. X. Yan and Y. D. Li, AdV. Func. Mater. **15**, 763(2005).

[6] K. B. Zhou, X. Wang, X. M. Sun, Q. Peng and Y. D. Li, J. Catal. **229**, 206(2005).

[7] X. Wang and Y. D. Li, Angew. Chem., Int. Ed. **41**, 4790(2002).

[8] X. Wang, X. M. Sun, D. P. Yu, B. S. Zou and Y. D. Li, AdV. Mater. **15**, 1442(2003).

[9] X. Wang and Y. D. Li, Angew. Chem., Int. Ed. **42**, 3497(2003).

[10] Y. P. Fang, A. W. Xu, R. Q. Song, H. X. Zhang, L. P. You, J. C. Yu and H. Q. Liu, J. Am. Chem. Soc. **125**, 16025(2003).

[11] Y. W. Zhang, X. Sun, R. Si, L. P. You and C. H. Yan, J. Am. Chem. Soc. **127**, 3260(2005).

[12] R. Si, Y. W. Zhang, L. P. You and C. H. Yan, Angew. Chem., Int. Ed. **44**, 3256(2005).

[13] C. B. Murray, D. J. Norris and M. G. Bawendi, J. Am. Chem. Soc. **115**, 8706(1993).

[14] X. G. Peng, L. Manna, W. D. Yang, J. Wickham, E. Scher, A. Kadavanich and A. P. Alivisatos, Nature, **404**, 59(2000).

[15] C. B. Murray, C. R. Kagan and M. G. Bawendi, Science, **270**, 1335(1995).

[16] W. C. W. Chan and S. M. Nie, Science, **281**, 2016(1998).

[17] M. Bruchez, M. Moronne, P. Gin, S. Weiss and A. P. Alivisatos, Science, **281**, 2013(1998).

[18] M. Yu, J. Lin, Z. Wang, J. Fu, S. Wang, H. J. Zhang and Y. C. Han, Chem. Mater. **14**, 2224(2002).

[19] H. Guo, N. Dong, M. Yin, W. P. Zhang, L. R. Lou and S. D. Xia, J. Phys. Chem. B **108**, 19205(2004).

[20] E. Rosa-Cruz, L. A. Diaz-Torres, R. A. Rodriguez-Rojas, M. A. Meneses Nava and O. Barbosa-Garcia, Appl. Phys. Lett. **83**, 4903(2003).

[21] Y. Q. Lei, H. W. Song, L. M. Yang, L. X. Yu, Z. X. Liu, G. H. Pan, X. Bai and L. B. Fan, J. Chem. Phys. **123**, 174710(2005).

[22] J. H. Zeng, J. Su, Z. H. Li, R. X. Ya and Y. D. Li, Adv. Mater. **17**, 2119(2005).

[23] F. Vetrone, J. C. Boyer, J. A. Capobianco, A. Speghini and M. Bettinelli, Chem Mater **15**, 2737(2003).

[24] D. Matsuura, Appl. Phys. Lett. **81**, 4526(2002).

[25] W. Liu, G. C. Farrington, F. Chaput and B. Dunn, J. Electrochem. Soc. **143**, 879(1996).

[26] Y. X. Pan, Q. Su, H. F. Xu, T. H. Chen, W. K. Ge, C. L. Yang and M. M. Wu, J. Solid. State. Chem. **74**, 69(2003).